UNIVERSITEIT VAN PRETORIA
UNIVERSITY OF PRETORIA
YUNIBESITHI YA PRETORIA

THE SYNTHESIS AND CHARACTERISATION OF FLUORINATED ETHYLENE PROPYLENE (FEP) COPOLYMERS

by

TANDO KILI

A dissertation submitted in partial fulfilment of
the requirements for the degree

Master of Science (Applied Sciences) in Chemical Technology

Supervisor: Prof. P.L. Crouse
Co-supervisor: Dr I.J. van der Walt

Department of Chemical Engineering,
Faculty of Engineering, Building Environment and Information Technology
University of Pretoria

December 2014

DECLARATION

I, Tando Kili (student number 10675371), hereby declare that the work on which this dissertation is based is original (except where acknowledgement have been made) and that neither the whole nor any part of the document has been, is being, or is to be submitted for another degree at this or any other university.

Signed _____

Date _____

DEDICATION

This dissertation is dedicated to my late mother and my family.

ACKNOWLEDGEMENTS

I would like to thank the Lord Almighty for giving me strength, courage and patience to complete this work.

I am very thankful to my supervisor, Prof Philip Crouse, for accepting me into his research group, his guidance and support.

I would also like to convey my sincere thanks to Cliff Thomson for training and assistance, and James Mabudafhasi for helping with experimentation, and Dr Jaco van der Walt for the technical management of the project at Necsa.

I am also grateful to the following institutes: DST's Fluoro-chemical Expansion Initiative (FEI), NRF's Innovation Scholarship, and Necsa for accommodating the technical work, and the NRF for financial assistance.

Last, but not least, I am grateful to my entire family for their patience and unconditional support during my studies.

SYNOPSIS

THE SYNTHESIS AND CHARACTERISATION OF FLUORINATED ETHYLENE PROPYELENE (FEP) COPOLYMERS

This work details research on the semi-continuous copolymerisation of tetrafluoroethylene (TFE) and hexafluoropropylene (HFP) in aqueous medium using different monomer ratios. A main objective of this dissertation was to understand the influence of changing parameters, such as monomer feed ratio and initiator concentration, on the properties of the polymer. The copolymerisation of TFE and HFP was carried out in ultra-pure water using a 300 mL Parr 316 stainless steel high-pressure reactor. The experiments were done at 85 and 100 °C with pressures in the range of 11 - 20 bar using ammonium persulfate as the free radical initiator. Different monomer feed compositions were studied: 10, 19, 20, 22, 26, 38, 39, 40, 44 and 46 mol % HFP. The pressure of the reaction was found to be dependent on the amount of HFP in the feed stream.

The following techniques were used to provide a comprehensive understanding of the as-polymerised FEP: FTIR, TGA-FTIR, SEM, DSC, XRD and ^{19}F NMR. Solid state ^{19}F NMR spectroscopy was used to elucidate the structure and determine the composition of FEP copolymers. The results revealed a successful incorporation of the HFP monomer in the copolymers by peaks at -67.44, -70.46 and -112.10 ppm due to $–CF_3$ and $–CF_2$ units of the HFP monomer and also by a peak at -183.42 ppm due to –CF unit of the HFP monomer. Results from DSC indicated that the melting temperature (determined by the highest peak of the first heating observed in the thermograms) and heat of fusion decreased from 324.28 to 278.71 °C and 73.05 to 36.60 J/g respectively as the mol % HFP increases in the copolymer. The XRD analysis showed that the FEP polymers are semi-crystalline with increase in the amorphous region as the concentration of HFP increases from 0.96 to 3.80 mol % HFP.

SEM analysis showed that the FEP samples consists of spheres and rods at low HFP concentration in the monomer feed and spheres at high HFP. The TG analysis revealed that the copolymers are thermally stable up to 460 °C; after that they start to decompose. The decomposition can be resolved into a two-step process by taking the first derivative of the

TGA curve. The evolved gas analysis using FTIR indicated that the first step corresponded to the elimination of HFP species (weak peak intensity at 1391 and 1790 cm^{-1} corresponding to C-F of CF_3 in C_3F_6 and C=C of C_2F_6) in addition to strong bands at 1032, 1184 and 1328 cm^{-1} attributed to the CF_2 moiety. The second corresponded to the degradation of the PTFE backbone chain to monomer component or unit.

TABLE OF CONTENTS

LIST OF ABBREVIATIONS

FEI	Fluorochemical Expansion Initiative
FEP	Fluorinated Ethylene Propylene
TFE	Tetrafluoroethylene
HFP	Hexafluoropropylene
MFI	Melt Flow Index
OFCB	Octafluorocyclobutane
PFIB	Perfluoroisobutylene
COF_2	Carbonyl fluoride
FTIR	Fourier Transform Infrared
DSC	Differential Scanning Calorimetry
SEM	Scanning Electron Microscopy
NMR	Nuclear Magnetic Resonance
TGA	Thermogravimetric Analysis
PFA	Perfluoroalkoxy
PFAVE	Perfluorinated alkyl vinyl ethers
PPVE	Perfluoropropylvinyl ether
IR	Infrared
APS	Ammonium persulfate

KPS	Potassium persulfate
PTFE	Polytetrafluoroethylene
FEP	Fluorinated ethylene propylene
ATR	Attenuated Total Reflectance
PR	Production Rate
MAS	Magic Spinning Angle
CSA	Chemical shift anisotropy
DTG	Derivative Thermogravimetry
XRD	X-ray Diffraction
A_{CF2}	Absorbance area of CF_2 vibration
A_{CF3}	Absorbance area of CF_3 vibration
T_{d10}	10 % decomposition temperature
RF	Radio Frequency
DD	Dipolar Decoupling
CP	Cross polarisation
CSA	Chemical shift anisotropy
o.d.	Outside diameter

LIST OF FIGURES

LIST OF TABLES

RESEARCH OUTPUTS EMINATING FROM THIS RESEARCH

Conference proceedings

T. Kili, M.L. Mabudafhasi, J.C. Thompson,I.J. van der Walt, P.L. Crouse, "The synthesis and characterisation of fluorinated ethylene propylene copolymers "FEP"), SACI National 2013 convention, East London, South Africa, Dec. 2013 (Oral presentation).

T. Kili, M.L. Mabudafhasi, J.C. Thompson, I.J. van der Walt, P.L. Crouse, "Synthesis and characterisation of fluorinated ethylene-propylene (FEP) copolymers", 12th International Chemistry Conference Africa 2013 at University of Pretoria in Pretoria, July 2013 (Poster presentation).

Peer-reviewed articles submitted

T. Kili, M.L. Mabudafhasi, J.C. Thompson, I.J. van der Walt, G. Silly, P.L. Crouse, "The suspension synthesis fluorinated ethylene propylene copolymers (FEP), submitted to *Journal of Polymer Science: Part A*, September 2014.

1.1 BACKGROUND

Fluorspar (calcium fluoride, CaF_2) is a mineral found naturally and is the primary source of fluorine for all fluorochemicals internationally. South Africa has the largest fluorspar reserves in the world. Most of the mined fluorspar in South Africa is exported as an unbeneficiated raw material at a price US$0.1/kg (Department of Trade and Industry, 2005). Only 5 % of the fluorspar mined in South Africa is beneficiated to fluorochemical products. The South African Government realised an opportunity to beneficiate the raw fluorspar by conversion into value-added fluoro-chemical products. In 2005 the SA government set up the Fluorochemical Expansion Initiative (FEI) with the strategic goal of expanding the beneficiation of fluorspar in South Africa (Department of Trade and Industry, 2005). Pelchem a wholly-owned subsidiary of Necsa, situated at the Pelindaba site near Pretoria was tasked with championing FEI.

Fluoropolymers are very attractive compounds because of their versatility (they cover the range of thermoplastics, elastomers, etc.) and their unique physical, and chemical properties (Ameduri et al, 2001). These properties result from the low polarisability and the strong electronegativity of the fluorine atom, the small van der Waals radius (1.32 Å) and the strong C-F bond (485 kJ/mol) as compared to the C-H bond (415 kJ/mol) or C-C bond (348 kJ/mol) (Simon and Kaminsky, 1998; Ameduri et al, 2001). Because of the strong C-F bond, fluoropolymers exhibit distinctive properties such as: high thermal stability, chemical resistance (e.g., to acids, bases and solvents), resistance to aging, low wettability and attractive low surface properties. They find industrial applications in areas such as aerospace, water-repellent textile finishing, pipes and hoses, valves, thermocouple wells, gaskets, heat exchangers and O-rings dynamic seals (Ge et al, 2006; Gudipati et al, 2004; Ellis et al, 2003).

Polytetrafluoroethylene (PTFE) is the most important fluoropolymer. PTFE is a perfluorinated homopolymer of the tetrafluoroethylene (TFE) monomer. It was discovered in 1938 by Dr Roy Plunkett of Du Pont Company (Simon and Kaminsky, 1998). The discovery of PTFE paved the way for solving industrial material problems by replacing costly exotic

metals with an economical plastic (Ebnesajjad, 2003). PTFE has unique desired properties such as high chemical and physical resistance, excellent thermal stability, low surface area energy, flame and weather resistance, non-tackiness, soil-proofing ability, good electric insulation, etc. The thermal stability of PTFE allows its applications at temperatures up to 260 °C (Simon and Kaminsky, 1998; Kim et al, 1999a; Kim et al, 1999b; Endo et al, 2004).

For industrial applications, PTFE is usually required to have a high molecular weight in order to minimise excessive crystallisation (White et al, 1998; Endo et al, 2004). However, the high molecular weight required makes processing using conventional processing techniques such as injection moulding difficult due to high melt viscosity. Hence special alternative processing technology such as powder sintering and paste extrusion is required to process PTFE powders (Endo et al, 2004). The PTFE homopolymer is highly crystalline, insoluble in common organic solvents and not easily cross-linked (Ameduri et al, 2001).

To overcome these undesired properties, PTFE underwent the typical evolutionary process of the other polymers families through copolymerisation of tetrafluoroethylene monomer with a variety of comonomers, such as hexafluorpropylene (HFP) in poly(tetrafluoroethylene-co-hexafluoropropylene) (FEP) and perfluoroalkyl vinyl ethers (e.g. perfluoropropylvinyl ether (PFA) in poly(tetrafluoroethylene-co-perfluoroalkylvinyl ether) (PFAVE) (Endo et al, 2004). The introduction of the comonomer results a semi-crystalline copolymer with molecular weight, crystallinity and melt viscosity lower in comparison to PTFE. The new fluoropolymers can be processed by a conventional techniques such as melt processing (extrusion and injection), and dispersion and solution coating methods (Ebnesajjad, 2003; Endo et al, 2004; White et al, 1998).

1.2 AIM OF THE STUDY

The aim of the study was to develop the technology for the on-specification synthesis of TFE/HFP copolymers, using in-house produced TFE and HFP.

The objectives of this investigation were:

- To obtain insight into the methods of synthesis and characterisation of TFE/HFP copolymers through a literature review;
- To study the semi-continuous copolymerisation in aqueous medium using different monomer feed ratios;
- To investigate the influence of changing parameters such as, monomer feed ratio, reaction temperature and initiator concentration on the properties of the polymer;
- To investigate the properties of the synthesised polymer using FTIR, DSC, SEM, ^{19}F-NMR, TGA-FTIR and XRD.

2.1 FLUORINATED ETHYLENE PROPYLENE (FEP)

Fluorinated ethylene propylene (FEP) is a random perfluorinated copolymer of tetrafluoroethylene (TFE) and hexafluoropropylene (HFP) monomers and has a branched molecular structure containing $-CF_2-CF_2-$ and $-CF_2-CF(CF_3)-$ units. The copolymer retains most of the unique properties of PTFE whilst the viscosity is low enough that conventional processing technologies can be utilised (Teng, 2012). The incorporation of HFP monomer in the PTFE chain reduces the melting point from 327 ˚C for PTFE to around 260 ˚C for FEP (Drobny, 2009). The FEP copolymer structure has a tertiary carbon at the branch point bonded to a pendent perfluoromethyl group, CF_3, shown in Figure 2-1. This carbon is believed to be less stable compare to primary and second carbons in the polymer chain. (Ebnesajjad, 2003).

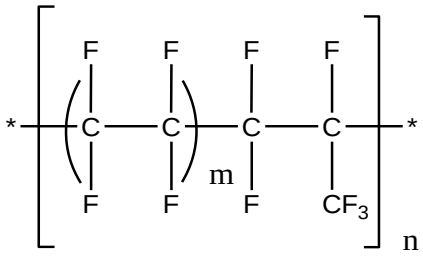

Figure 2-1 Schematic structure of FEP

Table 2-1 presents a comparison of the properties of FEP and PTFE. It can be see that the melting point, processing temperature, degradation temperature, and upper continuous-use temperature of FEP are all notably reduced compare to PTFE, the most affected being the use temperature. The reduction in thermal stability is due to the tertiary carbon bonded to the perfluoromethyl group that is susceptible to oxidation. FEP crystallinity is half that of PTFE even though its molecular weight of FEP is significantly lower to that of PTFE. The reduced crystallinity is caused by the disruption of crystallisation by CF_3 side chains. The

melt viscosity of FEP is almost one hundred million times lower than PTFE, thus making FEP melt-processible thermoplastic polymers. (Ebnesajjad, 2003)

Table 2-1 Comparison of FEP and PTFE properties (Ebnesajjad, 2003).

Property	**PTFE**	**FEP**
Melting Point	327	265
Processing Temperature	400	360
TGA Loss Temperature 1 %/hr, ˚C	465	380
Upper Continuous Use Temperature, ˚C	260	200
Melt Viscosity (380 ˚C), Poise	10^{11}-10^{12}	10^{4}-10^{5}
Crystallinity of Virgin Polymer, % wt	92-98	40-50

Commercial FEP copolymers are available in different melt flow indexes (MFI) (also called melt flow rate) grades and composition ranges that allow a selection of physical properties and processing characteristics, which are suitable for specific processing equipment and end-use requirements. The comparison of the Teflon® FEP grades properties are shown in Table 2-2.

- The highest MFI grades find use in applications where high extrusion rates or easier flow are required. They are more suitable for conventional injection moulding techniques. One of the core applications is for wire coating, such as plenum primaries. (Gangal, 2000; Gangal and Brothers, 2010)
- The intermediate MFI grades are used in applications that require more stress crack resistance. These find applications in cable jacketing, tubing, films, and coatings over wire-braid constructions such as coaxial cables and insulation of small wires sizes where high current loads or excessive thermal cycling may occur such as heater cables. (Gangal, 2000; Gangal and Brothers, 2010)
- The lower MFI grade finds applications as liners for processing equipment and thick films. The MFI is significantly lower compare to other MFI grades; therefore it is

unsuitable processing using conventional injection moulding. It has superior stress crack resistance and mechanical properties that are superior to the other product grades. (Gangal, 2000; Gangal and Brothers, 2010)

Table 2-2 Properties of Teflon® FEP fluorocarbon grades[a] (Gangal, 2000; Gangal and Brothers, 2010).

Mechanical properties	**ASTM method**	**Teflon® FEP 4100**	**Teflon® FEP 100**	**Teflon® FEP 140**	**Teflon® FEP 160**
Melt flow number, g/10 min	D2116	22	7.0	3.0	1.5
Specific gravity	D792	2.13-2.17	2.13-2.17	2.13-2.17	2.13-2.17
Tensile strength at 23 °C, MPa	D1708	20	23	30	31
Elongation at 23 °C, %	D1708	300	325	325	305
Compressive strength, MPa	D695	N/A	21	21	23
Flexural strength at 23 °C, MPa	D790		18	18	18
Impact strength at 23 °C, J/m	D256	No break	No Break	No Break	No Break
Flexural modulus at 23 °C, MPa	D790	655	620	620	586
Hardness durometer, Shore D	D2240	55	56	56	57
Coefficient of friction, metal/film	D1894	0.25	0.27	0.27	0.235
Deformation under load at 23 °C, 6.9 MPa, 23 hr, %	D621	0.5	0.5	0.5	0.5
Water absorption, 24 h, %	D570	0.004	0.004	0.004	0.004
Linear coefficient of expansion, mm/mm·°C	E831				
0-100 °C		N/A	13.5×10^{-5}	13.9×10^{-5}	7.6×10^{-5}
100-150 °C			20.8×10^{-5}	21.2×10^{-5}	11.5×10^{-5}
150-200 °C			26.6×10^{-5}	27.0×10^{-5}	14.2×10^{-5}

[a]Compression-moulded specimens; property data on extruded specimens are similar

FEP is available in pellet, flakes, and dispersion form. FEP copolymers with high stress-crack resistance and high extrusion rates can be improved by modification with perfluoroalkyl vinyl ethers monomers such as perfluoropropylvinyl ether (PPVE). The use of perfluoroalkyl vinyl ethers improves performance without affecting the chemical inertness and thermal stability. FEP copolymer dispersion are available commercially as a 55 wt % aqueous dispersion containing 6 % non-ionic surfactant and a small amount of anionic dispersing agent with an average particle size of ca 200 nm. (Gangal, 2000; Gangal and Brothers, 2010)

2.1.1 Chemical properties

FEP polymer is resistant to most chemicals and solvents, even at elevated temperatures and pressures. However, it suffers attack from fluorine, molten alkali metal, and molten sodium hydroxide. Organic solvents absorption is less than 1 % even at high temperatures and not affected by exposure times. FEP absorption of solvents and chemicals does not reduce its chemical integrity and the process can be reversed. (Gangal and Brothers, 2010)

2.1.2 Permeation to gases

The FEP polymer has permeation rates of vapours and gases that significantly lower compared to other polymers. Since FEP polymers are melt-processed, they have a zero void content and permeation happens by molecular diffusion. Because of its low permeability, FEP polymers find extensive use in the chemical industry (Gangal, 2000; Gangal and Brothers, 2010). Some permeation characteristics are shown in Table 2-3 and Table 2-4 and are comparable to those of PTFE. An inverse relationship between permeability and film thickness also applies to FEP. (Gangal and Brothers, 2010)

2.1.3 Electrical and optical properties

FEP polymers are the most valuable and versatile electrical insulators (Gangal, 2000; Ebnesajjad, 2003). Within the recommended service temperature range, PTFE and FEP exhibit similar electrical properties as electrical insulators. The volume resistivity of FEP polymers (i.e. greater than 10^{17} Ω·cm) is unaffected by the continuous immersion in water (Drobny, 2009) and surface resistivity is more than 10^{15} Ω/sq. The dielectric constant of FEP is unaffected at low frequencies (~2) but gradually decrease with increasing frequency at

frequencies higher than 100 MHz The FEP has higher dissipation factor than PTFE and this arises from the fact that the molecular structure of FEP is asymmetrical compare to PTFE structure (Gangal, 2000; Gangal and Brothers, 2010). The dielectric strength is high and independent on thermal aging at 200 °C (Drobny, 2009). The dielectric properties weaken with the introduction of corona discharge at high frequencies.

Table 2-3 Permeability of FEP fluorocarbon resin to liquid vapours. (Gangal, 2000; Gangal and Brothers, 2010).

	Permeability constant, 10^{15} mol/(m·s·Pa)		
Vapour	**23 °C**	**35 °C**	**50 °C**
Acetic acid		9.07	
Acetone	0.37		3.23
Benzene	0.75		
Carbon tetrachloride	0.24	0.41	
Decane	112.18		33.48
Dipentene	23.50		10.57
Ethyl acetate	0.27	2.06	4.09
Ethanol	1.61	4.66	
Sulfuric acid, 98%	21.70		
Toluene	5.38		
Water	8.14	20.32	18.26

2.1.4 Optical properties

FEP films transmit more ultraviolet, visible light, and infrared radiation compared ordinary window glass. The refractive index of FEP film is 1.341 - 1.347 (Drobny, 2009; Gangal and Brothers, 2010).

Table 2-4 Permeability of FEP fluorocarbon resin to gases (Gangal, 2000).

Gases	Permeability constant, 10^{15} mol/(m·s·Pa) at 20 °C
O_2	18.69
H_2	113.47
N_2	6.10
H_2	40.15
CH_4	3.17

2.1.5 Thermal stability

The FEP polymer is thermally stable and is melt-processed at ca 270 °C. The thermal stability of the polymer is dependent on the temperature and exposure time, therefore the stability is limited. The thermal degradation increases significantly for short periods above 280 °C and occurs at lower temperatures with longer hold times. The hourly weight loss of FEP polymers is presented in Table 2-5 (Gangal, 2000). The FEP polymer degradation is negligible if the melt flow rate change during moulding is less than 10 %. The physical properties decreases with continuing exposure above 205 °C and which is the result for the lower temperature rating for FEP plastics (Gangal, 2000; Gangal and Brothers, 2010).

2.1.6 Radiation effects

FEP is attacked by radiation, and its degradation in air starts at dose of 0.2 Mrad which is 10 times higher than that of PTFE (Ebnesajjad, 2011; Gangal, 2000; Gangal and Brothers, 2010). The primary effect of radiation is the degradation to small molecules. Effects on molecular weight can be reduced by the absence of oxygen. Cross-linking is prevalent when FEP is highly irradiated at elevated temperatures in the absence of oxygen thus negating molecular degradation. Effects on mechanical properties depend on total dosage but are independent of the dose rate. Surface modification by vacuum UV radiation is better compared to plasma treatment. (Gangal, 2000; Gangal and Brothers, 2010)

Table 2-5 Weight loss of FEP polymers as a function of temperature (Gangal, 2000)

Wight loss, %	0.0004	0.001	0.01	0.02	0.08	0.3
Temperature, °C	230	260	290	320	340	370

2.1.7 Transitions and relaxations

Only a single first-order transition is observed, i.e., the melting point (Ebnesajjad, 2011; Gangal and Brothers, 2010). Melting of the polymer increases the volume by 8 %. The presence of the HFP comonomer causes crystal changes which increase the intramolecular distance, thus reducing the melting point (Gangal, 2000).

The relaxation temperature is affected by the HFP content, i.e., increases with HFP content. Increasing HFP content leads to relaxing and untwisting of the helical conformation of the PTFE chain in order to accommodate the perfluoromethyl group in the HFP unit resulting in a less ordered crystalline structure. (Gangal, 2000; Gangal and Brothers, 2010)

2.1.8 Mechanical properties

The FEP polymers retains most of the unique properties of PTFE with main with difference being the reduced continuous use temperature of ~200 compared to 260 °C for PTFE. The flexibility at low temperatures and the low coefficients of friction and stability at high temperature are unaffected by fabrication conditions. FEP does not have the first-order transition at 19 °C observed for PTFE, thus doesn't exhibit marked change in volume at room temperature. The polymers are useful above -267 °C and exhibit flexibility above -79 °C. (White et al, 1998; Gangal, 2000; Gangal and Brothers, 2010)

2.2 MONOMERS

2.2.1 TFE monomer

TFE, (structure shown in Figure 2-2), is a colourless, tasteless, odourless, non-toxic gas that boils at -76.3 ˚C and freezes at -142.5 ˚C. It is stored as a liquid with a vapour pressure of 1

MPa at -20 ˚C. TFE is polymerised usually above its critical temperature of 33.3 ˚C and below its critical pressure 3.94 MPa (Drobny, 2009). The polymerisation reaction is highly exothermic and it generates 41.12 kcal/mol of heat so cooling during reaction is important. TFE has a reported heat of formation of -151.9 kcal/mol. TFE monomer disproportionate violently to yield carbon and carbon tetrafluoride in the absence of air (Drobny, 2009).

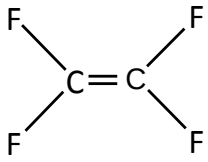

Figure 2-2 Structure of TFE.

The reaction generates a comparable amount of energy to an explosion of black powder. The decomposition is thermally initiated; therefore, the equipment for handling and polymerisation of TFE has to be without hot spots. The flammability limits in air are 14-43 vol. %. In the presence of air and oxygen, the TFE forms explosive mixtures. TFE can be stored in steel cylinder under controlled conditions with a use of a suitable inhibitor, such as α-pinene, terpene and d-limonene. Table 2-6 lists the summary of the properties of TFE (Drobny, 2009; Ebnesajjad, 2003).

2.2.2 Synthesis TFE monomer

The commercial manufacturing process of TFE consists of the following steps:

$$CaF_2 + H_2SO_4 \rightarrow CaSO_4 + 2HF \quad (1)$$

$$CH_4 + 3Cl_2 \rightarrow CHCl_3 + 3HCl \quad (2)$$

The first step produces hydrogen fluoride from fluorspar and the second step yields trichloromethane (chloroform, $CHCl_3$). The chloroform is then partially fluorinated with

hydrogen fluoride to chlorodifluoromethane, using antimony trifluoride as a catalyst in the third step.

Table 2-6 Physical properties of tetrafluoroethylene (Drobny, 2009; Ebnesajjad, 2003)

Property	**Value**
Molecular weight, g/mol	100.02
Boiling point at 101.3 kPa, °C	-76.3
Freezing point, °C	-142.5
Critical temperature, °C	33.3
Critical pressure, MPa	3.92
Critical density, g/cm^3	0.58
Liquid density vs temperature (°C), g/cm^3	
-100 < T < -40	1.202 - 0.004T
-40 < T < 8	1.1507 - 0.0069T - 0.000037T^2
8 < T < 30	1.11325 - 0.0029T - 0.00025T^2
Vapour pressure at T K, kPa	
196 < T < 273.15	$\log_{10} P = 6.4593 - 875.14/T$
273.15 < T < 306.45	$\log_{10} P = 6.4289 - 866.84/T$
Dielectric constant at 28 °C	
at 101.3 kPa	1.0017
at 858 kPa	1.015
Thermal conductivity at 30 °C, mW/(m·K)	15.5
Heat of formation for ideal gas at 25 °C, ΔH, kJ/mol	-635.5
Heat of polymerisation at 25 °C, ΔH, kJ/mol	-172.0
Flammability limits in air at 101.3 kPa, vol. %	14 - 43
Ignition temperature, °C	600 - 800

$$CHCl_3 + 2HF \rightarrow CHClF_2 + 2HCl \quad (3)$$

Finally, the chlorodifluoromethane produced in the third step is subjected to pyrolysis to convert it to tetrafluoroethylene.

$$2CHClF_2 \rightleftharpoons CF_2{=}CF_2 + 2HCl \quad (4)$$

The pyrolysis is a non-catalytic gas-phase reaction occurring in a flow reactor at atmospheric or subatmospheric pressures and at temperatures 560 to 900 ˚C with yields as high as 95 %. The last step is usually conducted at the manufacturing site for PTFE because of the difficulty of handling and danger transporting the monomer (Ebnesajjad, 2003). The major by-product of this process is HCl, although other halogenated products can form. The most significant being hexafluoropropylene (HFP), perfluorocyclobutane (OFCB), 1-chloro-1, 1, 2, 2-tetrafluoroethane with trace amounts of others such as perfluoroisobutylene (PFIB) which is very toxic. Because large amount of corrosive acids are used and generated, the reactor has to be manufactured from highly corrosion resistant materials such as platinum-lined nickel reactors. (Drobny, 2009)

The superheated steam is used as diluent to improve the process efficiency. After pyrolysis, gas stream is cooled then scrubbed by water and alkali to remove the acids and then dried by calcium chloride or sulfuric acid. Subsequently, it is compressed and cryogenically distilled to recover the unreacted chlorodifluoromethane and to obtain a highly purified TFE (Drobny, 2009). The disadvantage of this process is the product of HCl as a by-product, and low conversion (~20 %) of chlorodifluoromethane, requiring a large recycle stream (van der Walt, 2007).

2.2.3 HFP monomer

HFP monomer (Figure 2-3) is a colourless, odourless, tasteless and a relatively low toxic gas, which boils at -29.4 ˚C and freezes at -156.2 ˚C. HFP is extremely stable w.r.t. autopolymerisation compared to TFE and may be stored in liquid state without the addition of telogens (Drobny, 2009). A summary of the properties of HFP is listed in Table 2-7.

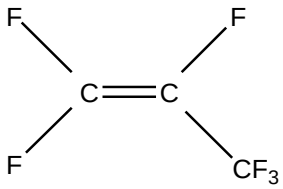

Figure 2-3 Structure of HFP.

HFP is thermally stable up to 400-500 ˚C. At 600 ˚C under vacuum, HFP decomposes and produces octafluoro-2-butene ($CF_3CF=CFCF_3$) and octafluoroisobutylene ($(CF_3)_2C=CF_2$). Under γ-radiation and in the presence oxygen it produces a 1:1 mole ratio of carbonyl fluoride (COF_2) and trifluoroacetyl fluoride (CF_3COF). Under basic conditions and presence of hydrogen peroxide, HFP forms hexafluoropropylene epoxide, which is a precursor for preparation of perfluoroalkylvinyl ether (Ebnesajjad, 2003).

2.2.4 Synthesis of HFP monomer

HFP can be prepared by the thermal cracking of tetrafluoroethylene in a stainless steel tube at 700-800 ˚C under reduced pressure. Octafluorocyclobutane (TFE dimer), octafluoroisobutylene are the major by-products of cracking. The presence of chlorodifluoromethane in small amounts (3 to 10 10 %) can inhibit the formation of polymer. Thermal decomposition of PTFE under vacuum (2.667 kPa) at 860 ˚C produces 58 % HFP (Drobny, 2009; Ebnesajjad, 2003; Gangal, 2000; Gangal and Brothers, 2010).

Table 2-7 Physical properties of hexafluoropropylene (Gangal, 2000; Gangal and Brothers, 2010).

Property	**Value**
Molecular weight, g/mol	150.021
Boiling point at 101.3 kPa, °C	-29.4
Freezing point, °C	-156.2
Critical temperature, °C	85
Critical pressure, MPa	3.254
Critical density, g/cm^3	0.60
Vapour pressure at T K, kPa 243.75<T<358.15	$\log_{10}P_{kPa} = 6.6938-1139.156/T$
Heat of formation for ideal gas at, 25 °C, ΔH, kJ/mol	-1078.6
Flammability limits in air at 101 kPa	Non-flammable for all mixtures
Heat of combustion, kJ/mol	879
Toxicity, LC_{50} (rat), 4 h[a], ppm	3000

[a]Exposure resulting in fatality of 50% of rats in 4 hours

HF reaction with 3-chloro-pentafluoro-1-propene (CF_2=CF-CF_2Cl) at 200 ˚C, under activated carbon catalyst yields HFP (Gangal, 2000; Gangal and Brothers, 2010). HFP can also be prepared from catalytic degradation of fluoroform (CHF_3) at 800-1000 ˚C in a platinum-lined nickel reactor. Another method is the co-pyrolysis of fluoroform and chlorotrifluoroethylene (CF_2=CFCl), or chlorodifluoromethane and 1-chloro-1, 2, 2, 2-tetrafluoroethane ($CHClFCF_3$), giving good yields of HFP (Gangal, 2000) (Gangal and Brothers, 2010).

Another method involves the pyrolysis of a mixture of TFE and carbon dioxide at atmospheric pressure at 700-900 ˚C. Conversions of 20-80 % and HFP yields better than 80 % were obtained. The unreacted TFE and carbon dioxide were distilled from the product and recycled back to the system. HFP can also be synthesised from hexachloropropylene via a multi-step process beginning with fluorination. The later steps convert the initial products to CF_3-CFCl-CF_3 which is then dehalogenated to HFP. Other techniques reported on the

synthesis of HFP from the mixture of a variety of linear and cyclic three-carbons with a partially halogenated three-carbon acyclic hydrocarbon. (Ebnesajjad, 2003)

2.3 FEP SYNTHESIS

Sauer (1951) published information on tetrafluoroethylene and hexafluoropropylene with the objective to provide a new and improved method of polymerisation for high molecular weight copolymers comprising hexafluoropropylene. This objective was accomplished by subjecting a mixture comprising HFP and another ethylenically unsaturated polymerisable compound to polymerisation conditions. The polymerisation was carried out using the following method:

- A high-pressure stainless steel reactor was flushed with oxygen-free nitrogen, and then charged with deoxygenated water, ammonium persulfate (APS) and sodium pyrophosphate.
- The reactor was closed, evacuated, cooled and is then charged with HFP and TFE.
- The reactor was agitated and heated to 55-64 °C for 9.8 hours and a pressure of 250-650 atm is maintained by water injection.
- The reactor was cooled to room temperature and the unreacted gases collected.
- The copolymer was discharged from the reactor, washed with distilled water, suspended for 3 hours in refluxing solution of concentrated HCl and acetic acid, filtered, washed with water, and air-dried at a pressure of 200 mmHg at 60 °C for 48 hours. The results and reaction parameters from the experiments done can be seen in Table 2-8.

Table 2-8 Summary of experiments performed by Sauer (1951).

	Example 1	Example 2	Example3
Water, parts	200	200	50
APS, parts	0.15	0.15	0.2
$Na_4P_2O_7$, parts	1.0	1.0	0
HFP, parts	20	15	7.5
TFE, parts	60	85	20
Temperature, °C	55-64	60-61	57-80
Reaction time, hr	9.8	9.2	14.5
Pressure, atm	250-650	460-500	50-100
%HFP in copolymer	20	13.4	Not reported
%TFE in copolymer	80	86.6	Not reported
Melt temperature, °C	310	325-330	320
Copolymer amount, parts	37.2	18	24
Tensile strength, psi	2000	1750	1750
Elongation, %	300	230	84
Dielectric constant	2.17	2.18	Not reported

APS = ammonium persulfate; $Na_4P_2O_7$ = sodium pyrophosphate

Bro and Sandt (1960) produced a copolymer of TFE and HFP with specific melt viscosity of 1×10^3 to 3×10^5 poises measured at 380 °C under a shear stress of 44.8 kPa and specific IR ratio (Appendix E) 1.5 to 6 making the copolymer melt processable by extrusion techniques. The crystalline melting points of the copolymers range from 242 to 305 °C with preferred melting points in the range of 256-287 °C, which falls within the limits of the four sided figure, DEFG (specific IR ratio of 3×10^4 to 1×10^5 poises) in Figure 2-4. The copolymer within DEFG limit can be fabricated at practical rates via melt extrusion into thin tough homogeneous shaped articles, such as films, filament, tubing and wire covering etc. The copolymer of the invention was produced by an inorganic free-radical initiator in aqueous medium while regulating the monomer composition and initiator concentration. The

polymerisation reaction was performed at temperatures that range from 50 to 150 °C, at pressures ranging from 2.0 to 7.1 MPa for 10 to 180 minutes.

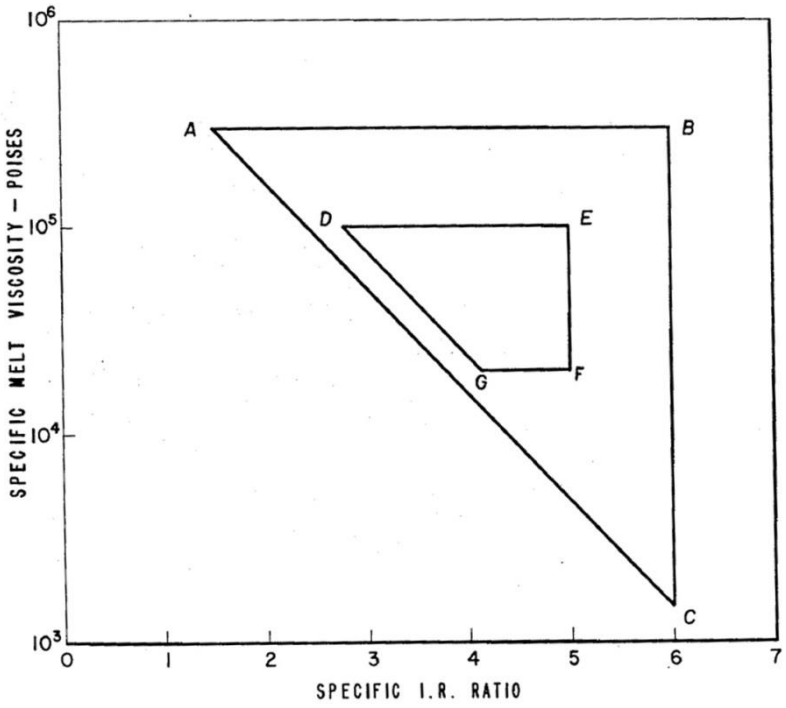

Figure 2-4 A plot of specific melt viscosity vs specific IR ratio of the FEP copolymers (Bro and Sandt, 1960).

The monomer feed weight ratio (TFE/HFP) ranged from 3/7 to 9/1 and initiator present in concentrations that effectively generate active free radicals in the range of 4×10^{-3} - 3×10^{-6} mol/(min·L) of solution.

The reactions were performed using the following method:

- A cylindrical horizontal, water jacketed paddle-stirred stainless steel reactor was charged with demineralised water.
- The reactor was purged of gases by warming the charge and then heating to 95 °C.

- The reactor was then pressured to 1.72 MPa with deoxygenated hexafluoropropylene (HFP) and 0.1 molal APS was added to the reactor and stirred for 15 minutes.
- A mixture containing 75 % TFE and 25 % HFP was added to the reactor to pressure the reactor to 4.48 MPa.
- Then a 0.0052 molal solution of APS was continuously added at 0.0455 parts per minute, so the calculated concentration of undecomposed persulfate was maintained at 2.1 x 10^{-4} molal.
- The stirring and 0.0052 molal APS addition was continued until the pressure dropped; thereafter for 80 minutes a pressure of 4.48 MPa was maintained by adding 75 % TFE and 25 % HFP.
- After 80 minutes the stirring was stopped, vapour in the reactor sampled then vented and contents discharged. The summary and the results of the reaction examples are reported in Table 2-9.

Miller (1952) produced a perfluorinated polymeric material of high chemical stability and mechanical characteristics which was easy to process using conventional methods. This was achieved by using a bis-trichloroacetyl peroxide $(CCl_3CO)_2O_2$ as an initiator and the use of low temperatures and moderate pressures. This was achieved by charging an evacuated glass polymerisation reactor with 0.0068 g of $(CCl_3CO)_2O_2$ in dichloromethane solvent at -30 °C. The reactor was evacuated to a low pressure and charged with 32.2 g HFP (purified by distillation from phosphorus pentoxide) and 3.6 g TFE (purified by distillation through sulphuric acid and phosphorus pentoxide) at liquid air temperatures -194 °C. The reactor was evacuated then pumped to low pressure and temperature raised to approximately -16 °C. The reactor was maintained under these conditions for 10 days and then 2.9 g of a chemically stable solid product was discharged. The product was compressed about 26.8 % of when a 0.635 cm diameter area of a 1.587 cm diameter sample, 0.457 mm thick was subjected to a pressure of about 6.89 MPa at 125°C for 10 minutes. When the pressure was released, the compressed sample recovered to about 77.8 % of its reduction in thickness in 10 minutes.

Table 2-9 Summary of examples and results for the copolymerisation of TFE and HFP using APS and KPS (Bro and Sandt, 1960).

	Ex. 1	Ex. 2	Ex. 3	Ex. 4	Ex. 5
Initial HFP charged, MPa	1.72	1.72	3.31	3.31	3.10
%HFP	25	25	25	25	25
%TFE	75	75	75	75	75
Initiator	APS	KPS	KPS	KPS	KPS
First initiator con. Added, molal	0.1	0.0236	0.0236	0.0236	0.0236
Final initiator con. Added, molal	0.0052	0.0088	0.0088	0.0104	0.0098
Initiator dosing rate, part/min	0.0455	0.0168	0.0168	0.0168	0.0168
Reaction pressure, bar	4.48	4.48	4.48	4.48	4.48
Melting T, °C	280	272	261	279	265
Melt viscosity, poise	7×10^4	6.1×10^4	4.4×10^4	2×10^5	1.2×10^4
Specific IR ratio	3.40	3.66	4.70	3.41	4.41
Specific volatile content, %	0.14	0.15	0.15	0.15	0.25
Reaction time, minutes	80	80	80	80	80
Active free radicals, mol/(min·L)	2.08×10^{-5}	1.25×10^{-5}	1.25×10^{-5}	1.5×10^{-5}	1.45×10^{-5}

APS = ammonium persulfate; KPS = potassium persulfate; HFP = hexafluoropropylene; TFE = tetrafluoroethylene

Cleaver (1960) investigated the use of new polymerisation catalysts such as nitrogen fluorides for the polymerisation of unsaturated monomers capable of addition polymerisation with improved properties. This was achieved by a process that consisted of the addition of a nitrogen fluoride groups such as dinitrogen difluoride (N_2F_2), dinitrogen tetrafluoride (N_2F_4) and nitrogen fluorides of the general formula, (FNX_1X_2) where X can be the same or different and represent fluorine or perfluoroaliphatic hydrocarbon radicals, i.e., perfluoroalkyl or perfluoroalicyclic groups, to a monomer at 300 °C, using the following method:

A pressure reactor was charged with unsaturated monomer and reaction medium, if any. Then the reactor was connected to an evacuated system, cooled to about -80 °C and evacuated to remove oxygen. A required amount of nitrogen fluoride was then injected and the system was maintained at the selected polymerisation temperature for the required period, after which the polymer was recovered. The amount of the initiator used was at least 0.0001 % by weight of the unsaturated monomer being polymerised. The conditions of the experiments are depicted in Table 2-10.

Table 2-10 Parameters and results of copolymerisation of TFE and HFP with nitrogen fluorides and with solvents: [a] cyclic HFP dimer and [b] perfluorodimethylcyclobutane (Cleaver, 1960).

	Ex. XIV	Ex. XVIIA	Ex. XVIIB	Ex. XXIX	Ex. XXX
Reactor size, mL	80	80	80	80	80
HFP, g	30	30	30	30	31
TFE, g	10	10	10	20.3	10
Reaction time, min	120	120	120	750	720
Reaction Temp, °C	120	75	75	152	155
Solvent amount, mL	20[a]	20[a]	20[a]	20[b]	20[b]
Catalyst	NF_3	N_2F_2	N_2F_2	N_2F_4	N_2F_4
Catalyst weight, mg	300	3	6	45	37
Product weight, g	2.2	7.5	8	15.7	5.7
mol % HFP in copolymer	NR	NR	NR	13	15

NR = Not reported

A process for the polymerisation of perfluorinated monomers in a perfluorinated medium using a highly fluorinated initiator was investigated by Bro et al (1961). In their study they used a peroxygenated acids catalyst having a general formula R_fCOOOH formed by a

reaction between a hydrogen peroxide and a fluorinated acid according to the equations depicted below:

$$R_fCOOH + H_2O_2 \rightleftharpoons R_fCOOOH + H_2O \quad (1)$$

or by the reaction of a fluorinated acid anhydride with H_2O_2

$$(R_fCO)_2O + H_2O_2 \rightleftharpoons R_fCOOOH + H_2O \quad (2)$$

where R_f is a perfluoroalkyl or an omega-hydrofluoroalkyl radical. The catalyst may be used from temperatures below 0 to 100 °C At higher temperatures the catalyst decomposition rate is too fast to be practical for most fluorinated monomers. The amount of catalyst that can be utilised depends on the polymerisation conditions as well as the monomer and may vary from 0.001 % to 10 % by weight of the H_2O_2 based on the weight of the monomer. Results and experimental parameters are shown in Table 2-11.

Table 2-11 Reaction parameters of FEP polymerisation (Bro et al, 1961).

	Ex. IX	**Ex. X**	**Ex. XI**
Reactor size	180	85	180
Solvent amount, mL	50	0	50
Fluorinated acid	5 g[a]	5 g[b]	50 mL[b]
30 % H_2O_2	0.25 g	0.25 g	1 g
HFP	30 g	30 mL	30 g
TFE	15 g	20 g	15 g
Temperature, °C	50	50	50
Time, min	60	60	60
Solid product weight, g	18.4	11.4	4.5
wt % HFP	9	14	

[a]trifluoroacetic anhydride; [b]trifluoroacetic acid and solvent = perfluoro-dimethylcyclobutane

Eleuterio (1962) investigated a method of preparing amorphous copolymers of HFP and TFE. The author argued that the FEP polymers created at the time were normally crystalline, in a sense that after being heated to temperatures of 300 °C and allowed to cool in air to room temperature, they exhibited X-ray diffraction patterns characteristic of crystalline materials. The method used by the author to produce amorphous TFE/HFP copolymers involved heating a mixture of 70 to 99 wt % HFP and 1 to 30 wt % TFE at temperatures that ranged from 70-350 °C under pressures of 2000 - 10000 atm (202.6 - 1013.25 MPa) in the presence of a polymerisation initiator. The method used is illustrated by the following example (parts are by weight):

- A stainless steel vessel of 120 parts by weight capacity was charged with 85 parts by weight of perfluorodimethylcyclobutane, 0.15 parts of weight of bis (trifluoromethylthio) mercury [$(CF_3S)_2Hg$], and 2 parts of TFE.
- The reactor vessel was then pressurised with HFP to fill with liquid at room temperature, confined and heated at 200 °C for 4 h. A pressure of 3000 atm (303.9 MPa) was attained during the heating period
- The reactor vessel was cooled and unreacted monomer and solvent were flashed off and 5 parts of TFE/HFP polymer was obtained.

The polymer was moulded to a 0.0508 mm thick film by heating at 250 °C and cooled to room temperature. The resulting film was limp, transparent and completely amorphous when determined by X-ray. The film also showed a specific IR ratio of about 17. The polymer was soluble in perfluorodimethylcyclobutane and showed an inherent viscosity of 0.2 dL/g as measured at 25 °C. In a similar experiment, where 25 parts of TFE was charged instead of 2 parts produced a copolymer with specific IR ratio of 10.5 and 15 % crystallinity as determined by comparing areas under the crystalline and amorphous peaks from X-ray analysis. In a comparable run where 6 parts of TFE and 0.1 parts of cobalt trifluoride was charged. This produced 15 parts of copolymer with specific IR ratio of 22 and produced a film that was stiff, transparent and entirely amorphous. It was soluble in perfluorodimethylcyclobutane and exhibited inherent viscosity of 0.4 dL/g at 25 °C and 0.5 % concentration (g/100 ml solution) in that solvent calculated according to Equation 2-1

$$\eta_{inherent} = \frac{ln\left(\eta/\eta_0\right)}{0.5} \qquad 2.1$$

where η is the viscosity of the solution and η_0 is the viscosity of the solvent.

In a contrast run, 0.068 parts of bis (trichloroacetyl) peroxide, 32.2 parts HFP and 3.6 parts TFE were charged at cryogenic temperatures to an 80 water parts by weight capacity reactor vessel and warmed to -16 °C and maintained at this temperature under autogenous pressure until the reaction was stopped. The obtained solid polymer was pressed into a film at 350 °C and allowed to cool in air at room temperature. The resulting film was brittle and had a crystallinity of about 50 % determined by X-ray analysis. The conclusion was that to achieve amorphous TFE/HFP copolymers, high pressures of least 2000-10000 atm and temperatures in the range of 100 to 300 °C are required.

Feiring et al (1993) investigated polymerisation conducted in the presence of an initiator and solvent containing only C, F and H and optionally ether oxygen or alcohol which didn't cause appreciable transfer that can interfere with the polymerisation. A 400 ml pressure tube was loaded with 200 mL of water was chilled to -20 °C and 5 mL of 0.05 M HFPO dimer peroxide initiator in 1, 1, 2, 2-tetrafluorocyclobutane solvent added. The tube was sealed, evacuated and filled with 204 g of HFP and 50 g of TFE. The tube was heated for at 33 to35 °C for 4 hours, filtered, washed with methanol/Freon® 113, dried under vacuum and 73 g of white powder was recovered. The IR analysis found 75 wt. % HFP and no detectable end groups. Melt extrusion at 372 °C with a 15 kg weight gave a translucent bubble free ribbon at 0.05 g/min. A duplicate run at 33 to 36 °C gave 34 g of white powder. Table 2-12 shows the results with the presence of other hydrofluorocarbon solvents under similar conditions. The only exception is that the amount of initiator was varied from 5 to 10 mL of a 0.05 to a 033 M solution.

Table 2-12 Summary of the results of TFE and HFP copolymerisation using different hydrocarbon solvents (Feiring et al., 1993).

Solvent	Yield, g	% HFP	Melt index at 372 °C
CF_3CH_2OH	17	4.6	0 (15 kg)
CF_3CH_2OH	17	5.6	0 (15 kg)
1, 1, 2, 2-tetrafluorocyclobutane	37	7.5	0.05 (15kg)
1, 1, 2, 2-tetrafluorocyclobutane	34	8.4	0.05 (15 kg)
Bis(trifluoromethyl)dioxolane	33	8.3	0.5 (15 kg)
Bis(trifluoromethyl)dioxolane	35	7.9	0.6 (15 kg)
$CF_3CFHCFHCF_2CF_3$	40	9.8	1.0 (15 kg)
$CF_3CFHCFHCF_2CF_3$	43	8.6	1.3 (15 kg)
$CF_3CFHCF_2OCH_3$	30	8.4	1.3 (5 kg)
$CF_3CFHCF_2OCH_3$	30	8.1	0.4 (5 kg)
$C_nF_{2n+1}H$, n = 6 – 8 (trace I_2)[1]	42	8.6	1.8 (5 kg)
$C_nF_{2n+1}H$, n = 6 – 8 (trace I_2)	39	8.8	1.3 (5 kg)
$HCF_2CF_2CF_2CF_2H$	35	9.5	0.4 (15 kg)
$HCF_2CF_2CF_2CF_2H$	42	9.2	0.4 (15 kg)

[1]Chain transfer agent

Feiring et al. (2000) described the use of perfluoroalkylsulfonlyl chloride, i.e. perfluorobutanesulfonyl chloride, as an initiator and showed that it reduces the ionic end groups that result from the use of APS or ionic initiators resulting in fluorocarbon-ended polymers. Comparative results and reaction conditions between perlfuoroalkylsulfonyl chloride and ammonium persulfate are show in Table 2-13.

Table 2-13 Summary of perfluorobutanesulfonyl chloride and APS results (Feiring et al., 2000).

	Perfluorobutanesulfonyl chloride	**APS**
Reactor volume, ml	1000	1000
Water volume, ml	600	600
Surfactant	Ammonium perfluorononanoate	Ammonium perfluorononanoate
Surfactant mass, g	1.45	1.45
Initiator mass, g, in 25 ml water	0.65	0.46
Reaction temp, °C	100	100
Reaction pressure, bar	44	44
Mass TFE, g	50	50
Mass HFP, g	120	120
Polymer mass, g	47.4	48.8
Melting temperature, °C	283.1	275.6
Carboxylic acid ends per 10^6 C	106	2922

3.1 CHEMICALS/MATERIALS USED

Ammonium persulfate was purchased at Sigma-Aldrich (Reagent grade, 98 %) and used without purification. Tetrafluoroethylene (TFE) was produced in-house by pyrolysis of polytetrafluoroethylene (PTFE) using a plasma reactor in the Department of Applied Chemistry at the South African Nuclear Energy Corporation (Necsa). The TFE was then triple distilled to the purity of 99.96 ± 0.03 % using a 1.5 m long Podbielniak-type low temperature distillation column and was collected and stored in a 50 L cylinder at a pressure of ≤ 2 bar. HFP was obtained from Necsa with a purity of 99.9 % and was distilled once to an improved purity of 99.97 ± 0.02 % using the same distillation column used for TFE distillation and stored in a 2 L vessel. Ultra-pure water (18.0 Ω) from a Millipore Milli-Q machine was obtained from Pelindaba Analytical Labs (PAL) at Necsa.

3.2 POLYMERISATION

3.2.1 Apparatus

The experimental apparatus used for the polymerisation, illustrated in Figure 3-1, consists of the following:

- The reactor is a 300 mL stainless steel Parr 4561 316 high-pressure autoclave fitted with ~207 bar bursting disk, a thermocouple, a baffle and gas entrapment stirrer and also monomer and initiator inlet fittings.
- A Parr 4848 Reactor controller unit connected to the reactor was used to set and control temperature, stirring speed, and monitor the pressure of the reaction.
- A Bronkhorst Coriolis mass flow meter with a data logger was used to monitor the monomer consumed.
- A series 1 liquid dosing pump used to dose ultra-pure water and initiator solution.
- A Vacutec vacuum pump was used to evacuate the polymerisation system.

- The system also contains a water container, U-tube and thermostat-controlled vessel for degassing the monomers. The vessel was also used for building and maintaining pressure for the reaction.

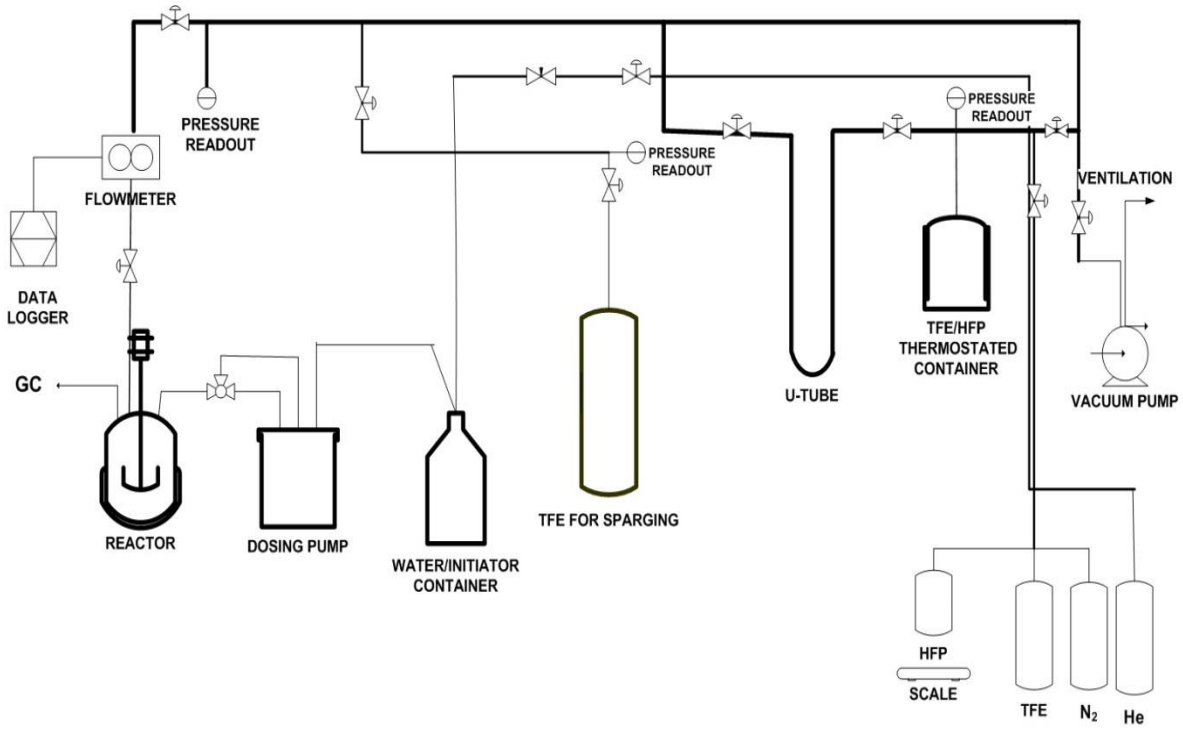

Figure 3-1 A schematic of the semi-continuous polymerisation apparatus.

3.2.2 Polymerisation Procedure

From the literature it is evident that the polymerisations are done at reaction pressure above the critical pressure of TFE monomer. The HFP usually constitute a large amount (above 50 %) due to low reactivity compared to TFE. For safety reason reaction pressure less than 20 bar were chosen compare to pressures up to 40 bar in the literature. This done to ensure temperature of the used to heat the transfer vessel to build reaction pressure does not exceed the critical temperature (33.3 °C) of TFE monomer when the HFP content in the mixture is increased. The following conditions were chosen according to literature and modification of TFE experiments performed in the lab.

In a typical reaction the reactor was pressurised with nitrogen at 20-25 bar to check for leakage of the system and to remove oxygen. The reactor was left under vacuum until the introduction of the monomer and water. The required amount of TFE and HFP was transferred thermo-stated vessel, 3 freeze-thaw cycles between the thermo-stated transfer vessel and U-tube were preform to reduce O_2 content. The transfer vessel heated to obtain the desired pressure, then the reactor and the system were pressurised with the TFE/HFP mixture. Then 150 mL of He/TFE sparged ultra-pure water was dosed into the reactor at 10 mL/min. After loading of water in the reactor was finished, agitation at 600 rpm and heating were started. When the reaction temperature stabilised, agitation speed was increased to 1500 rpm. Then the initiator solution was dosed into the reactor (10 minutes for between 10 - 20 mol % HFP content, 20 minutes for between 30 - 40 mol % HFP and > 25 minutes for between 40 - 50 mol % HFP content) and reaction started. During the polymerisation, a mixture with an appropriate composition of the gas monomers was continuously fed to the reactor to maintain a constant pressure. Then the reaction was terminated by stopping the TFE/HFP supply, the unreacted monomer mixture was vented off, then reactor cooled down to room temperature and the opened. The reaction parameters for all the experiments are summarised in Table 3-1.

Table 3-1 Reaction parameters used to copolymerise TFE and HFP.

Experiment name	TFE/HFP ratio in feed	Temp (°C)	[APS] (M)	APS dosing rate (mL/min)	Reaction pressure (bar)	Water (mL)	Agitation speed (rpm)
ETK0417	78/22	85	0.006	1.0	20.1	150	1500
ETK0418	74/26	85	0.006	1.0	18.4	150	1500
ETK0509	80/20	85	0.006	1.0	17.9	150	1500
ETK0511	54/46	85	0.006	1.0	13.2	150	1500
ETK0515	61/39	85	0.006	1.0	14.5	150	1500
ETK0801	56/44	85	0.006	1.0	11.5	150	1500
ETK0823	81/19	85	0.006	1.0	19.0	150	1500
ETK0831	90/10	85	0.006	1.0	19.0	150	1500
ETK0905	62/38	85	0.006	1.0	15.0	150	1500
ETK1017	60/40	100	0.006	1.0	15.3	150	1500
ETK1023	61/39	100	0.006	2.5	15.5	150	1500
ETK1024	61/39	100	0.006	0.5	14.6	150	1500

3.2.3 Product work-up

The copolymers were separated from water by sieving and washed with ultra-purity water to remove impurities, i.e. initiator traces present and dried in the oven overnight (more than 12 hours). For copolymers synthesised using ~50 and ~60 mol % HFP, where the yields were low, the resulting product was transferred into a petri dish and the water evaporated. The resulting powder was scraped and washed with ultra-pure water and dried in the oven as above.

3.3 MATERIALS CHARACTERISATION

The following analysis: ^{19}F NMR, FTIR, TGA-FTIR, DSC, SEM and XRD were used for the characterisation of the as-polymerised FEP polymers. The background theory on each analysis is shown in the Appendices.

3.3.1 ^{19}F NMR analysis

Solid-state ^{19}F NMR spectra for the powdered sample were recorded on a Varian VNMR 600 Solid spectrometer with a magnetic field strength of 14.1 Tesla. A T3 quadruple resonance MAS probe HFXY with Vespel stator and Zirconia pencil MAS motor was used. The experiments were conducted using one pulse method with 16 scans. The experiments conducted at 20 kHz spinning rate, a 3.2 mm o.d. probe was used. For those conducted at 55 kHz spinning rate, a 1.2 mm o.d. probe was used. The probes were kept at 10 °C.

3.3.2 FTIR analysis

The infrared spectra for the study were measured with a Perkin Elmer Spectrum 100 FTIR spectrometer in the ATR mode to obtain IR spectra. Typically 32 scans were taken in the range of 600 to 4000 cm^{-1} at a resolution of 4 cm^{-1} and averaged to get one spectrum. The powdered samples were brought in contact with one side of the internal reflection element using an adjustable spring pressure arm to ensure approximately the same pressures for all the samples.

3.3.3 TGA-FTIR analysis

A PerkinElmer thermogravimetric analyser (TGA 4000) was employed in determining the thermal stability of the commercial and as-polymerised FEP samples. Analyses were performed in an atmosphere of nitrogen at 20 mL/min. TGA scans were performed over a temperature range of 30 to 650 °C at a heating rate of 10 °C/min for polymerised FEP copolymers and 30 to 950 °C at 10 °C/min for commercial FEP. The evolved gaseous products were transferred via a heated line to a PerkinElmer Spectrum 100 FTIR equipped with a transmission gas cell. The transfer line and IR gas cell were kept at 225 °C and transfer of sample from TGA to the cell occurred at a rate of 40 mL/min. The FTIR spectra (4.0 cm^{-1}

resolution, range 4000 to 450 cm^{-1}) were recorded every 0.6 s and automatically stored for later analysis.

3.3.4 DSC analysis

The DSC measurements for the as polymerised FEP samples were recorded on a PerkinElmer DSC 4000. The DSC thermograms were obtained by using a heating rate and cooling rate of 20 °C/min within the temperature range of 100 to 350 °C under nitrogen purge. The DSC was calibrated with two metals standards, i.e. Indium and zinc, of known melting temperature and enthalpy. The enthalpy of fusion, enthalpy of crystallisation, first melting (T_{m1}), second melting (T_{m2}), crystallisation (T_c), and onset temperature of the FEP copolymers were obtained by integrating the area for the first, second heating and cooling peak from DSC chromatograms using Pyris software. In all cases, polymer samples weighed 7 to 10 mg, using a closed aluminium pan. The weight crystallinity fraction (also called degree of crystallinity) was evaluated applying the relationship

$$X_c = \Delta H_f / \Delta H_f^o \qquad 3.1$$

where ΔH_f and ΔH_f^o are heat of fusion of the measured samples and theoretical 100% crystalline sample, respectively (Frick et al, 2011). For this, a value of 82.05 Jg^{-1} for ΔH_f^o of 100 % PTFE as reported in literature was used (Marega, 2004; Frick et al, 2011).

3.3.5 SEM analysis

The morphology of the samples was determined by ultra-high resolution field emission SEM (Zeiss Ultra Plus 55) with resolution 0.6 nm and specimen size 5 mm diameter x 0.6 mm high. The samples were placed on a specimen stub lined with a double-sided adhesive tape. The surface was coated with a very thin layer of graphite by sputtering techniques. Then the samples were placed inside the SEM vacuum column and evacuated. The samples where then analysed with SEM in ultra-high vacuum mode at an accelerating voltage of 2 kV, low enough to prevent radiation damage and images were taken.

3.3.6 XRD analysis

X-ray diffraction analyses were performed using PANalytical X'Pert PRO powder X-ray diffractometer with Fe-filtered Co K_α tube as a radiation source. The data were collected for diffraction angle 2θ ranging from 5 to 60° at an interval of 0.02°.

4.1 RESULTS

4.1.1 Experimental conditions and yields

The reaction scheme for the aqueous suspension polymerisation of TFE and HFP using ammonium persulfate as a free radical initiator is shown in Figure 4-1. Table 4-1 details the summary of the reaction and results for the polymerisation of TFE and HFP. The reaction was performed by freezing the desired amount of HFP and TFE monomer in a TFE/HFP thermostat-controlled transfer vessel, followed by heating to the desired temperature. The heating temperature was maintained in order to have a constant feed ratio for the duration of the experiment. The HFP and TFE monomers are not soluble in water so agitation was maintained during the experiment.

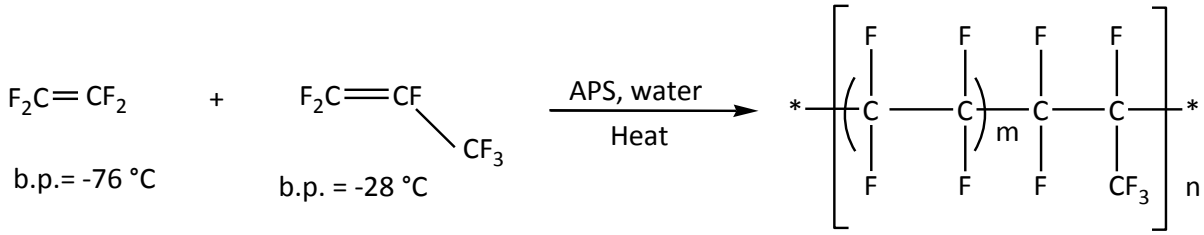

Figure 4-1 Polymerisation scheme of TFE and HFP copolymers using ammonium persulfate initiator.

The pressure for the reactions depended on the concentration of HFP in the monomer feed, as shown in Table 4-1. The reduction in pressure can be attributed to the HFP monomer having a low vapour pressure compared to TFE, *i.e.*, increasing the HFP amount affects the total pressure of the transfer vessel. A Bronkhorst Coriolis mass flow meter was used to monitor the monomer feed flow during the reaction. The flow meter was calibrated for TFE monomer; hence the flow rates recorded were not accurate. The flow meter was used as an indication of reaction occurrence.

The polymer obtained from a monomer feed containing less than 30 mol % HFP was obtained as a white free flowing powder (Figure 4-2) compared to the agglomerated PTFE homopolymer. The polymer yield was separated by sieving and washed with 50 mL ultra-pure water three times and dried at 80 °C for more than 12 hours. In the case of higher than 40 mol % HFP, the resulting polymer contained a small amount of suspended powder, as shown in Figure 4-2 and was transferred from the reactor to a petri dish to evaporate the water. The resulting off-white powder was then washed with ultra-pure water and dried at 80 °C for 12 hours.

Figure 4-2 TFE/HFP copolymer product obtained prepared using (A) 20 mol % HFP and (B) 40 mol % HFP in the feed.

From Figure 4-3, showing monomer flow rate against time, it can be observed that the flow rate decreases with increasing HFP concentration in the gaseous monomer feed ratio. The pressure reduction due to increasing HFP concentration can be a contributing factor. The apparent weight rate of suspension copolymerisation (R_{app}) of TFE and HFP in water was determined gravimetrically from the polymer yield according to Equation 4.1, where Δt_p = time of polymerisation, P_m = monomer conversion = polymer yield and L = volume of

reaction water (Beginn et al, 2006). The measured values are listed in Table 4.1 and shown in Figure 4-4.

$$R_{app} = {}^{P_m}\!/_{(\Delta t_p . L)} \qquad 4\text{-}1$$

From Figure 4-4, it was observed that the apparent production rate reduces with increased HFP concentration in the monomer feed.

Table 4-1 TFE/HFP reaction parameters and results.

Experiment	mol % HFP in feed	P (bar)	Temp (°C)	APS dosing rate (mL/min)	Time (min)	Yield (g)	R_{app} (g/(minL)) x 10^{-4}	mol % HFP in copolymer
ETK0511	46	13.2	85	1.0	80	1.97	0.164	3.80
ETK0801	44	11.5	85	1.0	70	2.09	0.199	2.33
ETK0515	39	14.5	85	1.0	50	3.38	0.450	1.65
ETK0905	38	15.0	85	1.0	77	5.72	0.495	2.12
ETK0418	26	18.4	85	1.0	40	9.52	1.587	1.06
ETK0417	22	20.1	85	1.0	40	11.60	1.933	1.19
ETK0509	20	17.9	85	1.0	50	15.92	2.123	1.00
ETK0823	19	19.0	85	1.0	50	16.58	2.211	0.51
ETK0831	10	18.6	85	1.0	50	15.26	2.035	0.96
ETK1017	40	15.3	100	1.0	62	4.27	0.459	2.55
ETK1023	39	15.5	100	2.5	50	3.71	0.494	3.30
ETK1024	39	14.6	100	0.5	70	7.25	0.690	3.24

The initiator (APS) concentration = 0.006 mol/L, agitation speed = 1500 rpm, water volume = 150 mL.

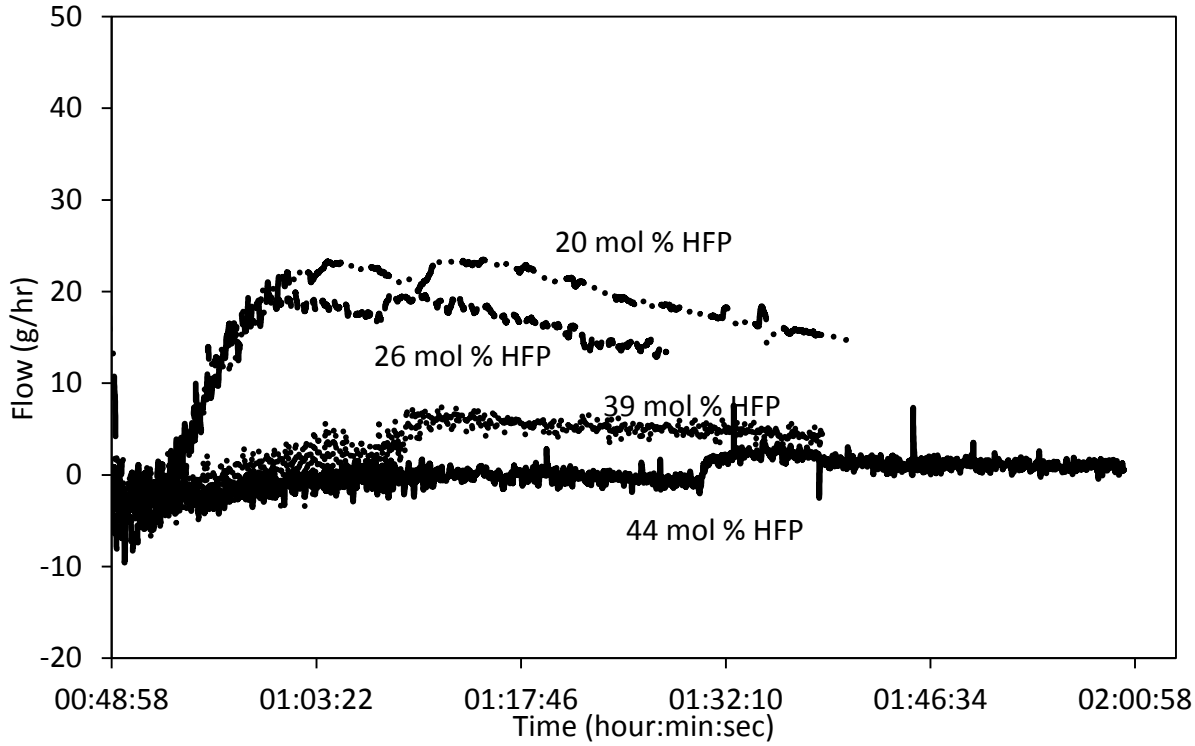

Figure 4-3 Polymerisation monitoring curves showing flow rate of monomer against time during polymerisation.

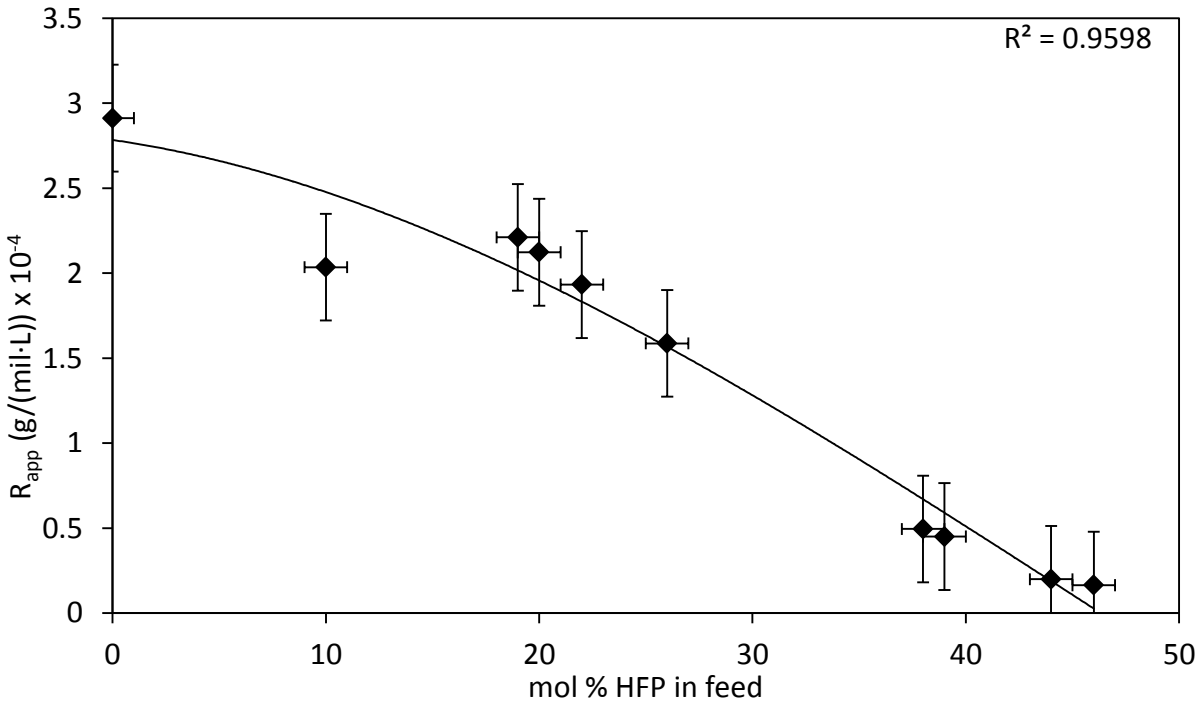

Figure 4-4 The apparent production rate of TFE/HFP copolymerisation R_{app}.

4.1.2 Solid state ^{19}F NMR Analysis

Perfluorinated polymers such as FEP are insoluble in conventional organic solvents, so a high-resolution solid state ^{19}F NMR with MAS (magic angle spinning) spectroscopy applying spinning speed of 20 kHz and 55 kHz was used to determine the chemical structure of the polymerised FEP copolymers. Four samples were analysed with TFE/HFP monomer feed ratios: 90/10 (ETK0831), 80/20 (ETK0509), 74/26 (ETK0418) and 54/46 (ETK0511). Table 4-2 shows relevant chemical shift assignment of the ^{19}F NMR spectrum of FEP from the literature (Scheler, 1998; Forsythe et al, 2001; Lappan et al, 2002). Figure 4-5 shows the major sequence of repeating units and characteristic peak assignments of the fluorine nuclei for the FEP copolymer. All the chemical shift assignments were taken relative to $CFCl_3$. The spectrum shown in Figure 4-6, shows that all the spectra have a presence of a sharp intense isotropic peak at -121 ppm due to the $-CF_2-CF_2-$ structure, weak intensity isotropic peaks at -67 ppm and -70 ppm due to the pendant $-CF_3$ of $-CF_2CF(CF_3)-$ unit and a weak isotropic peak at -184 ppm belonging to -CF of $-CF_2CF(CF_3)-$ unit. Another peak at -110 ppm is due to the $-CF_2$ adjacent to $-CF_2CF(CF_3)-$ group (Feiring et al, 2000; Forsythe et al, 2001). The isotropic peaks were associated with sides spinning bands at -27, -50, -86, -153 ppm, -192 ppm and -228 ppm; these peaks are highlighted in Figure 4-6.

Table 4-2 Chemical shift assignment of FEP copolymer from literature (Scheler, 1998; Forsythe et al, 2001; Lappan et al, 2002).

Chemical shift (ppm)	Assignment
-68 to -75	$-CF_3$
-110 to -112	$-CF_2CF(CF_3)$
-115 to -130	$-CF_2CF_2-$
-183 to -187	$-CF_2CF(CF_3)$

The spinning side bands indicate that the ^{19}F-^{19}F homonuclear dipolar interactions cannot be completely averaged at the spinning rate of 20 kHz. From Figure 4-6, the peak at -184 ppm

for 26 mol % HFP in the feed overlapped with the spinning side band. The monomer composition was not calculated due to the interference of spinning side bands. Figure 4-7, represents spectra for ETK0831, ETK0418, ETK0509 and ETK0511, analysed using a spinning rate of 55 kHz and shows that at spinning rates of 55 kHz the spinning sidebands present at 20 kHz are completely averaged out (Hill et al., 2003). The spectrum shows peaks at -67.4418 ppm, -70.4698 ppm for -CF_3 from the HFP unit, -112.105 ppm due to -CF_2 of the HFP unit, -121.784 ppm for -CF_2 of the TFE group and -183.425 ppm for -CF belonging to HFP group. The HFP monomer composition for ETK0831, ETK0418, ETK0509 and ETK0511 copolymer at spinning rate of 55 kHz was calculated by the ratio of the integrated area of CF_3 and CF_2 using Equation 4-2 (Ahmed et al, 2006)).

$$\text{mol \% HFP} = \frac{{}^{I_{CF_3}}/_{3}}{{}^{I_{CF_2}}/_{2}} \qquad 4\text{-}2$$

where I_{CF_3} and I_{CF_2} is the area of the integral of the signals corresponding to the fluorine of the CF_3 group in HFP and CF_2 group of TFE and HFP in the copolymer, respectively.

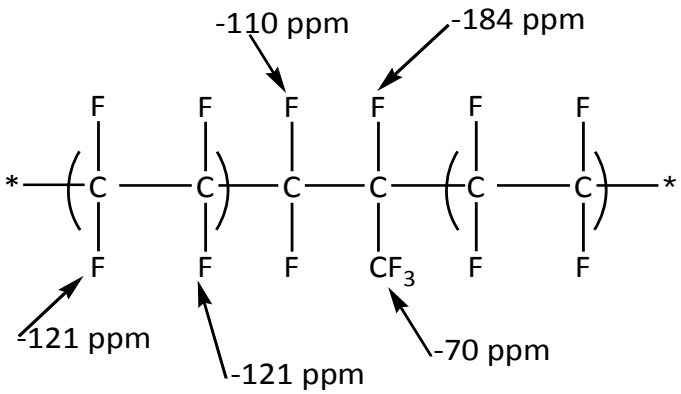

Figure 4-5 The major sequence of the repeating units and peak assignment.

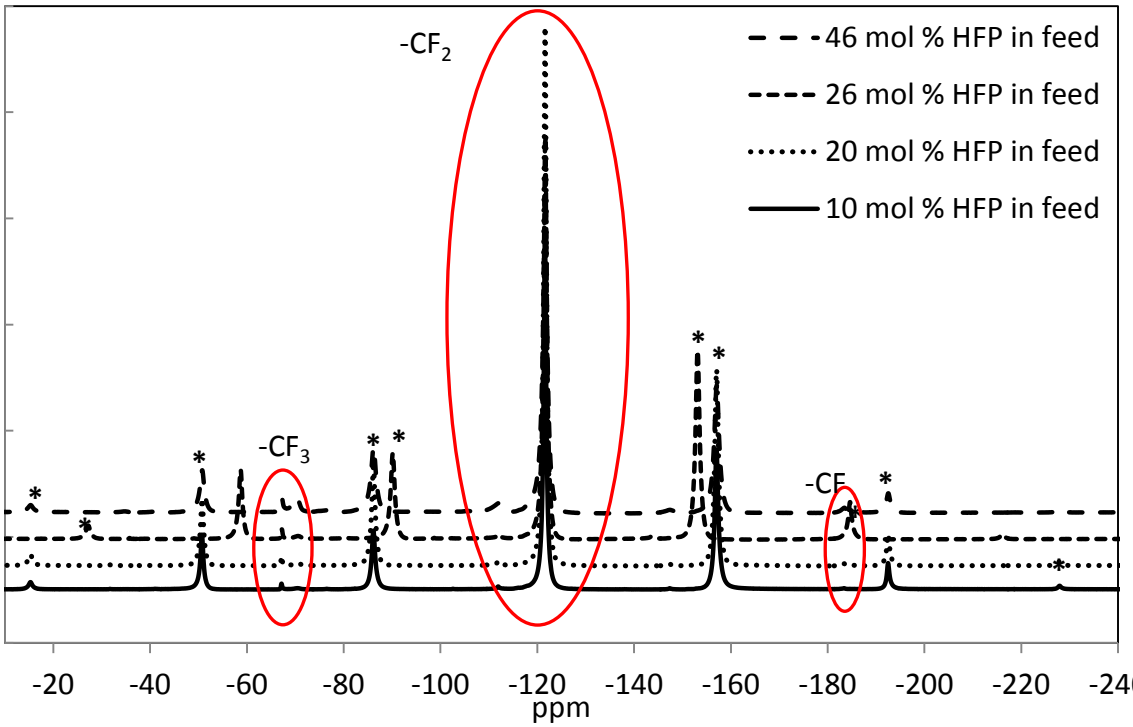

Figure 4-6 ^{19}F NMR spectra for 10 mol % HFP (ETK0831), 20 mol % HFP (ETK0509), 26 mol % HFP (ETK0418) and 46 mol % HFP (ETK0511) in the feed at 20 kHz spinning rates.* Denotes side spinning bands.

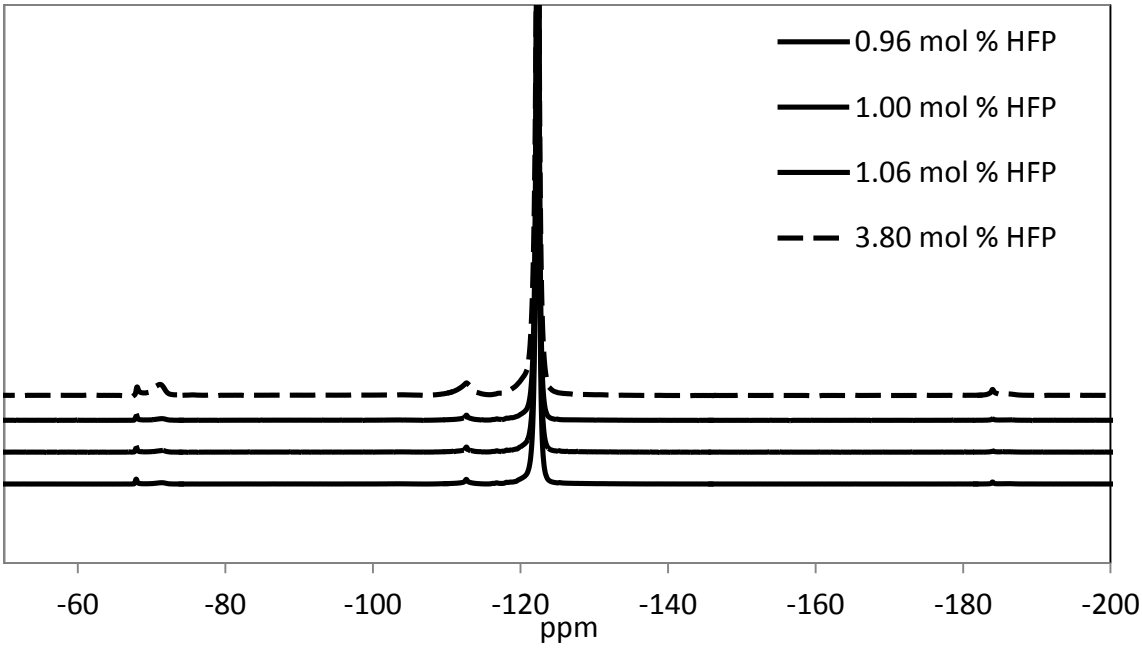

Figure 4-7 ^{19}F NMR spectra for 0.96 mol % HFP (ETK0831), 1.00 mol % HFP (ETK0509), 1.06 mol % HFP (ETK0418), 3.80 mol % HFP (ETK0511) in the copolymer at 55 kHz spinning rates.

4.1.3 FTIR analysis

ATR-FTIR spectra were recorded for all as-polymerised FEP, PTFE and commercial FEP. The FTIR spectra of commercial PTFE (DuPont PTFE 807N X) and commercial FEP (Dyneon FEP, in pellet form) are shown in Figure 4-8, to highlight differences between peaks for PTFE, and commercial FEP. Those of the 10 to 46 mol % HFP in the feed are shown in Figure 4-9. The assignment of the peaks was performed using the help of data from the literature (Ignatieva et al., 2002).

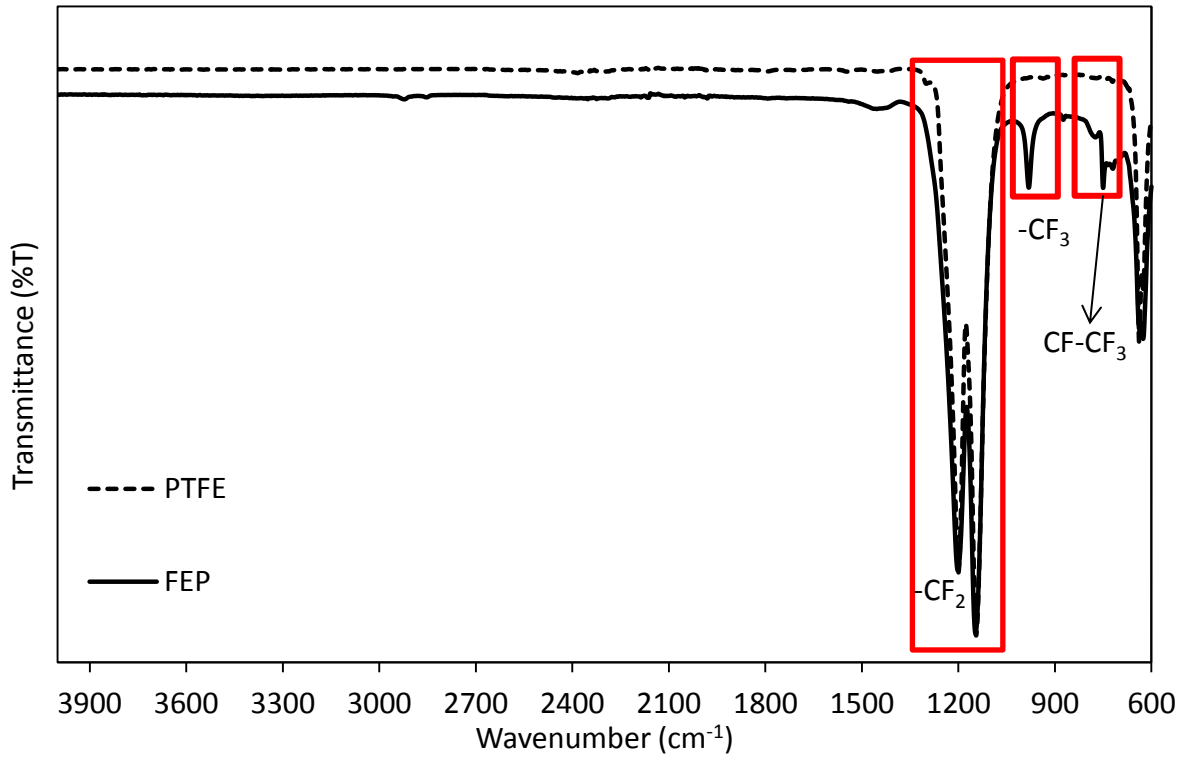

Figure 4-8 ATR-FTIR spectra of commmercial PTFE (A) and FEP (B).

The FTIR spectra of commercial PTFE shown in Figure 4-8 shows the most characteristic bands at 1144.48 and 1200.20 cm^{-1} and are attributed to the stretching vibration of the $-CF_2$ of the $-CF_2-CF_2-$ structure (Ignatieva et al, 2002). The FTIR spectra of commercial FEP were characterised by the presence of a new weak peak at 981.61 cm^{-1} that is assigned to the $-CF_3$

stretching vibration of the hexafluoropropylene unit and peak at 750.26 cm^{-1} characteristic of the CF-CF_3 group (Kostromina et al, 1986). The -CF_2-CF_2- bands at 1201.40 and 1146.45 cm^{-1} are still present. The combination band for –CF_2 stretching vibration at 2365 cm^{-1} from the PTFE and FEP spectra observed by other authors (Lunkwitz et al, 2004) was not detected.

In the case of as-polymerised FEP copolymers spectra (Figure 4-9), a shift to higher wavenumbers (2 to 4 cm^{-1} increase) is observed. Identifying bands characteristic of the -CF_2 stretching vibration and presence of the band for -CF_3 is also observed. These band and wavenumbers are depicted in Table 4-3. From the spectra it can be observed that the CF_3 and CF-CF_3 band intensities increases from 10 mol % HFP (ETK0831) in the feed ratio to 46 mol % HFP (ETK0511) showing evidence that HFP monomer was incorporated in the PTFE structure. From the ATR-FTIR spectroscopy of the as-polymerised copolymers it can be concluded that FEP copolymers with different HFP composition were successfully prepared using different TFE/HFP gaseous monomer feed ratios.

Table 4-3 Bands and wavenumbers for as-polymerised FEP copolymers, commercial FEP and commercial PTFE.

Sample Name	**mol % HFP in feed**	**-CF_2 (cm^{-1})**	**-CF_2 (cm^{-1})**	**-CF_3 (cm^{-1})**
PTFE 807N X		1200.00	1144.48	
Dyneon FEP		1201.40	1146.45	981.44
ETK0831	10	1203.90	1148.17	982.53
ETK0823	19	1204.26	1148.49	982.75
ETK0905	39	1202.05	1146.92	981.77
ETK0801	44	1202.2	1147.18	981.74
ETK0511	46	1202.72	11148.08	981.61

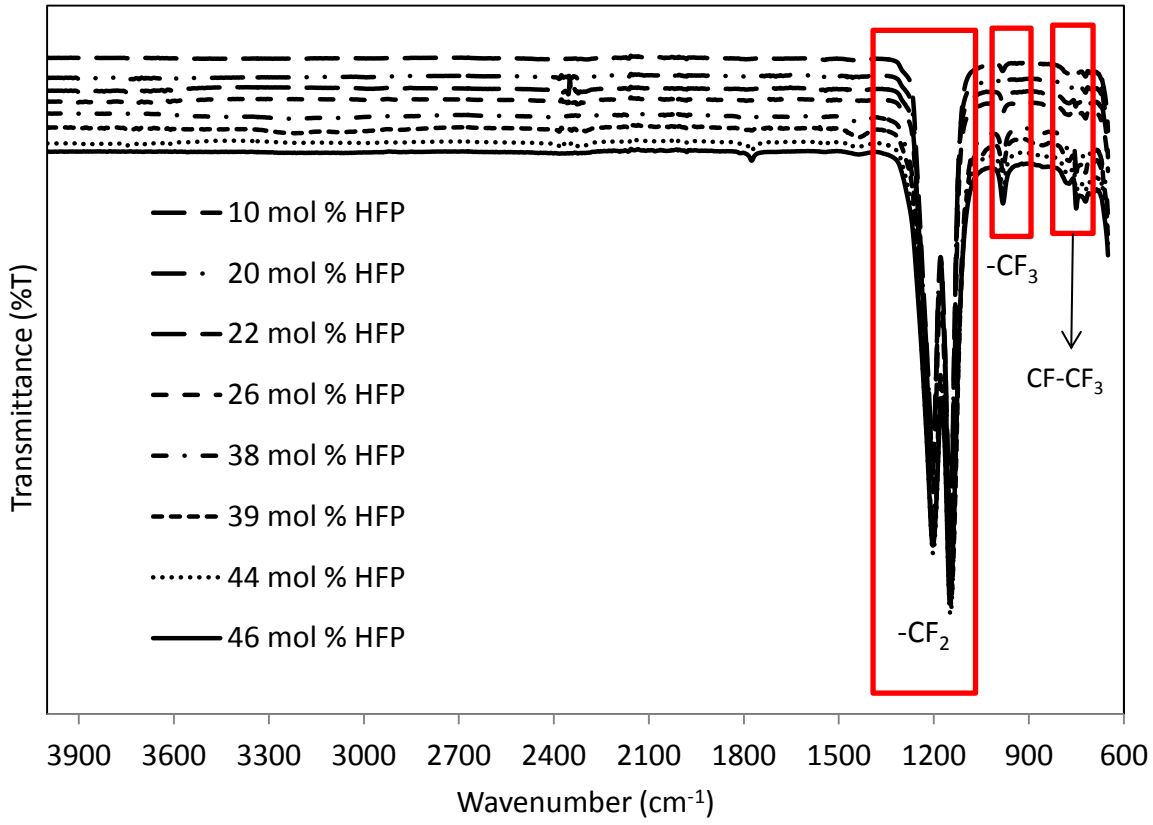

Figure 4-9 FTIR spectra of as-polymerised FEP copolymers using various monomer feed ratio.

Figure 4-10 shows the area of absorbance ratio for intensities of the $-CF_3$ (Abs(981 cm^{-1}) and $-CF_2$ (Abs(1146 cm^{-1}) + Abs(1202 cm^{-1})) vibration band of $-CF_2-CFCF_3-$ and $-CF_2-CF_2-$, respectively. The mathematical expression obtained for the curve is:

$$y = 8 \times 10^{-6}x^2 - 0.0003x + 0.0036$$

where y is the absorbance ratio and x is the mol % HFP in the feed. These ratios can be taken as relative measure of the degree of HFP incorporation in the copolymers. From the Figure 4-10, an increase in the absorbance ratio with an increase of the HFP concentration in the gaseous feed ratio is observed. This observation can be taken as indication of an increase of the incorporation of HFP monomer in the copolymer chain. The FTIR results were used to determine the HFP composition for the remainder of the FEP samples.

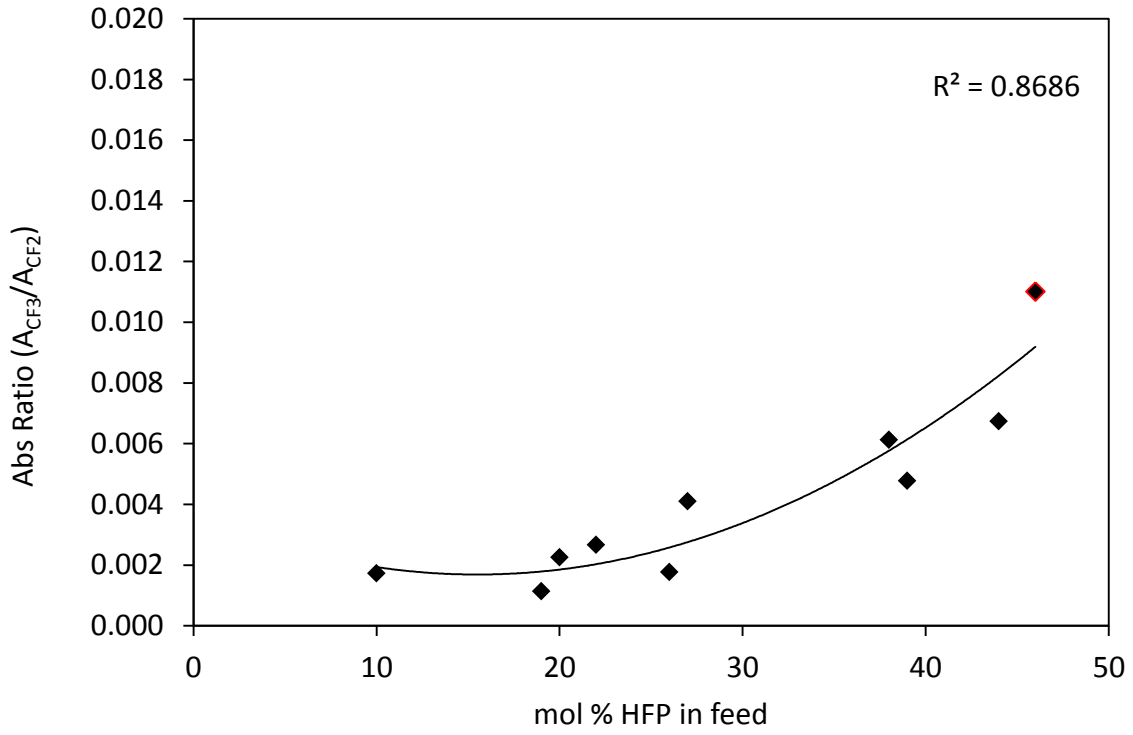

Figure 4-10 Absorbance ratio versus mol % HFP in the monomer feed. The dashed line represents the absorbance ratio of commercial FEP.

The FTIR absorbance ratio data for the different FEP copolymers prepared using various feed ratios were used to determine the HFP composition for the copolymers. The data were calibrated against the results from the ^{19}F NMR data performed with MAS spinning rates of 55 kHz using Equation 4-2.

$$\text{mol \% HFP} = \text{(Absorbance ratio)} / A \times \text{B mol \% HFP} \qquad 4\text{-}2$$

where A and B represent the absorbance ratio and HFP content (from ^{19}F NMR), respectively for ETK0831, ETK0418, ETK0509 and ETK0511 samples. The results for HFP composition are not 100 % accurate but they can be used as an approximation for the HFP composition for all the as-polymerised copolymers, (shown in Table 4-4 and Figure 4-11). The figure represents that an increase in IR absorbance ratio results in linear increase of the HFP content from ^{19}F NMR analysis. The solid line represents the best fit of the experimental data.

Table 4-4 Summary of the calculated mol % HFP in copolymer.

Sample	mol % HFP in the feed	Absorbance ratio	Calculated mol % HFP in copolymer
ETK0831	10	0.0017	0.96
ETK0823	19	0.0011	0.51
ETK0509	20	0.0023	1.00
ETK0417	22	0.0027	1.19
ETK0418	26	0.0018	1.06
ETK0515	39	0.0048	1.65
ETK0905	38	0.0061	2.12
ETK0801	44	0.0067	2.33
ETK0511	46	0.0110	3.80
ETK1024	39	0.0096	3.24
ETK1023	39	0.0094	3.30
ETK1017	40	0.0074	2.55

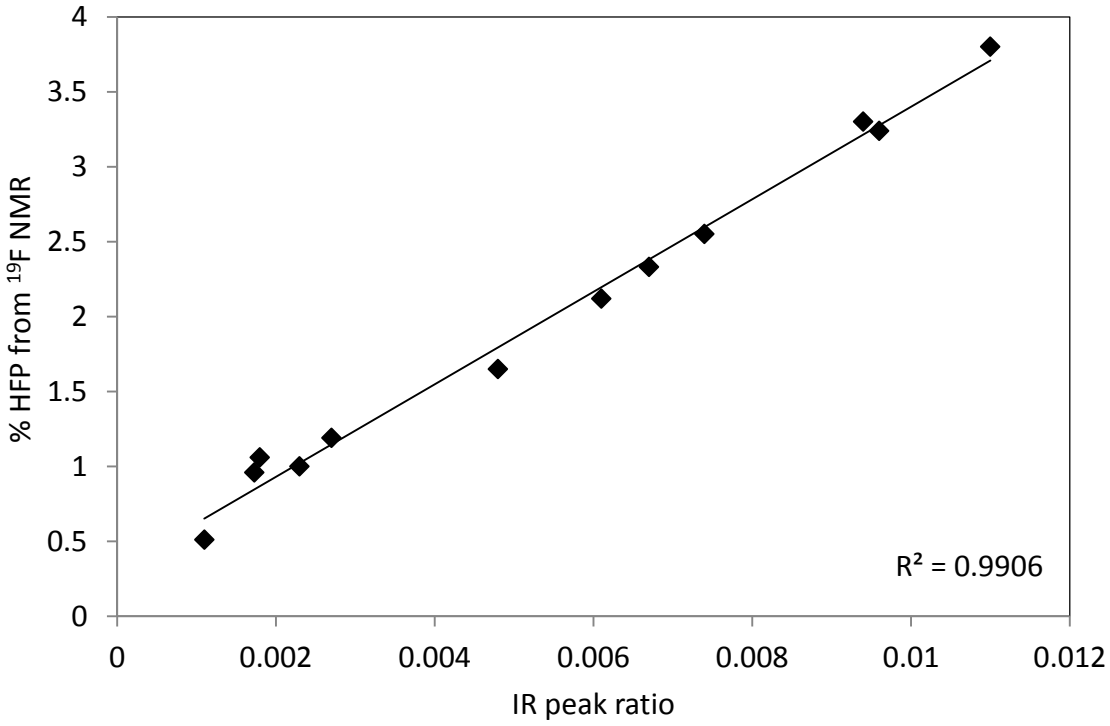

Figure 4-11 Relationship between IR peak ratio and ^{19}F NMR percentage HFP.

4.1.4 TGA-FTIR analysis

Thermogravimetric analysis, coupled with Fourier-transform infrared spectroscopy (TGA-FTIR), is an established technique used for studying thermal degradation of materials. In this study TGA-FTIR was used to examine the thermal stabilities and evolved gases of as-polymerised FEP copolymers and compare them to commercial FEP (Dyneon FEP). Figure 4-12 presents the mass loss on heating for the various FEP copolymers and commercial FEP. It is observed that the thermal stabilities of the copolymers decrease with increasing HFP concentration (indicated by dashed arrow in Figure 4-12). The corresponding values of derivative thermogravimetry (DTG), 10% decomposition (T_{d10}) temperature and onset temperature are shown in Table 4-5.

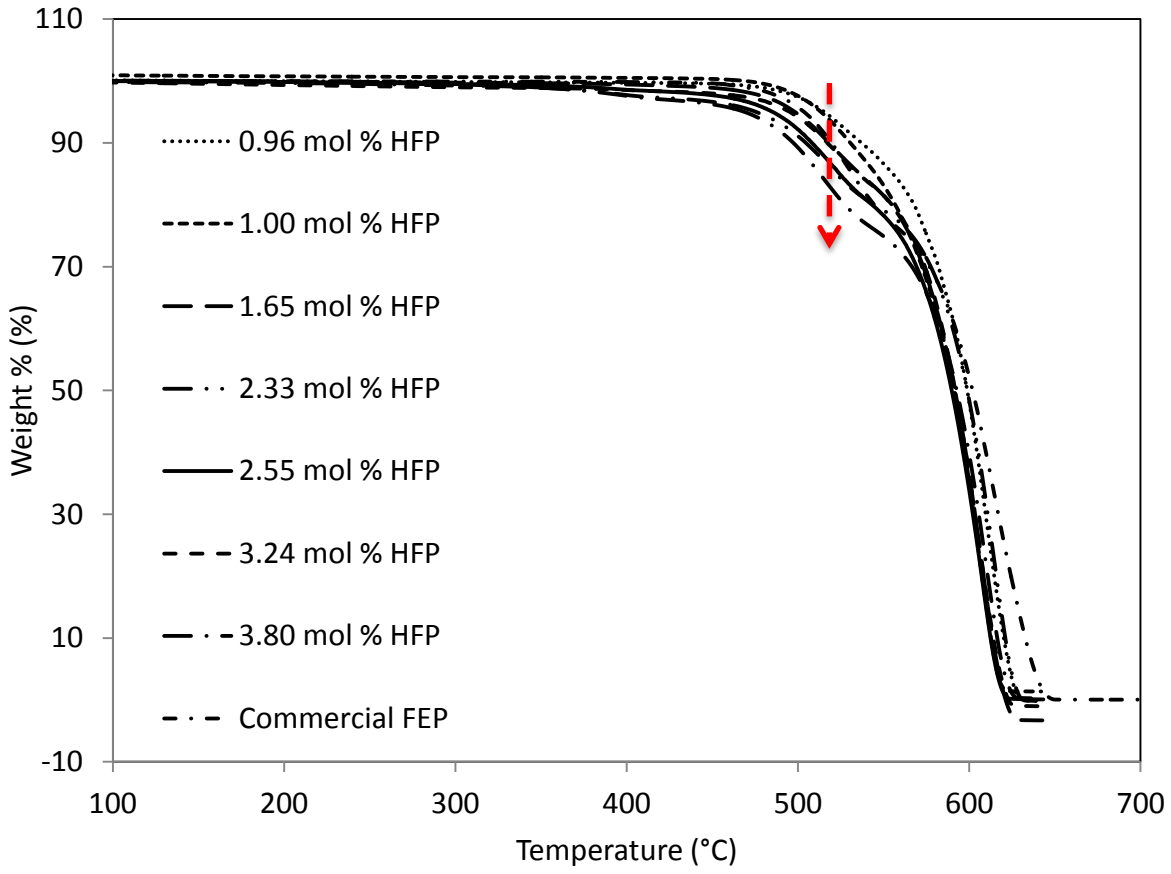

Figure 4-12 TGA thermograms for commercial and as-polymerised FEP under nitrogen atmosphere.

The T_{d10} is generally reduced as the HFP content is increased, as shown in Table 4-5. The first derivative of the decomposition curve for the commercial FEP sample examined in nitrogen atmosphere (Figure 4-13) exhibits a two-step process. This is different from the one-step process observed for commercial PTFE. The two step-processes observed for the thermal decomposition of the commercial FEP in the current study is in agreement with observation made by Gupta et al. (1994). The thermal degradation of FEP was reported to start at 450 °C, the first decomposition was observed at 515 °C followed by a second stage at 590 °C. Gupta and co-workers (1994) used FT-IR and MS techniques to propose a mechanism for the decomposition process. They proposed that the first stage of decomposition was assigned to the decomposition of the chain segments containing HFP units and the second stage at higher temperature was attributed to the degradation of the major monomer component, TFE.

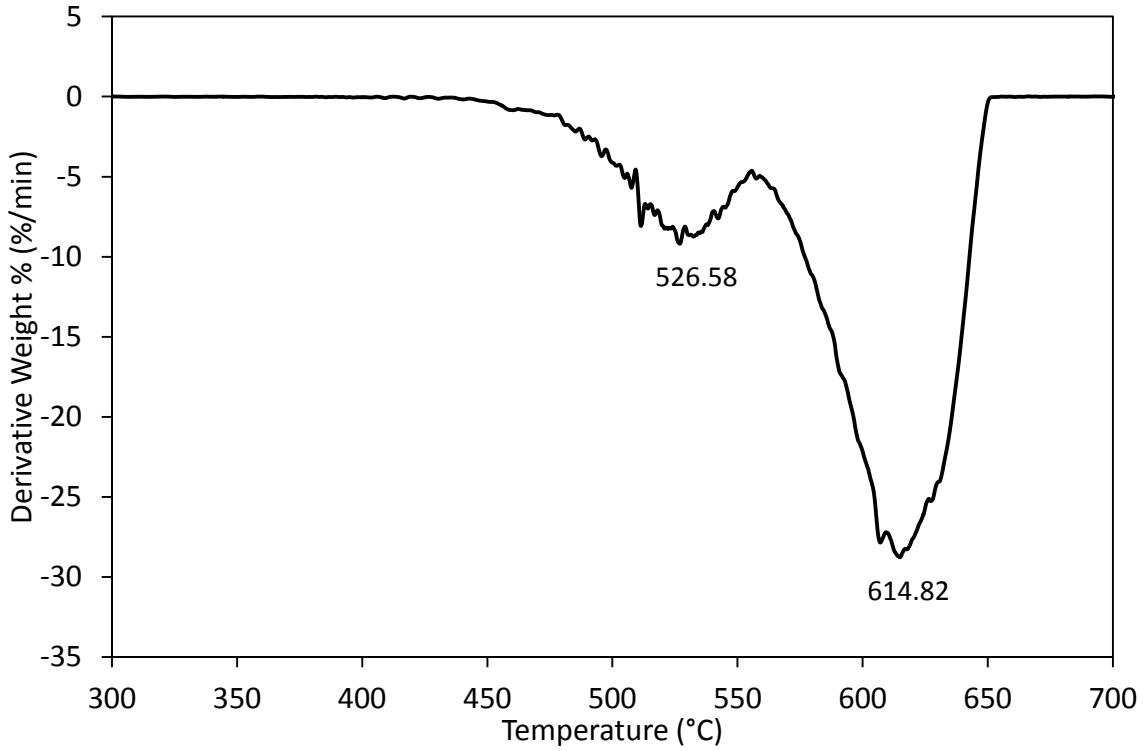

Figure 4-13 DTG plot of the thermogram in TG analysis of polymerised of commercial FEP in nitrogen atmosphere.

Table 4-5 Onset temperature, DTG and 10 % decomposition temperature.

Sample name	mol % HFP	Onset T_1 (°C)	Onset T_2 (°C)	DTG_1 peak (°C)	DTG_2 peak (°C)	% T_{d10} (°C)
Commercial FEP		496.00	583.96	526.58	614.82	519.57
ETK0831	0.96	497.20	584.83	523.49	614.82	537.05
ETK0509	1.00	505.25	585.20	528.21	606.86	530.41
ETK0418	1.06	497.84	583.50	519.72	606.63	528.72
ETK0515	1.65	495.74	583.83	512.04	607.83	518.1
ETK0801	2.33	486.71	589.33	517.09	616.05	504.43
ETK0511	3.80	486.84	585.77	514.46	609.29	497.24
ETK1017	2.55	484.03	581.16	516.70	607.88	508.08
ETK1023	3.30	477.78	582.52	513.20	608.34	486.21
ETK1024	3.24	491.58	580.10	517.10	604.98	517.10

The commercial FEP shows decomposition above 496 °C and can be resolved into two steps (Figure 4-13). The weight loss above 496 °C is due to the degradation of the FEP matrix under the influence of heat treatment. Figure 4-14 A and B presents an FTIR spectrum of gaseous evolution products of commercial FEP at 526 and 614 °C, respectively. The spectrum shows clear features representing organofluorine species. The sharp peak at 1034 cm^{-1} is due to the C-F stretching vibrations. The two peaks at 1180 and 1326 cm^{-1} are attributed to the CF_2 moiety (Gupta et al, 1994). The peak at 1390 cm^{-1} and 1790 cm^{-1} represent C-F stretch of CF_3 in $–CF_3$ group and the C=C stretch of C_2F_6, respectively. The C=C stretch in C_2F_4 is IR inactive. The peak intensities representing the HFP are noticeably very small compared to that of TFE (C_2F_4) at high degradation temperature (shown in Figure 4-14(B). This results from the fact that HFP is a minor component of the FEP copolymer.

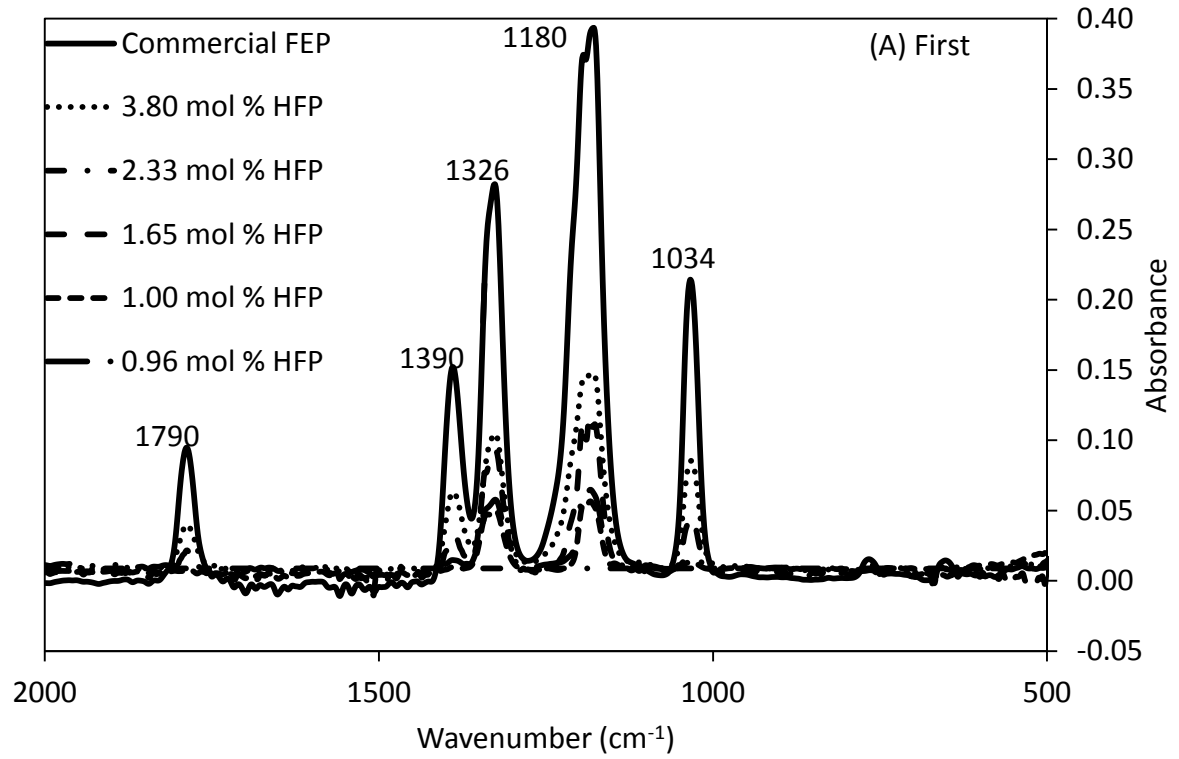

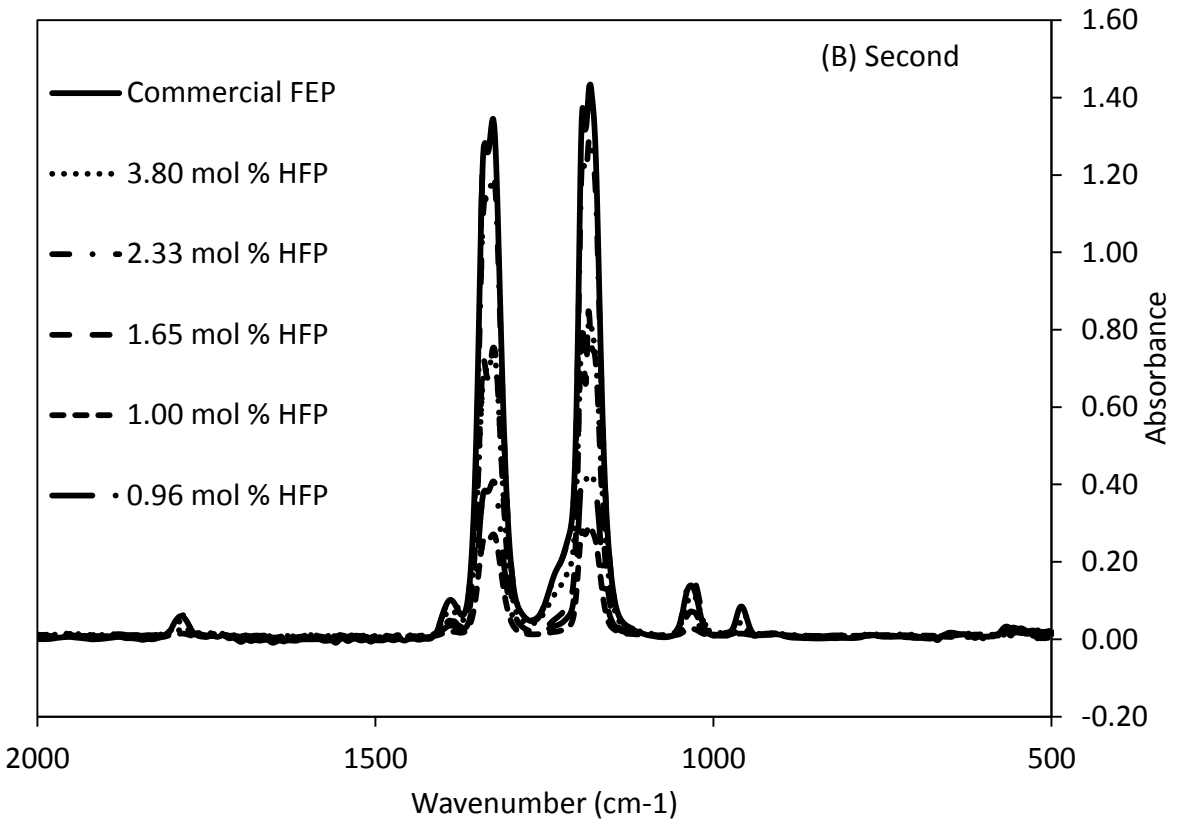

Figure 4-14 FTIR spectra of gaseous product for the first (A) and second (B) decomposition step for as-polymerised FEP copolymers.

Figure 4-15 presents the DTG of the as-polymerised FEP copolymers for 0.96, 1.00, 1.65, 2.33, 2.55, 3.24, 3.30 and 3.80 mol % HFP. The Figure 4-15 shows that the as-polymerised FEP copolymers also undergo two-step decomposition. The 3.30 mol % HFP, 2.33 and 3.80 mol % HFP copolymers showed a small decomposition step with onset temperatures of 339.64, 375.10 and 380.10 °C, respectively. The evolved gas products from this step were not detected by FTIR.

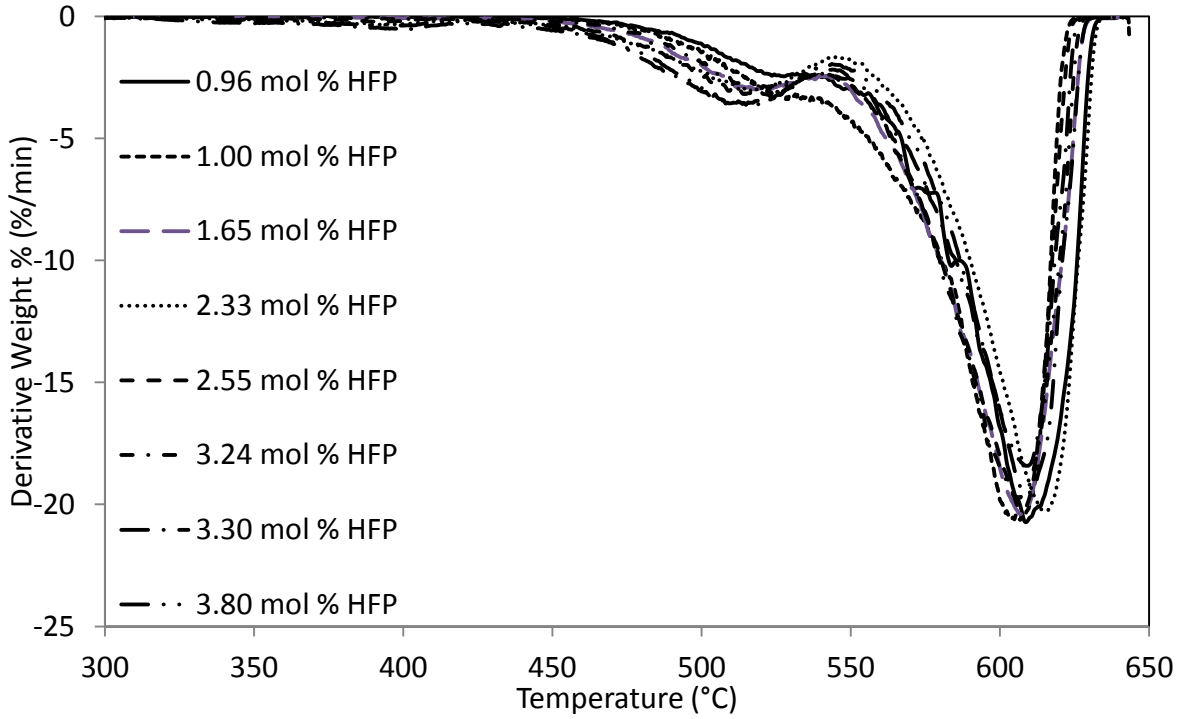

Figure 4-15 DTG pattern in TG analysis of polymerised FEP with different monomer feed ratios.

Figure 4-16 A and B show FTIR gas analyses for the first and second decomposition curves of the FEP copolymers prepared at 100 °C using different initiator dosing rates. From the FTIR spectra it can be observed that the intensity of the first decomposition step of the as-polymerised FEP copolymers is reduced compared to the second decomposition step. The evolved-gas spectra of all the as-polymerised FEP copolymers are found to be in a complete agreement with those of the commercial FEP spectra.

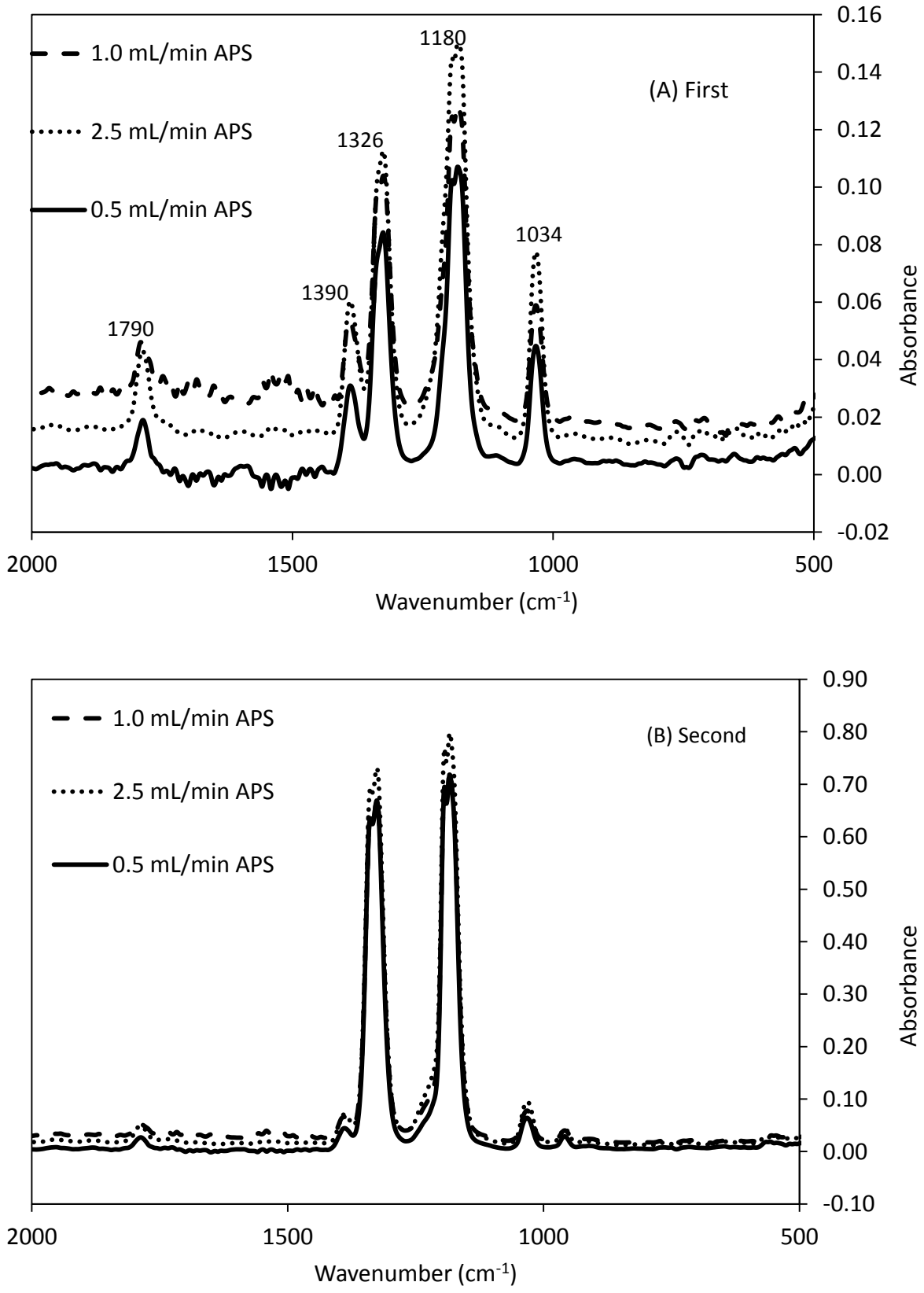

Figure 4-16 FTIR spectra of gaseous product for the (A) first and (B) second decomposition step for copolymers prepared at 100 °C using 0.5 mL/min APS (3.24 mol % HFP), 1.0 mL/min APS (2.55 mol % HFP) and 2.5 mL/min APS (3.30 mol % HFP).

4.1.5 DSC analysis

The DSC analysis was used to investigate the effects of increasing HFP composition in the PTFE chain on the melting temperature and melting enthalpy of the as-polymerised FEP copolymers. The maximum of the first heating, and second heating from the DSC thermograms were used to determine the first and second melting temperature. Figure 4-17 shows the first and second melting temperature curves for DuPont 807N X PTFE, and FEP samples. Figure 4-18 shows first and second melting curves of FEP copolymers prepared at 100 °C at 0.5, 1.0 and 2.5 mL/min APS initiator dosing rate. The DSC data, such as the melting temperature, melting enthalpy and degree of crystallisation for the first and second step of all the studied samples are listed in Table 4-6.

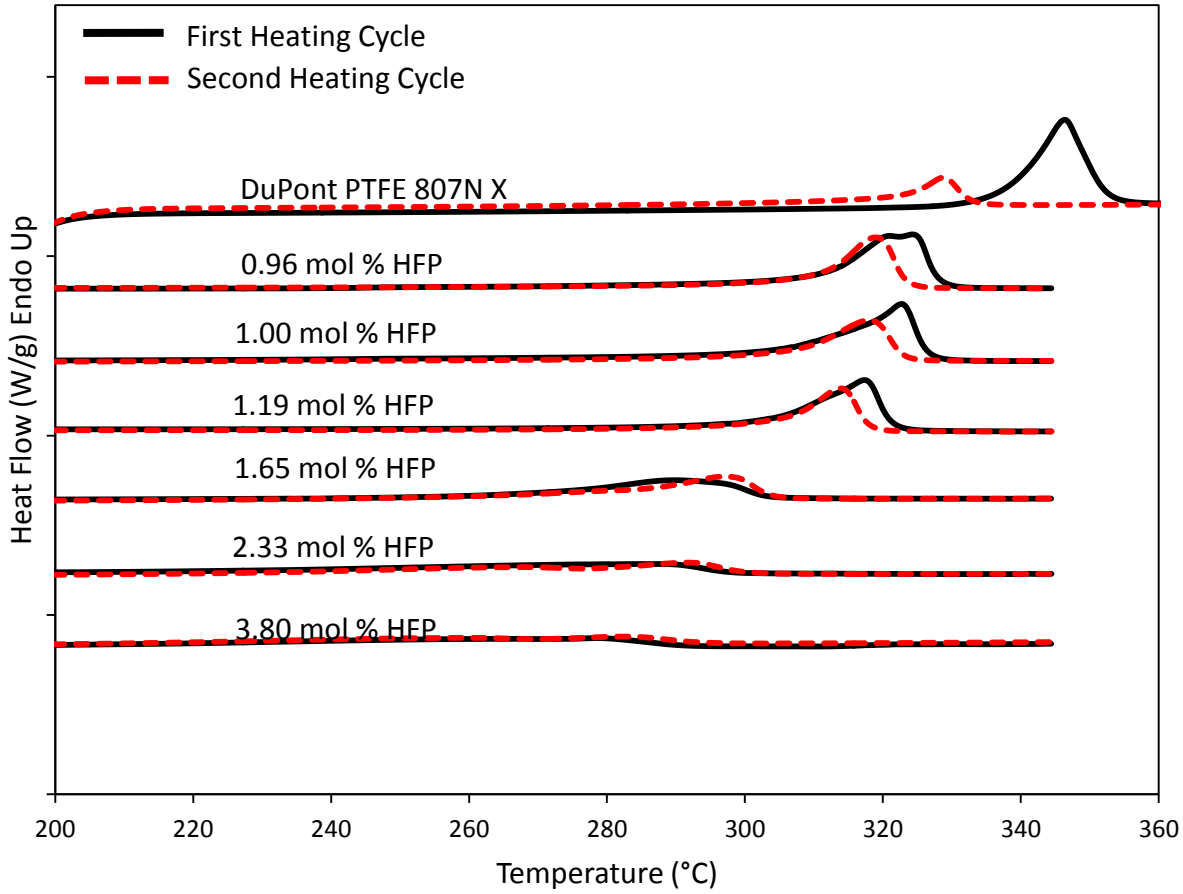

Figure 4-17 A DSC thermograms showing T_{m1} and T_{m2} of DuPont 807N X, and as-polymerised FEP copolymer using different feed ratios.

From Figure 4-17 and Table 4-6, it is evident that the melting peak temperatures (T_{m1}) of the 807N X PTFE exceed their crystallised melt temperature, T_{m2} and is above the equilibrium melting temperature, T_m^O, 332 °C (Enzo, G, 2001; Pucciariello, 1999). This behaviour is due to the fact that melting of the virgin PTFE consisting of extended chain crystals, and with equilibrium melting temperature that is irreversible. On cooling PTFE polymers forms a kinetically stable folded-chain with a lower melting temperature (Frick et al, 2012). Subsequent melting and re-crystallisation of the folded chain structure is reversible. The virgin PTFE consists mostly of extended chain, whereas PTFE crystallised from the melt consists entirely of folded chain crystals and has a spherulitic structure (Starkweather et al, 1989; Frick et al, 2012). The melting enthalpy of PTFE samples is high indicating a high degree of crystallinity developed during polymerisation (Suwa et al, 1973).

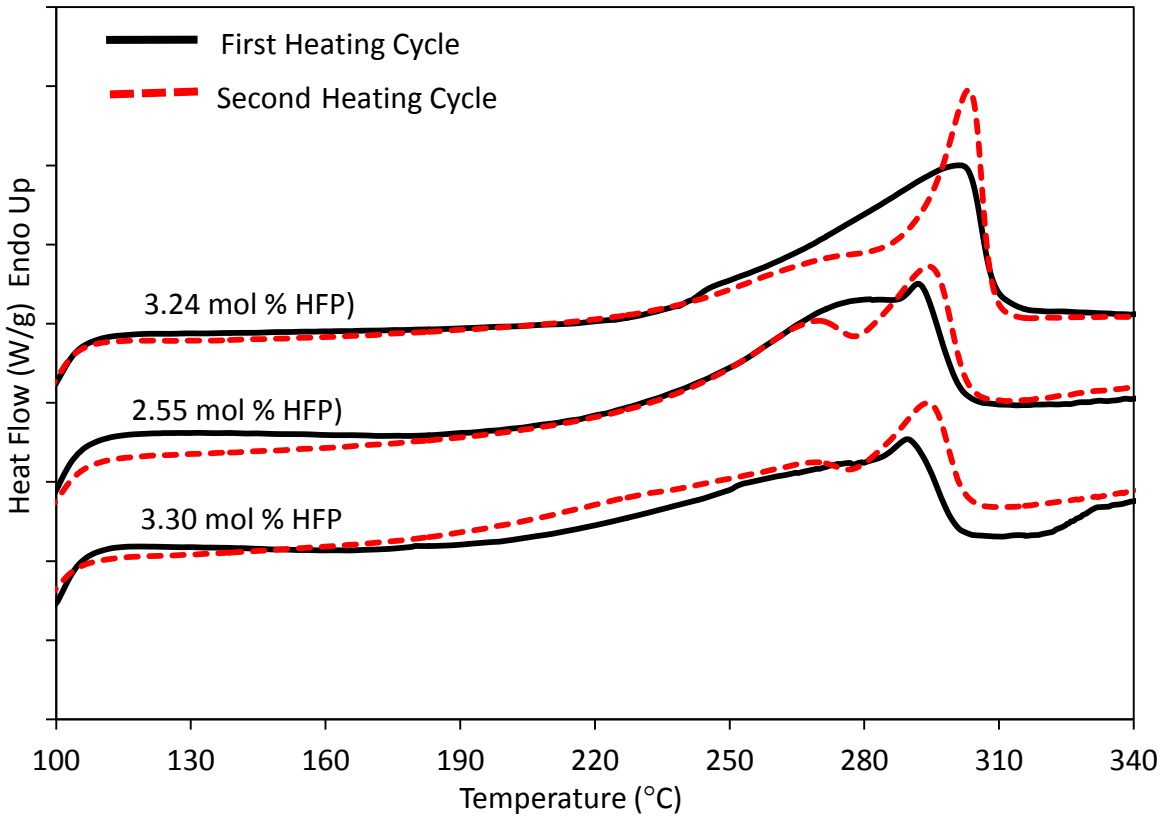

Figure 4-18 A DSC thermograms showing first and second heating of FEP copolymers containing 3.24 mol % HFP (0.5 mL/min APS), 2.55 mol % HFP (1.0 mL/min APS) and 3.30 mol % HFP (2.5 mL/min APS) prepared using different initiator dosing rate at 100°C.

Melting and crystallisation behaviour of PTFE is changed due to the incorporation of branched comonomer (Frick et al, 2012). The DSC traces of as-polymerised FEP, and DuPont 807N X PTFE show the presence of melt transitions (Figure 4-17). In general, increasing comonomer content the endotherm peak broadens compared with virgin PTFE and the heat of fusion and melting temperatures decreases (Frick et al, 2012). Comparing the melting behaviour of PTFE and as-polymerised FEP and commercial FEP a noticeable decrease in the melting temperature with increasing incorporation of comonomer into the PTFE chain can be observed (Table 4-6).

Table 4-6 Melting peak temperature, melting enthalpy and degree of crystallisation from DSC analysis.

Experimental name	**HFP content (mol %)**	**T_{m1} (°C)**	**ΔH_{f1} (J/g)**	**T_{m2} (°C)**	**ΔH_{f2} (J/g)**	**X_{c1} (%)**	**X_{c2} (%)**
DuPont 807N X		346.36	65.8990	328.82	21.0821	80.3	25.7
Dyneon FEP		250.39	29.8414	246.97	25.1417	36.4	30.6
ETK0831	0.96	324.28	73.0572	318.90	47.9717	89.0	58.5
ETK0509	1.00	322.72	71.0702	318.01	44.4911	86.6	54.2
ETK0417	1.19	317.30	58.7766	313.88	41.7466	71.6	50.9
ETK0515	1.65	289.84	41.5637	297.02	42.1647	50.7	51.4
ETK0905	2.12	290.76	40.8476	300.99	41.8312	49.8	51.0
ETK0801	2.33	287.85	38.2080	291.71	38.1612	46.6	46.5
ETK0511	3.80	278.71	36.6051	282.03	36.1369	44.6	44.0
ETK1017	2.55	292.08	42.8905	294.35	42.1151	52.3	51.3
ETK1023	3.30	289.51	35.7043	293.90	35.3250	43.5	43.1
ETK1024	3.24	301.15	46.3670	303.31	43.9203	56.5	53.5

The melting temperatures of as-polymerised FEP and commercial FEP were determined to be lower than the melting temperature of PTFE. From Table 4-6, the melting temperature decreases with an increase of the HFP monomer content in copolymer from 324.28 °C (0.96 mol % HFP) down to 278.71 °C (3.80 mol % HFP) and subsequently, the melting enthalpy was reduced from 73.0572 to 36.6051 J/g showing a decrease in degree of crystallinity.

Figure 4-18 shows the first and second heating of the FEP copolymers synthesised at 100 °C using different initiator dosing rate of 0.5, 1.0 and 2.5 mL/min. Comparing 3.24 mol % HFP (0.5 mL/min), 2.55 mol % HFP (1.0 mL/min), and 3.30 mol % HFP (2.5 mL/min), the copolymer DSC thermograms are characterised by a broad first melting, shown in Figure 4-18. The second melting curve is characterised by a broad peak with two shoulders and higher melting compared the first heating curve. This can be attributed to different molecular weights or crystalline structures in the copolymer.

Figure 4-19 represents the dependence of T_{m1}, T_{m2} and T_c of the copolymers on the HFP monomer content in the copolymer. The T_{m1} and T_{m2} decreases as the HFP content in the FEP copolymers increase from 0 to 3.80 mol % HFP. These observations are in accordance with the expectations (Friedman, 2002; Guerra et al, 1998), since an increase of the HFP unit in the copolymer also increases the number of $-CF_3$ groups attached to the polymer chain. The increase in the $-CF_3$ units impedes effective chain packing and hinders crystallisation. The reduction in effective packing results in a decrease in the interaction energy between the crystallised chain and the melting enthalpy becomes reduced.

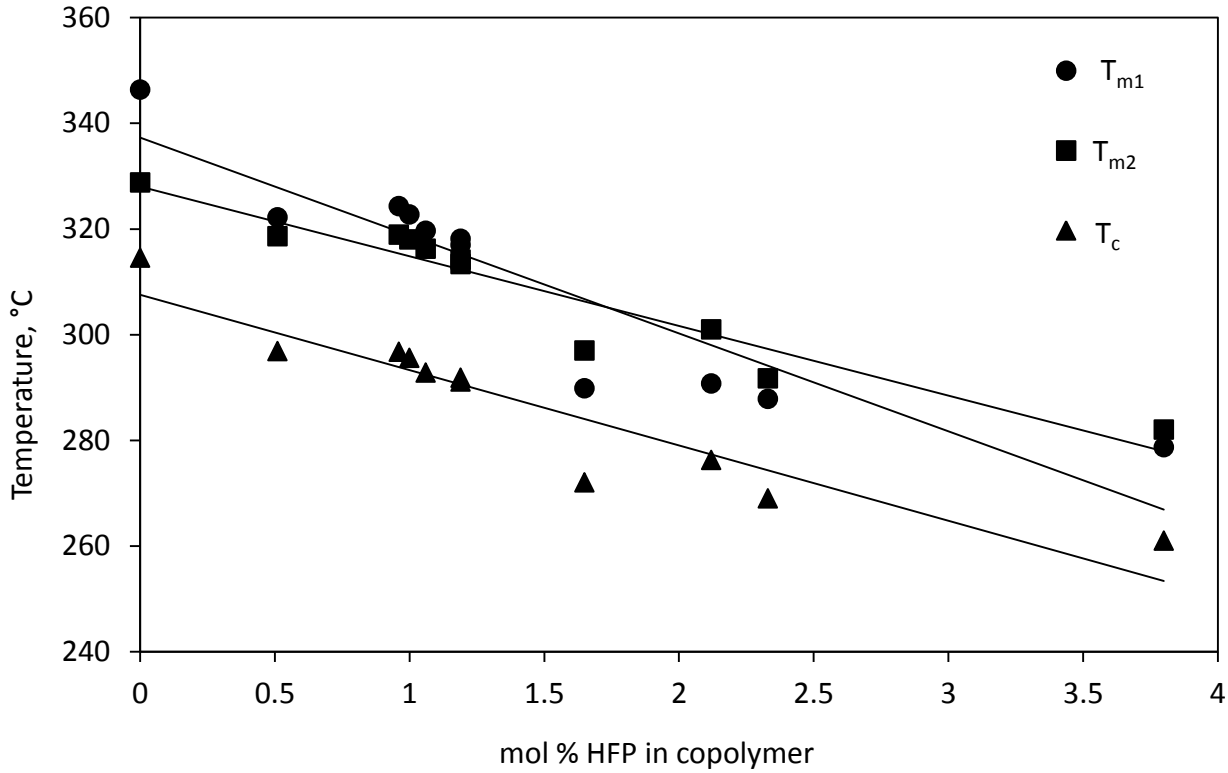

Figure 4-19 Effect of mol % HFP in the feed on $T_{m1,}$ T_{m2} and T_c of FEP copolymers.

The heat of fusion, ΔH_f, is one of the other important parameters that can provide useful information regarding the changes in the copolymer due to different starting feed ratios. The heat of melting is a measure of crystallinity in the polymer matrix. The heat of fusion per unit mass of polymer obtained in the current investigation was determined from the peak area in the DSC thermograms for as-polymerised FEP for various HFP concentrations. A plot of ΔH_f as a function of HFP content in the copolymer is presented in Figure 4-20. The heat of fusion displays a decrease with increase in HFP content in the copolymer. Consequently a decrease in heat of fusion for the FEP copolymer, correspond to a decrease in crystallinity that may be attributed the increase in HFP composition in the copolymer. The heat of fusion was used to determine the degree of crystallinity of copolymers. The results obtained for crystallinity of the commercial FEP and PTFE, and as-polymerised FEP samples, are shown in Table 4-6. As stated, the crystallinity measurements using DSC were calculated from the heat of fusion of PTFE (Frick et al, 2012; Marega, 2004).

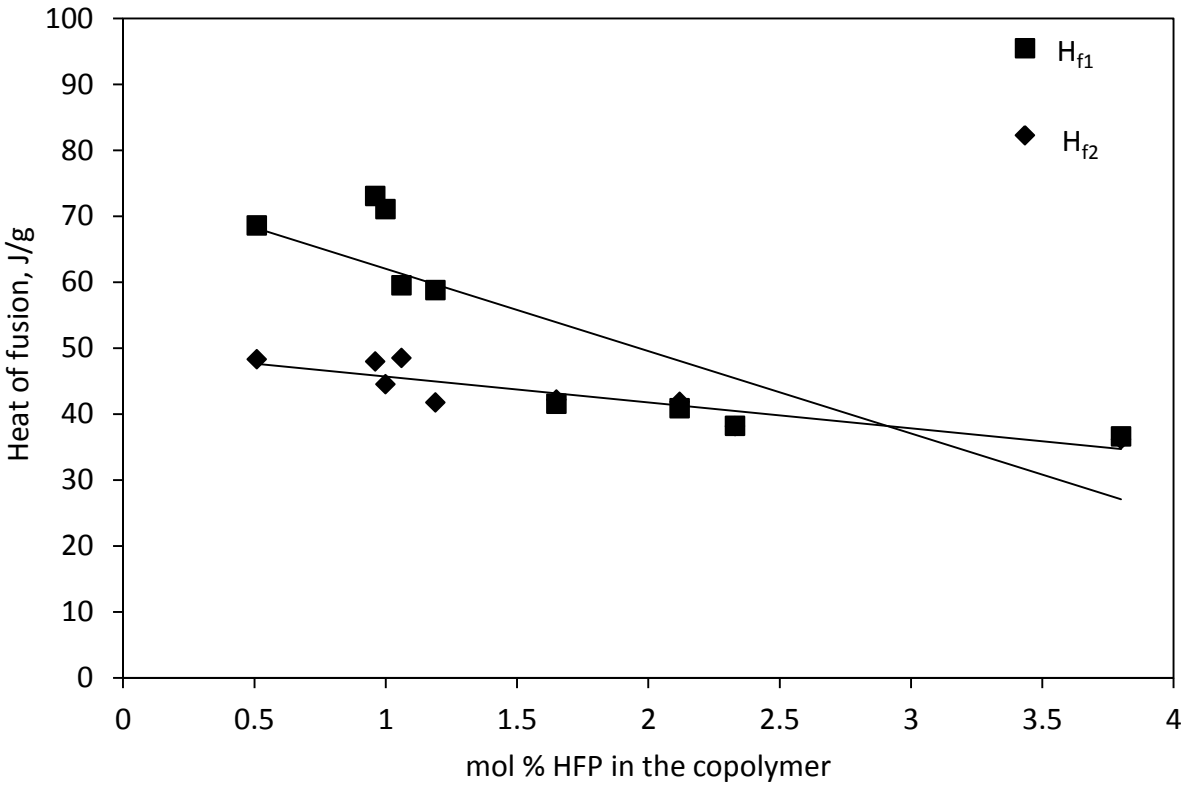

Figure 4-20 The variation in the heat of fusion as a function of mol % HFP in the copolymer of as-polymerised FEP.

4.1.6 XRD analysis

In order to determine the effect of changing the gaseous monomer feed ratio of the crystal structure of the copolymers, X-ray powder diffraction analysis was performed. The X-ray diffraction patterns of the as-polymerised FEP copolymers were compared to those of commercial PTFE (DuPont 807N X). Figure 4-21 shows the X-ray diffraction of scan for commercial PTFE. The X-ray diffraction patterns show that the commercial PTFE has a semi crystalline nature, which is in good agreement with the literature. From the diffraction patterns the most intense peak occurs at an interplanar spacing, d, of 4.89 Å (2θ = 21.09°) for commercial. This intense peak indexed as 100, arises from the lateral two-dimensional hexagonal packing of PTFE molecules. Three weak peaks are also observed see (Figure 4-21) at 2.82 Å (2θ = 36.9°), 2.42 Å (43.3°) and 2.18 Å (48.5°) respectively, and correspond to the 110, 107 and 108 diffraction signals (Bolz and Eby, 1965).

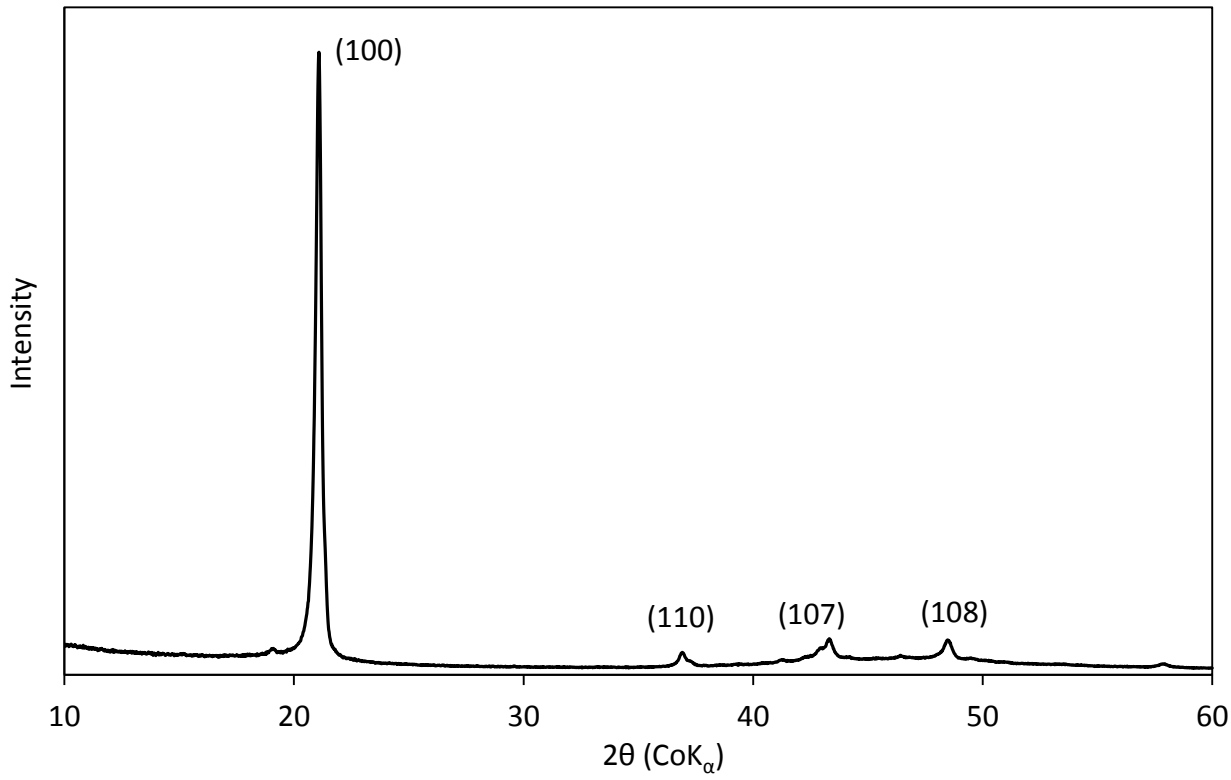

Figure 4-21 X-ray powder diffraction pattern of DuPont PTFE 807N X.

The Figure 4-22 and Figure 4-23 present the X-ray diffraction scans for 0.96, 1.00 and 1.06, and 1.65 and 3.80 mol % HFP copolymers, respectively. When compared to the commercial PTFE, a trend is observed. The peaks are shifted to lower diffraction angle with increasing HFP concentration copolymer. This shift is illustrated in Table 4-7. The intensity of the higher-order peaks decreases for 0.96 mol % HFP to 3.80 mol % HFP in the copolymer such that 110, 107 and 108 diffraction signals are reduced and no longer visible for the copolymers. The diffraction peak half-widths progressively increase with HFP content in the copolymer. The amorphous contribution to the scattering profile increases with HFP concentration in the copolymer (see Table 4-7). The value of the interplanar spacing of the hexagonal unit cell of the commercial PTFE is 4.89 Å, and a deviation is observed (Table 4-7 for the as-polymerised FEP copolymers to 4.99 Å for 3.80 mol % HFP copolymer. The deviation confirms that the $-CF_3$ group is at least partially included in the crystal phase (Kostromina et al, 1986; Marigo et al., 1996).

Table 4-7 X-ray diffraction data for commercial PTFE and as-polymerised FEP samples.

Name	**mol % HFP in copolymer**	**2θ (°)**	**d_{100} (Å)**
PTFE 807N X		21.09	4.89
ETK 0831	0.96	20.82	4.95
ETK 0509	1.00	20.80	4.96
ETK 0418	1.06	20.94	4.93
ETK 0515	1.65	20.71	4.98
ETK 0511	3.80	20.67	4.99

The broadening of the diffraction peaks and the gradual disappearance of the peaks at 110, 107 and 108 with increasing HFP concentration in the copolymer suggest less ordered and/or smaller crystals compared to the PTFE structure.

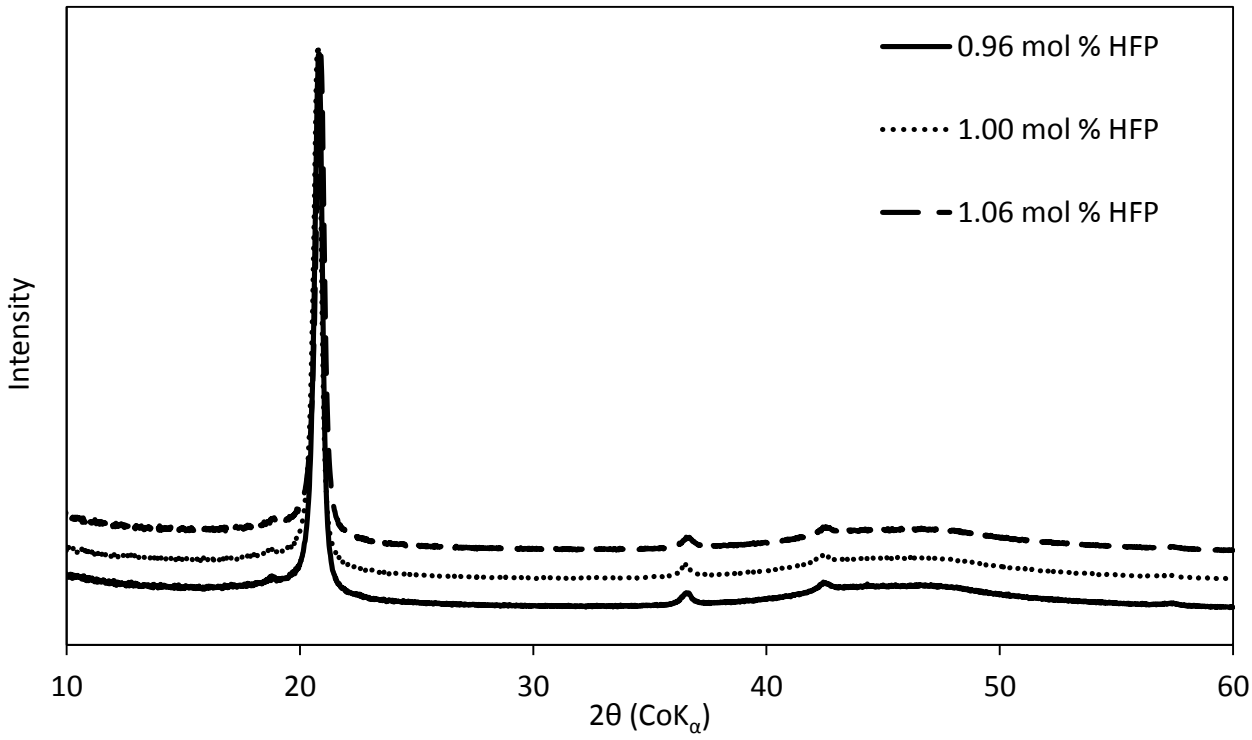

Figure 4-22 X-ray powder diffraction pattern of 0.96, 1.00 and 1.06 mol % HFP in the copolymer.

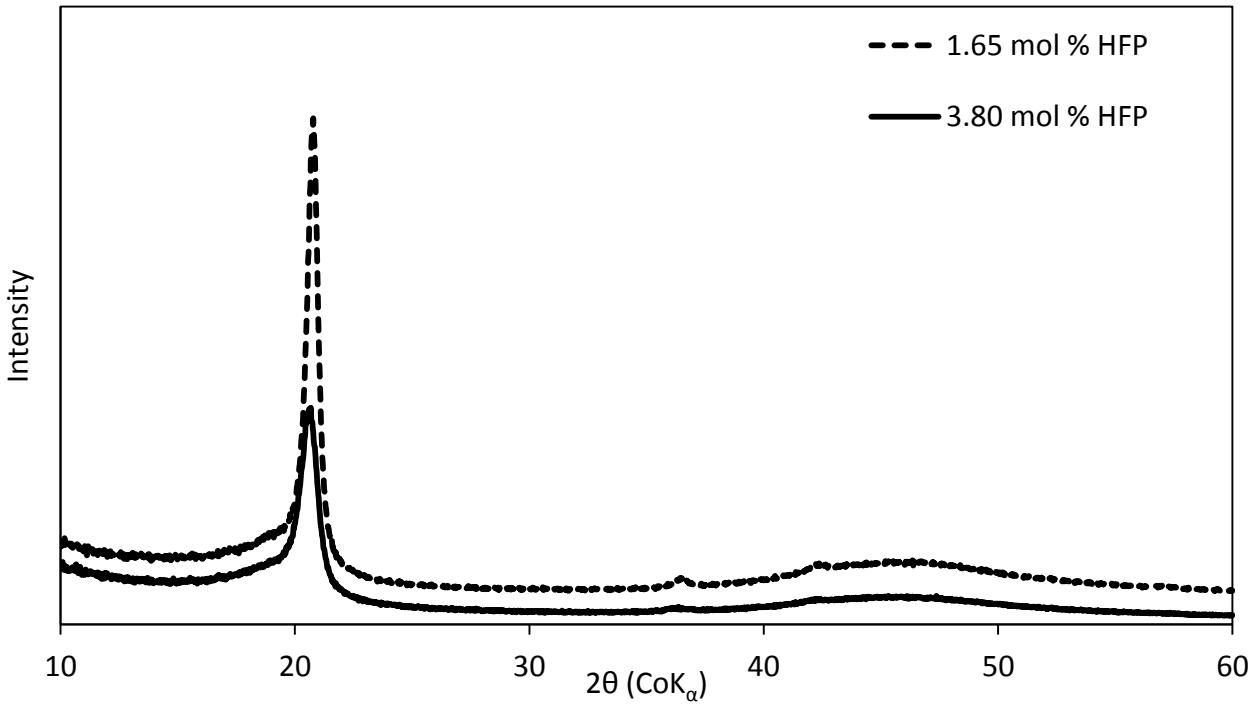

Figure 4-23 X-ray powder diffraction pattern of 1.65 and 3.80 mol % HFP in the copolymer.

This broadening is more pronounced as the HFP content is increased. It is also apparent from the DSC results that the crystallinity decreases with increasing HFP concentration in the copolymer, showing increased incorporation of HFP in the crystal phase. This results in the disruption of the regular helical conformation of the chain by forming chain defects.

4.1.7 SEM analysis

The SEM analysis was performed to observe morphological changes of the synthesised FEP coplymers. Distinctive morphological differences of FEP coplymers were obtained depending on the monomer feed ratios. In order to see if there is a significant change in the morphology of as-polymerised FEP copolymers, the morphology of PTFE has to be reviewed. Rahl et al (1972) found that non-spherical, ribbon-shaped crystals were found in the early stages of the polymerisation. The ribbons are chain-extended single crystals with chain axis parallel to the long axis of the ribbons. The work was done on emulsion-grade PTFE at various stages of the polymerisation. Seguchi and co-workers (1974) suggested that polymer morphology strongly depends on the polymerisation conditions such as emulsifiers (surfactant). They found that polymerisation carried without emulsifying agent and polymerisation carried out for longer periods consisted of spherical to elliptical particles with a diameter of 100 Å and spherical particles dominate.

The Figure 4-24 illustrates that SEM micrographs of the as-polymerised FEP copolymer powders (synthesised using different monomer feed ratios) with different HFP unit concentrations consists of two different particle population, namely rods and spherical globules. It was not possible to determine which of the crystal morphology was dominant from the SEM micrographs. The effect of HFP content in the copolymer was investigated on the population of the rods and spheres to establish if a trend is present. A trend is observed from low HFP to high HFP unit concentration. At low HFP comonomer content, i.e., 0.96 mol % HFP shown in Figure 4-24 (A), the morphology is consists of both the rod-like and spherical crystal particles and 1.19 mol % HFP (Figure 4-24(B)), the rods are reduced and spherical crystal particles dominate.

For copolymers containing 1.65 and 3.80 mol % HFP (shown in Figure 4-24(C) and (D), respectively), the rod-like particles are completely absent and spherical particles predominate. This can be a result of the increased incorporation of HFP in PTFE chain thus reducing crystallinity and melting temperature. A comparison on the effect of initiator dosing and temperature of the morphology of the resulting copolymers was made. Figure 4-25 shows SEM images for 3.24, 2.55 and 3.30 mol % HFP copolymers. From the micrograph it can be observed that spherical globules particles predominate and rod-like

particles are completely absent. These results compare very well with the morphology of the FEP copolymer prepared from 60/40 TFE/HFP using 1.0 mL/min APS at 85 °C (see Figure 4-24 (C), 1.65 mol % HFP). The spherical globules appear to be fused together, showing that agglomeration is prevalent for polymerisation done at higher temperatures using different dosing rates.

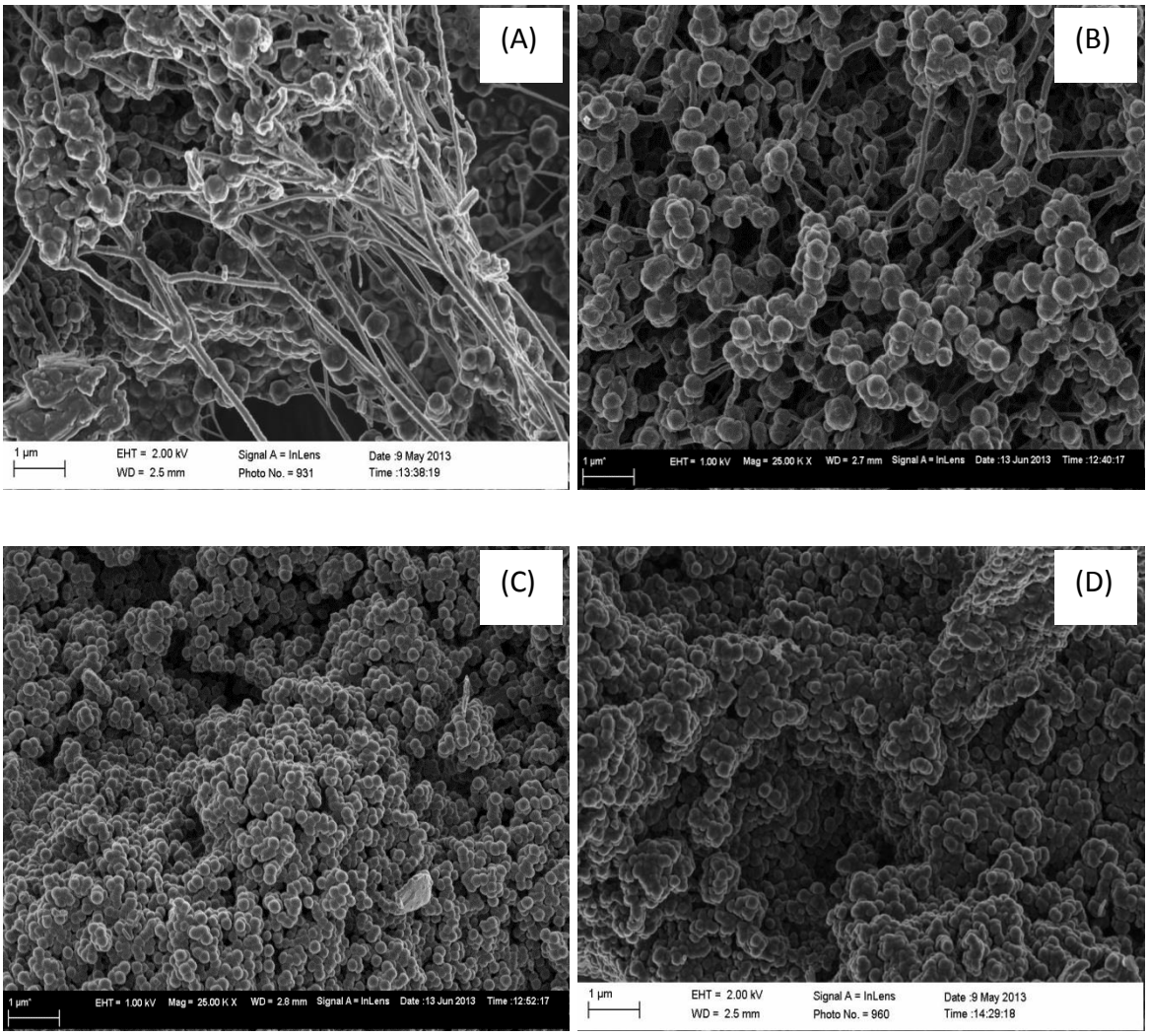

Figure 4-24 SEM micrographs of (A) 0.96 mol % HFP, (B) 1.19 mol % HFP, (C) 1.65 mol % HFP and (D) 3.80 mol % HFP in the FEP copolymer.

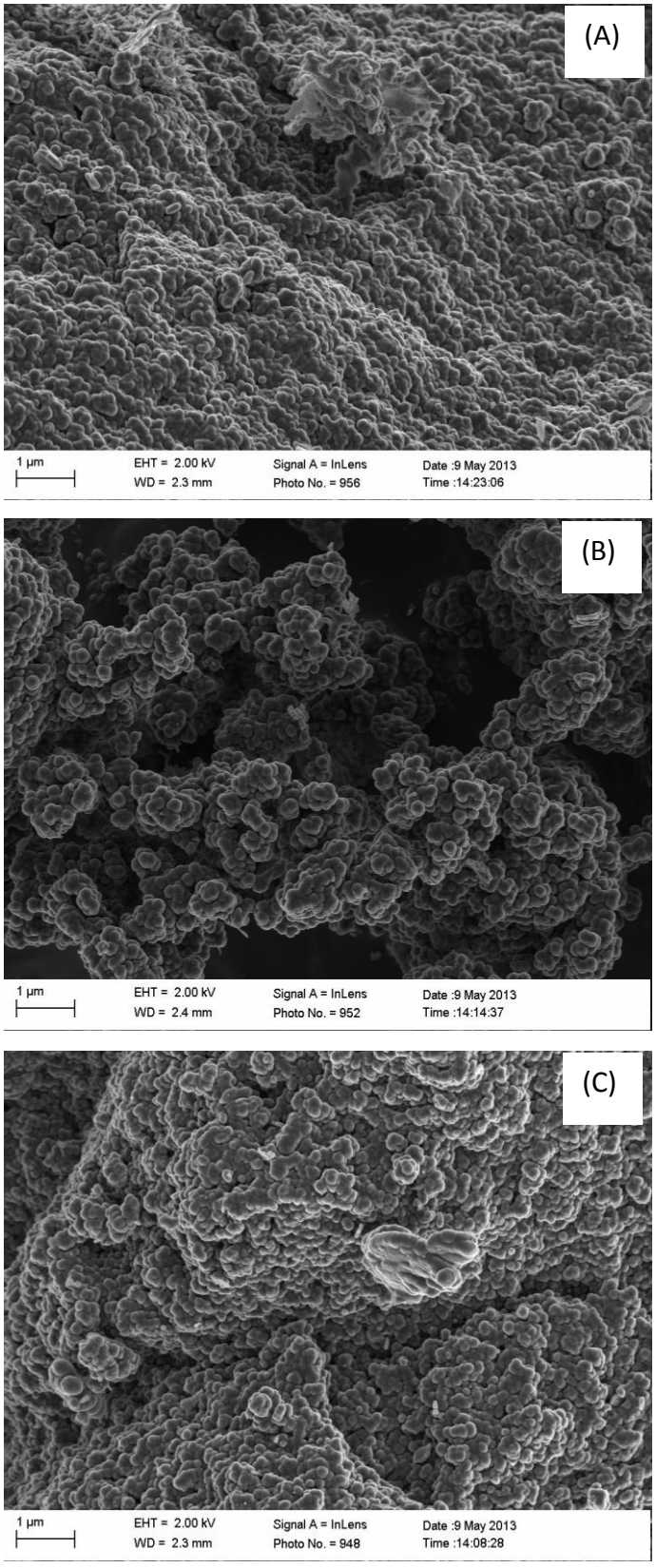

Figure 4-25 FEP SEM micrographs for A) 3.24 mol % HFP, 0.5 mL/min APS B) 2.55 mol % HFP, 1.0 mL/min APS and C) 3.30 mol % HFP, 2.5 mL/min APS synthesised using , and mL/min APS dosing rate at 100 °C .

CHAPTER 5 CONCLUSIONS

PTFE (homopolymer of TFE) is the most important fluoropolymer (Simon and Kaminsky, 1998), and it has unique desired properties but has a disadvantage of being difficult to process using conventional processing techniques. In order to overcome these undesirable properties, the TFE can be copolymerised with HFP monomer to form FEP. The aim of the study was to develop the technology for an on-specification polymerisation of FEP copolymers using TFE and HFP. The main objective of this work was to investigate the copolymerisation in TFE and HFP in aqueous medium using different TFE/HFP feed stream ratio. In this study it has been shown that changing the feed stream ratio, polymer products with different thermal properties, crystallinity and morphology were successfully synthesised using suspension polymerisation. Chemical structure and HFP content analysis of the synthesised polymers was accomplished by using, ^{19}F NMR and FTIR. The thermal properties and crystallinity of the polymers were analysed using DSC, TGA and XRD. The morphology change with charging feed stream ratio was determined by using SEM analysis.

Suspension polymerisation of FEP copolymers was carried out using different concentrations HFP in the gaseous monomer feed. The experiments were performed at 85 and 100 °C using a 1.0 mL/min initiator feed rate at 85 °C for all the experiments, and 0.5, 1.0, and 2.5 mL/min feed rates at 100 °C . For the different initiator dosing rates, a constant ratio of 60 mol % TFE and 40 mol % HFP were chosen based on experiments results done at 85 °C. The pressure of the experiments ranged between 11 to 20 bar, and was found to be dependent on the concentration of the HFP monomer in the feed ratio.

The ^{19}F NMR MAS and FTIR analysis confirmed the chemical structure the prepared FEP copolymers. The ^{19}F NMR results preformed spinning rates of 20 kHz showed the presence of side spinning bands on top of the FEP characteristic peaks. The analysis was performed at 55 kHz and the side spinning bands were completely averaged in the characteristic peak range. For analysis at 55 kHz, the HFP composition in the copolymer was determined to be 0.96, 1.00, 1.06 and 3.80 mol % HFP. These values were used to calibrate the FTIR absorbance ratio data to calculate the HFP composition in the copolymers.

The FTIR analysis revealed that the resulting copolymers show the presence of a -CF_3 symmetric stretching band which represent incorporation of HFP into the PTFE chain. It also revealed that the -CF_3 band increases with as the mol % HFP in the feed increases. This was corroborated by a plot of absorbance ratio of CF_3/CF_2, which showed increased as the HFP concentration in the feed increases.

The TGA analysis of the copolymers in nitrogen atmosphere showed that the copolymers are stable and start to decompose above 490 °C. Analysis of the evolved gaseous products from the TGA was done using an FTIR cell coupled to the TGA. The results revealed that copolymers undergo a two-step decomposition process; the first step is due to the evolution of the hexafluoropropylene monomer unit and the second at high temperatures is attributed to the degradation of the tetrafluoroethylene monomer unit. A different trend was observed for the copolymers with 3.30 mol % HFP (using different initiator dosing rate and temperature, see Section 3.2.2), 2.33 and 3.80 mol % HFP. They showed a 3 step decomposition process with first onset decomposition temperatures of 339.64, 375.10 and 380.10 °C, respectively. The evolved gas products from these steps were not detected by FTIR.

The XRD analysis showed that the crystallinity of PTFE is decreased by an increase of HFP in the copolymer. The changes in XRD patterns of these copolymers clearly indicate that coordination between the comonomers is consistence with results reported in the literature (Marigo et al, 1996). The decrease in crystallinity is an indication of incorporation of HFP in the PTFE chain. The DSC results showed a decrease in the melting temperature (T_{m1}) and crystallinity of the as-polymerised copolymers as the concentration of the HFP unit in the feed copolymer. The melting temperature decreased from 324.28 (0.96 mol % HFP) to 278.71 °C (3.80 mol % HFP).

Scanning electron micrographs showed that the as-polymerised FEP copolymers powder consists of rod-like particles and spherical globules at low HFP content. The population of the rods is significantly reduced as the HFP content of the copolymers increase.

REFERENCES

Ahmed, TS, DeSimone, JM, Roberts, GW (2006) "Copolymerisation of Vinylidene with Hexafluoropropylene in supercritical carbon dioxide", Macromolecules, 39, 15 – 18.

Alia, A, Ganapathy, S, de Groot, HJM (2009) "Magic angle spinning (MAS) NMR: a new tool to study the spatial and electronic structure of photosynthetic complexes", *Photosynth. Res.,* 102, 415 – 425.

Ameduri, B, Boutevin, B and Kostov, G (2001) "Fluoroelastomers: synthesis, properties and applications", *Prog. Polym. Sc.*, 26(1), 105 – 187.

Beginn, U, Najjar, R, Ellmann, J, Vinokur, R, Martin, R (2006) "Copolymerisation of Vinylidene with Hexafluoropropylene in supercritical carbon dioxide", *Journal of Polymer Science: Part A: Polymer Chemistry*, 44, 1299 – 1316.

Bolz, CH and Eby, RK (1965) "Inclusion of perfluoromethyl group in the crystals of copolymers of tetrafluoroethylene and hexafluoropropylene", *Journal of Research of the National Bureau of Standards: A. Physics and Chemistry*, 69A (5), 481 – 492.

Breitmaier, E (2002) *Structure Elucidation by NMR in Organic Chemistry: A Practical Guide*, Third edition revised, John and Wiley & Sons Ltd, The Atrium, Southern Gate, Chichester, West Sussex, England.

Bro, MI, Convery, RJ, Schreyer, RC (1961) "Polymerisation of fluorine containing monomers", *US Patent 2988542*, assigned to E.I. Du Pont de Nemours and Company, Wilmington.

Bro, MI and Sandt, BW (1960) "Novel perfluorocarbon polymers", *US Patent 2946763*, assigned to E.I. Du Pont de Nemours and Company, Wilmington.

Cleaver, CS (1960) "Polymerization process using nitrogen fluorides", *US Patent 2963468*, assigned to E.I. Du Pont de Nemours and Company, Wilmington.

Dargaville, TR, George, GA, Hill, DJT, Whittaker, AK (2003) "An investigation of the thermal and tensile properties of PFA following γ radiolysis", *Macromolecules*, 36, 7132 – 7137.

Department of Trade and Industry of South Africa (2005) "Chemical sector development strategy report", Department of Trade and Industry, Pretoria, South Africa.

Drobny, JG (2009) *Technology of Polymers*, Second edition, Taylor and Francis group, LLC, CRC Press, Boca Raton, FL.

Ebnesajjad, S (2003) *Fluoroplastics: Melt Processible Fluoropolymers: The Definitive User's Guide and Databook*, Volume 2, Plastic Design Library, NY.

Ebnesajjad, S (2011) Introduction to Fluoropolymers, In: *Applied Plastics Engineering Handbook: Processing and Materials,* Elsevier Inc.

Eleuterio, HS (1962) "Amorphous copolymers of hexafluoropropylene and tetrafluoroethylene and their preparation", *US Patent 3062793*, assigned to E.I. Du Pont de Nemours and Company, Wilmington.

Ellis, DA, Martin, J. W., Muir, DCG, Mabury, SA (2003) "The use of ^{19}F NMR and mass spectrometry for elucidation of novel fluorinated acids and atmospheric fluoroacids precursors evolved in the thermolysis of fluoropolymers", *Analyst*, 128, 756 – 764.

Emmons, ED, Velisavljevic, N, Schroonover, JR, Dattelbaum, DM (2008) "High-pressure Raman spectroscopy and X-ray diffraction studies of terpolymer of tetrafluoroethylene-Hexafluoropropylene-Vinylidene Fluoride: THV 500", *Applied Spectroscopy*, 62 (2), 142-148

Endo, M, Ohnishi, A, Kutsumizu, S, Shimizu, T, Yano, S (2004) "Crystallisation of binary blends of polytetrafluoroethylene copolymer", *Polymer Journal*, 36 (9), 716 – 727.

Enzo, G (2001) "Featured article semi-crystalline fluorinated polymers", *Polymer International*, 50, 10 – 26.

Feiring, AE, Krespan, CG, Resnick, PR, Smart, BE, Treat, TA, Wheland, RC (1993) "Hydrocarbon solvents for fluoromonomer polymerization", *US Patent 5182342*, assigned to E.I. Du Pont de Nemours and Company, Wilmington.

Feiring, AE, Wonchoba, ER, Davidson, F, Percec, V, Barboiu, B (2000) "Fluorocarbon-Ended Polymers: Metal Catalysed Radical and Living Radical Polymerizations Initiated by Perfluoroalkylsulfonyl Halides", *Journal of Polymer Science: Part A: Polymer Chemistry*, 38, 3313 – 3335.

Forsythe, JS, Hill, DJT, Mohajerani, S, Whittaker, AK (2001) "Solid-state ^{19}F NMR determination of new structure formation in FEP following radiolysis at 300 and 363K", *Radiation Physics and Chemistry,* 60, 439 – 444.

Frick, A, Sich, D, Heinrich, G, Stern, Claudia, Schlipf, M (2012) "Classification of new-melt-processable PTFE: Comparison of emulsion- and suspension-polymerised materials", *Macromol. Mater. Eng.*, 297, 329 – 341.

Friedman, M and Walsh, G (2002) "High performance films; Review of new materials and trends" *Polymer Engineering and Science*, 42 (8), 1756 - 1788.

Gangal, SV (2000) Fluorine-Containing Polymers, Perfluorinated Ethylene-Propylene Copolymers, *Kirk-Othmer Encyclopaedia of Chemical Technology*, John Wiley and Sons, Inc., New York.

Gangal, SV and Brothers, PD (2010) Perfluorinated Polymers, Perfluorinated Ethylene-Propylene Copolymers, *Encyclopaedia of Polymer Science and Technology*, John Wiley and Sons, Inc., New York.

Ge, Z, Zhang, X, Dai, J (2006) "Synthesis and characterisation of a new fluorinated polyether glycol prepared by radical grafting of hexafluoropropylene onto polytetramethylene glycol", *European Polymer Journal*, 42, 395 – 401.

Gudipati, CS, Greenlief, CM, Johnson, JA, Prayongpan, P, Wooley, KL (2004) "Hyperbranched fluoropolymers and linear poly (ethylene glycol) based amphiphilic crosslinked network as efficient antifouling coatings: An insight into the surface compositions, topographies and morphologies" *Journal of Polymer Science: Part A: Polymer Chemistry*, 42, 6193 – 6208.

Guerra, G, Venditto, V, Natale, C, Rizzo, P, De Rosa, C (1998) "Structural variations in random copolymers of tetrafluoroethylene with kind and content of comonomer units', *Polymer*, 39 (14), 3205 - 3209.

Gupta, B, Highfield, TG and Scherer, GG (1994) "Proton-exchange membranes by radiation grafting of styrene onto FEP films. II: Mechanism of thermal degradation in copolymer membranes", *Journal of Applied Polymer Science*, 51, 1659 – 1666.

Hill, DJT, Mohajerani, S, Whittaker, AK, Scheler, U (2003) "Chain scission and branching in irradiated poly(tetrafluoroethylene-co-hexafluoropropylene)", *Polymer International*, 52, 1725 – 1733.

Ignatieva, LN, Tsvetnikov, AK, Livshits, AN, Saldin, VI, Buznik, VM (2002) "Spectroscopic study of modified polytetrafluoroethylene" *Journal of Structural Chemistry*, 43 (1), 64 – 68.

Kim, CU, Lee, JM, Ihm, SK (1999a) "Emulsion polymerisation of tetrafluoroethylene: Effects of reaction conditions on particle formation" *Journal of Fluorine Chemistry*, 96, 11 – 21.

Kim, CU, Lee, JM, Ihm, SK (1999b) "Emulsion polymerization of tetrafluoroethylene: Effects of reaction conditions on the polymerisation rate and polymer molecular weight", *Journal of Applied Polymer Science*, 73, 777 – 793.

Kostromina, SV, Kozlova, NV, Zubov, YuA, Chvalun, SN, Fedorovich, YeA and Ryvkin, GA (1986) "X-ray study of structural parameters of some tetrafluoroethylene copolymers", *Polymer Science USSR*, 28 (4), 992 – 998.

Lappan, U, Fuchs, B, Geißler, U, Scheler, U, Lunkwitz, K (2002) "Number-average molecular weight of radiation-degraded poly(tetrafluoroethylene). An end group analysis based on solid-state NMR and IR spectroscopy", *Polymer*, 43, 4325 – 4330.

Lee, TH, Boey, FYC, Khor, KA (1995) "X-ray diffraction analysis techniques for determining the polymer crystallinity in a polyphenylene sulphide composite", *Polymer Composite*, 16 (6), 481 – 488.

Lunkwitz, K, Lappan, U, Scheler, U (2004) "Modification of perfluorinated polymers by high-energy irradiation", *Journal of Fluorine Chemistry*, 125, 863 – 873.

Marega, C, Marigo, A, Causin, V, Kapeliouchko, V, Di Nicolo, E and Sanguineti, A (2004) "Relationship between the size of the latex beads and the solid-solid phase transitions in emulsion polymerised poly(tetrafluoroethyelene)", *Macromolecules*, 37, 5630 – 5637.

Marigo, A, Marega, C, Zannetti, R, Ajroldi, G (1996) "Lamellar morphology by small-angle x-ray scattering measurements in some perfluorinated copolymers of tetrafluoroethylene", *Macromoecules*, 29, 2197 – 2200.

McMurry, J (2004) *Organic Chemistry*, 6th edition, Brooks/Cole, Thomson Learning, CA, USA.

Miller, WT (1952) "Copolymers of perfluopropene and tetrafluoroethylene and method of making the same", *US Patent 2598283*, assigned to United State of Atomic Energy Commission.

Mulla, SM, Phale, PS, MR Saraf (2012) "Use of X-ray diffraction techniques for polymer characterisation and studying the effect of optical accessories", *Admet*, OM 006, 1-6.

Munekawa, S (1988) "Application of X-ray diffraction techniques to the semiconductor field", *The Rigaku Journal*, 5 (2), 31 – 34.

Pucciariello, R, Mancusi, C (1999) "Extreme thermal behaviours of polytetrafluoroethylene and random tetrafluoroethyelen fluorinated copolymers", *Journal of Applied Polymer science,* 73, 919 – 925.

Rahl, FJ, Evanco MA, Fredericks, RJ, Reimschuessel, AC (1972) "Studies of the morphology of emulsion-grade polytetrafluoroethylene", *Journal of Polymer Science: Part A-2*, 10, 1337 – 1349.

Robinson, JW, Frame, EMS, Frame II, GM (2005) *Undergraduate Instrument Analysis,* Marcel Dekker, New York.

Sauer, JC (1951) "Polymers of hexafluoropropylene", *US Patent 2549935*, assigned to E.I. Du Pont de Nemours and Company, Wilmington.

Scheler, U (1998) "High-speed MAS-NMR investigation on radiation-modified fluoropolymers", *Solid State Nuclear Magnetic Resonance*, 12, 9 – 13.

Seguchi, T, Suwa, T, Tamura, N, Takehisa, M (1974) "Morphology of polytetrafluoroethylene prepared by radiation-induced emulsion polymerisation", *Journal of Polymer Science-Polymer Physics Edition*, Vol. 12, 2567 – 2576.

Simon, CM, Kaminsky, W (1998) "Chemical recycling of polytetrafluoroethylene by pyrolysis" *Polymer Degradation and Stability*, 62, 1 – 7.

Smith, BC (2011) *Fundamentals of Fourier Transform Infrared Spectroscopy*, Second edition, Taylor & Francis Group LLC, CRC Press, Boca Raton, FL, US.

Söderlind, F (2008) "*Collodidal synthesis of metal oxide nanocrystal and thin films*", PhD Thesis, Linköping University, Sweden.

Suwa, T, Takehisa, M, Machi, S (1973) "Melting and crystallisation behaviour of poly(tetrafluoroethylene). New method for molecular weight measurement of poly(tetrafluoroethylene) using a differential scanning calorimetry", *Journal of Applied Polymer Science*, Vol. 17, 3253 – 3257.

Tanaka, S (1992) "*Theory of Power-compensated DSC*", Thermochimica Acta, 210, 67-76.

Teng, H (2012) "Overview of the development of the fluoropolymer industry", *Appl. Sci.,* 2, 496-512.

Wendlandt, WW (1985) *Thermal Methods of analysis*, Third edition, Wiley-Interscience, New York, US.

White, ML, Waddon, AJ, Atkins, EDT, Farris, RJ (1998) "Copolymerisation of hexafluoropropylene and tetrafluoroethylene: Effect of chain conformation and crystal structure", *Journal of Polymer Science: Part B: Polymer Physics*, 36, 2811 – 2819.

APPENDIX A THERMAL ANALYSIS

When matter is heated, it undergoes certain physical (melting, vaporisation, crystallisation, transition between crystals structures, changes in microstructure in metal, alloys and polymers, etc.), and chemical (oxidation, corrosion, decomposition, dehydration, chemisorption etc.) changes. The analytical techniques used to study changes in physical properties as a function of temperature are called thermal analysis techniques. They include thermogravimetric analysis (TGA), differential thermal analysis (DTA), differential scanning calorimetry (DSC), thermometric titration (TT), dynamic mechanical analysis (DMA), and thermomechanical analysis (TMA). Table A-1 represents a brief overview of some application for various thermal analysis methods. (Robinson et al, 2005)

Table A-1 The summary of some application of thermal analysis methods (Robinson et al, 2005).

Application	TGA	DSC, DTA	TMA	DMA
Compositional analysis	X	X		
Curring studies		X		
Glass transition		X	X	X
Heat of reaction		X		
Oxidative stability	X	X		
Corrosion	X	X		
Creep			X	X
Stress relaxation			X	X
Thermal stability	X	X		
Viscoelastic properties			X	X
Protein denaturation		X		
Shrinkage			X	X

A.1 Differential scanning calorimetry (DSC)

In DSC, difference in heat flow into a reference and sample are measured against temperature of the sample. The difference in heat flow is a difference in energy content. Modern DSC sample and reference pans are small and usually made of aluminium. They may or may not have lids. Sample size is generally 1-10 mg. Commercial DSC equipment can operate at temperatures from 180 to 700 °C, with specialised instruments capable of maximum temperatures of 1600 °C. The DSC must be able to be heated and cooled in a controlled manner. To achieve the very low end of the temperature range, a special liquid nitrogen cooling accessory is needed; for other cooling applications, electrical cooling or forced air is used.

The DSC measures the change in the heat flow rate between the sample and the reference sample while subjected to a controlled temperature program. There are two major types of DSC that are commonly in use in studying thermal properties of materials (Wendlandt, 1985; Tanaka, 1992):

Power-compensated DSC

The sample and reference temperature are controlled independently using identical separate ovens (Figure A-1). The temperature difference between the sample and the reference is maintained to zero by varying the power input to the two furnaces. This energy is then a measure of the enthalpy changes or heat capacity changes in the test sample relative to the reference. (Tanaka, 1992)

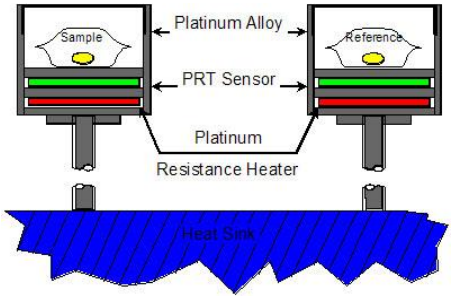

Figure A-1 Power compensated DSC.

Heat-flux DSC

The sample and reference material are enclosed in the same furnace together with a metallic block with high thermal conductivity that ensures a good heat-flow path between sample and reference (see Figure A-2). The enthalpy or heat capacity changes in the sample lead to a temperature differences relative to reference. This results in a certain heat-flow between sample and reference, because of the good thermal contact between the sample and reference. The temperature difference ΔT between sample and reference is recorded and related to the enthalpy change in the sample using calibration experiments. (Tanaka, 1992)

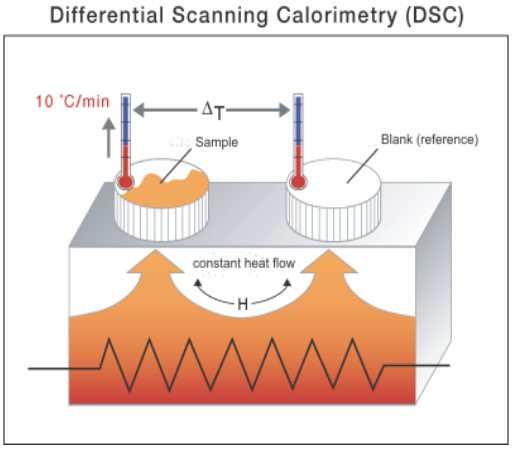

Figure A-2 Heat-flux DSC.

Differences in heat capacity can also be accurately measured and are observed as shifts in the baseline before and after an endothermic or exothermic event or as isolated baseline shifts due to a glass transition. Because DSC provides accurate quantitative analytical results, it is now the most used thermal analysis techniques. A typical DSC thermal curve for polyethylene terephthalate, the polymer is shown in Figure A-3. (Robinson et al, 2005)

DSC is used to study all type of reactions and transitions that can be studied using DTA, with the added advantage of accurate quantitative measurement of ΔH and C_p. Polymer chemist

use DSC extensively to study percent crystallinity, crystallisation rate, polymerisation kinetics, polymer degradation, and the effect of composition on the glass transition temperature, heat capacity, and other phase characteristics of polymer blends. Material scientists, physical chemists, and analytical chemist use DSC to study corrosion, oxidation, reduction, phase changes, catalysts, surface reactions, chemical adsorption and desorption, fundamental physical properties such as enthalpy, boiling point, and equilibrium vapour pressure. (Robinson et al, 2005)

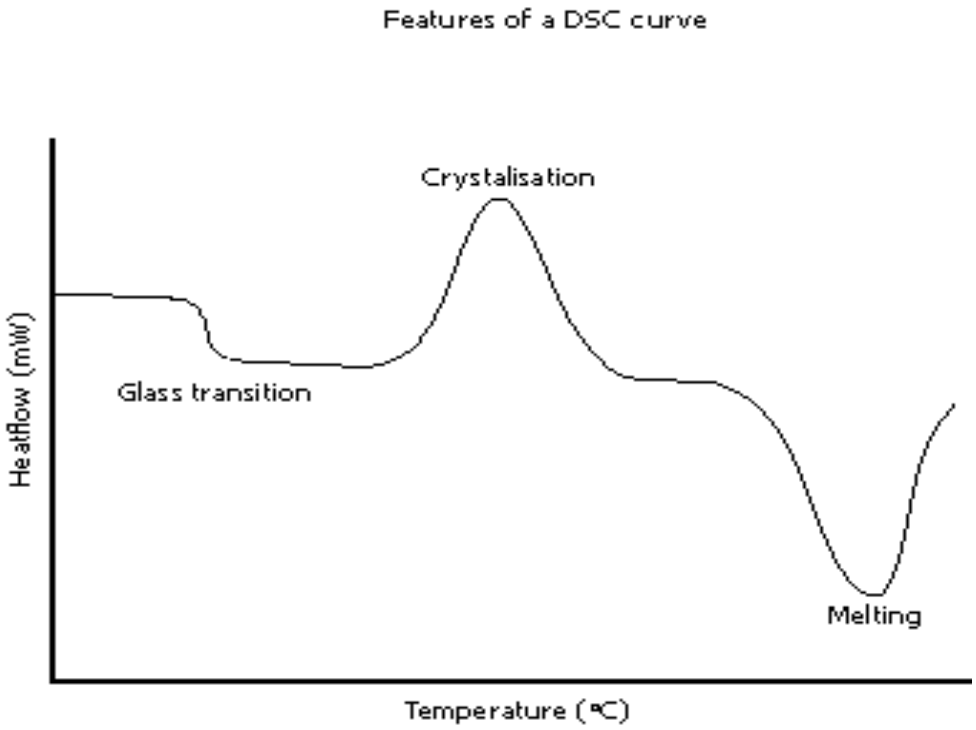

Figure A-3 DSC thermal curve of PET

A.2 Thermogravimetric analysis (TGA)

Thermogravimetric analysis measures weight (mass) of a sample in a specified atmosphere as a function of temperature. The most common temperature programme is a linear increase in temperature with time, although isothermal programs, stepped temperature programs can be used. The plot of the TGA analysis is a plot of mass (mass %) vs temperature, is called thermal curve. An example of a thermal curve is shown in Figure A-4. The mass or % mass is plotted along the y-axis and temperature (for a linear temperature ramp) along the x-axis (Robinson et al, 2005). The change in mass of a sample as the temperature changes, tells several things:

- It determines the temperature at which the material loses or gains weight. Loss of weight indicates decomposition or evaporation of the sample. A gain can indicate adsorption by the sample of a component in the atmosphere or a chemical reaction with the atmosphere.
- The temperature at which no weight change occurs indicates the temperature stability of the materials. These weight changes at certain temperatures are physical properties of chemical compounds under the conditions of the experiment (atmosphere, heating rate). (Robinson et al, 2005)

Modern TGA equipment have a sensitive balance, usually a microbalance, for continuously measuring sample weight, a furnace surrounding a sample holder, and a purge gas system for supplying an inert or reactive atmosphere. A computer generally controls the furnace and the data acquisition. (Robinson et al, 2005)

Examination of a TGA curve will show that a sample's weight loss associated with particular decomposition occurs over a considerable temperature range, not at a single temperature. When TGA is used to identify an unknown compound, this wide range is handicap because the uncertainty of identification in increased. This problem can be partially overcome by derivative thermogravimetry (DTG). In DTG, the first derivative of the TGA curve is plotted with respect to temperature. The plot that results has a change in mass with time, dm/dt, which is the rate of mas change, on the y-axis. (Robinson et al, 2005)

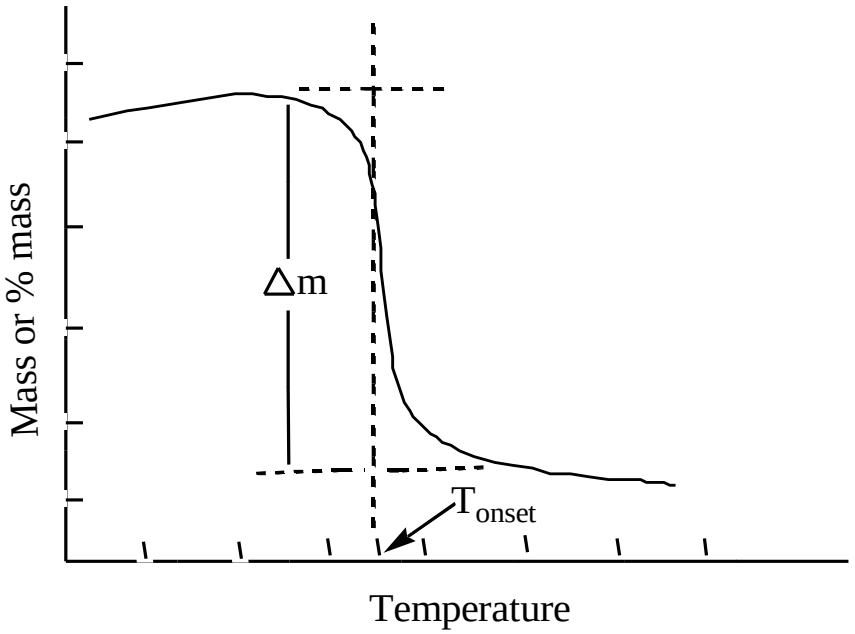

Figure A-4 A diagram illustrating measurement of the onset temperature, T_{onset}.

While the TGA provides useful data when mass change is involved in a reaction, the nature of the materials evolving is not known. The evolution of gases from the TGA may be determined using evolved gas detection (EGD) or evolved gas analysis if qualitative or quantitative analysis of the gas is required. These techniques are essentially a combination of thermal analysis and mass spectrometry (MS), GC-MS or other species-selective detectors, such as FTIR.

The evolved gases are carried through a heated transfer line to the FTIR or MS or other gas analyser. Nitrogen is used as a purge gas because it does not exhibit IR absorption. A FTIR instrument is less sensitive and less versatile than MS, but is cheaper and simpler. The interface is relatively simple, because FTIR normally operates at ambient pressure as does the thermal analyser. The IR spectra are simple to interpret and reference libraries of gas phase IR spectra are available for common gases and volatile organic compounds. This makes positive identification of the evolved gas straightforward if the gas is one of the gases that often accompany the decomposition of a material, e.g. H_2O, CO, or HCl. (Robinson et al, 2005)

APPENDIX B MOLECULAR SPECTROSCOPY

B.1 Fourier transforms infrared (FTIR) spectroscopy

Infrared spectroscopy is one of the oldest techniques employed for the molecular level characterisation of materials. In an infrared experiment, one usually measure the transmission, reflection, emission, or scattering of IR radiation, then calculates the absorption from the measured quantity.

Absorption of energy in the infrared region arises from changes in the vibrational energy of the molecules. There are two predominant types of vibrations that cause absorptions in an IR spectrum:

Stretching

This involves rhythmical displacement along the bond axis such that the interatomic distance alternately increase and decrease (Figure B-1(a))

Bending

This involves a change in bond angles between two bonds and an atom common to both (Figure B-1(b)).

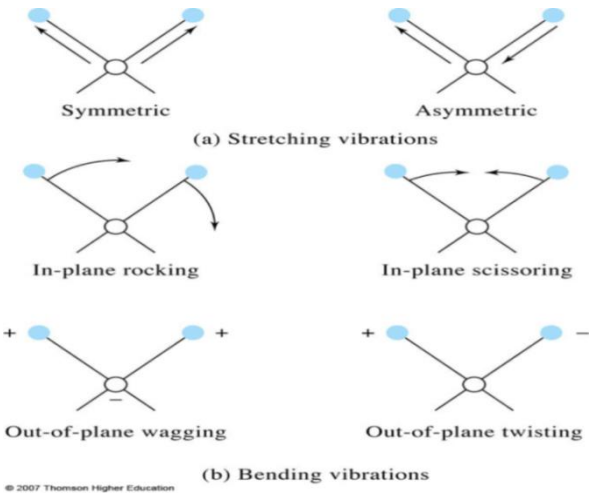

Figure B-1 Stretching and bending vibrations.

Only vibrations that produce a change in the electric dipole moment of the molecule are observed in the infrared spectrum. For example, stretching vibrations in homonuclear diatomic molecules like O_2, N_2 and Br_2 do not produce a change in dipole moment and hence these molecules are not IR active. On the other hand, molecules like CO and IBr are IR active because they contain a permanent dipole moment that will change as the bond is stretched or compressed. Linear molecules such as CO_2 do not have a net dipole moment, but can produce an IR spectrum because the two C=O bonds can stretch in an asymmetric fashion and also bend to produce changes in the dipole moment, shown in Figure B-2. (Robinson et al, 2005)

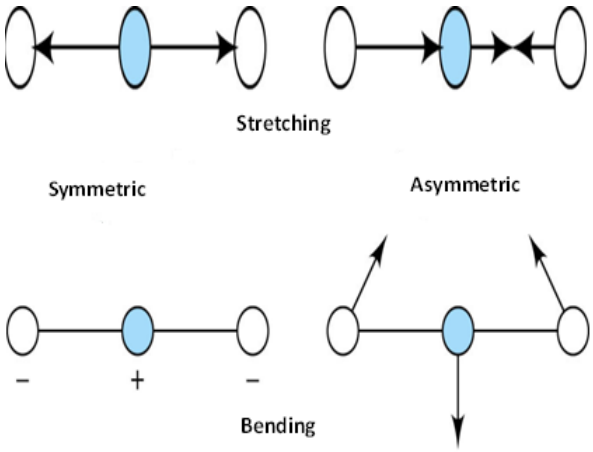

Figure B-2 Carbon dioxide (CO_2) stretching and bending vibrations.

Diatomic molecules can perform only one single vibrational modes motion. The number of possible vibrational modes of multi-atomic molecules can be calculated in the following:

Each single atom can move in three spatial directions corresponding to 3N spatial coordinates for N number of atoms. Thus the system of N points of mass has 3N degrees of freedom available. To describe the motion of such molecules, translational, rotational, and vibrational motions must be considered. Three coordinates or degree of freedom are required to describe translational motion and three degrees of freedom are required to describe rotational motion about a molecule's centre of gravity (Robinson et al, 2005). This

leaves 3N - 6 degree of freedom to describe vibrational motion. There are three 3N - 6 possible normal modes of vibration in a molecule for N atoms (Robinson et al, 2005; Söderlind, 2008). For example, the water molecule contains 3 atoms, so its 3 x 3 = 9 degrees of freedom and (3 x 3) - 6 = 3 normal modes of vibration. For water molecule, these normal modes of vibration are symmetric stretch, an asymmetric stretch, and a scissoring (bending) mode (Robinson et al, 2005). Linear molecules cannot rotate about the bond axis. As a result, only two degrees of freedom are needed to describe rotation, so linear molecules have 3N - 5 normal modes of vibration. The CO_2 molecules for example have 3 modes of vibration are shown, but 3N - 5 = 4 normal modes of vibration. (Robinson et al, 2005)

The infrared spectrum can be divided into three main regions: the far-infrared (< 400 cm^{-1}), the mid-infrared (400 - 4000 cm^{-1}) and the near-infrared (4000 - 13000 cm^{-1}). The most useful IR region is the mid-infrared region, but the near- and far-infrared regions do provide important information about certain materials. Generally there are fewer infrared bands in the 1800 - 4000 cm^{-1} region with many bands between 1500 cm^{-1} and 400 cm^{-1} called the fingerprint region. If two molecules have identical IR spectra, they are almost certainly identical (McMurry, 2004). Structural information can be extracted by understanding where the characteristic functional groups absorptions take place. Table B-1 list the characteristic IR bands of some of typical functional groups. The Figure B-3 illustrates the schematic diagram of a typical FTIR spectrometer.

The source

The black-body source emits infrared energy and then the beam is passed through an aperture which controls the amount of energy passed to the sample (and, ultimately, to the detector).

Sample

The beam enters the sample compartment, transmitted through or reflected off the surface of the sample, depending on the type of analysis. This is where specific frequencies of energy, which are uniquely characteristic of the sample, are absorbed.

Interferometer

The beam enters the interferometer where the spectral encoding takes place. The resulting interferogram signal then exits the interferometer.

Detector

The beam finally passes to the detector for final measurement. The detectors used are specially designed to measure the special interferogram signal.

The computer

The measured signal is digitised and sent to the computer where the Fourier transformation is performed. The final infrared spectrum is then presented to the user for interpretation and further manipulation.

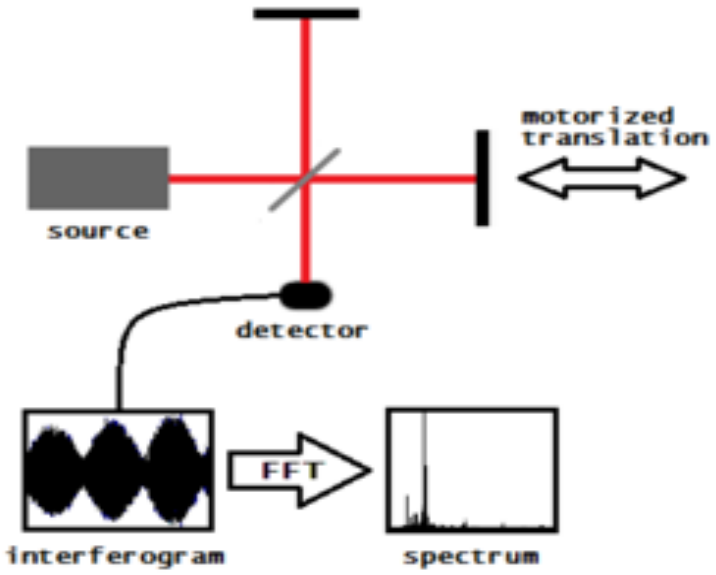

Figure B-3 Typical Fourier transform spectrometer.

Table B-1 Characteristic infrared absorption frequencies of some functional groups (McMurry, 2004).

Compound type	Functional group	Frequency (cm^{-1})	Frequency range (cm^{-1})
Alkanes, alkyl groups	C-H	2960 - 2850	Medium to strong
Alkenes	=C-H	3100 - 3020	Medium
	C=C	1680 - 1640	Medium
Alkynes	≡C-H	3300	Strong
	-C≡C-	2260 - 2100	Medium
Alkyl halides	C-Cl	800 - 600	Strong
	C-Br	600 - 500	Strong
	C-I	500	Strong
Alcohols	O-H	3650 - 3400	Strong, broad
	C-O	1150 - 1050	Strong
Amines	N-H	3500 - 3300	Medium
	C-N	1230 - 1030	Medium
Carbonyl compounds	C=O	1780 - 1670	Strong
Carboxylic acids	O-H	3100 - 2500	Strong, very broad
Nitriles	C≡N	2260 - 2210	Medium
Nitro compounds	NO_2	1540	Strong
Aromatics	C-H	3030	Weak
	Ring	2000 - 1660	Weak
		1600 - 1450	Medium

FTIR can be used for qualitative and quantitative analysis. Qualitative helps with the structural elucidation and compound identification. This is achieved by comparing spectra of the unknown sample to that of known molecule in order to identify the compound.

Quantitative analysis of absorption spectrometry is the use of Beer's Law to prepared calibration line relating absorbance to concentration. Once calibration is generated and validated it can be used to determine the concentration of molecules in unknown samples (Smith, 2011). For a single compound in a homogeneous medium, the absorbance at any frequency is expressed as,

$$A = \varepsilon l c \qquad \text{B1}$$

where A is the sample absorbance at a given frequency, ε is the molecular absorptivity at the frequency, l is the path length of source beam in the sample, and c is the concentration of the sample (Smith, 2011). Table B-2 lists the advantages and disadvantages of infrared spectroscopy as chemical analysis techniques. These attributes are for the techniques generally, are independent of the type or brand infrared spectrometer used.

Table B-2 Advantages and disadvantages of IR spectroscopy (Smith, 2011).

Advantages	**Disadvantages**
Almost universal	some molecules can't be detect (Not IR active)
Spectra are information rich	Mixture (Complex spectra to interpret)
Relatively fast and easy	Water (broad intense peaks can mask peaks from solute
Relatively inexpensive	
Sensitivity	

B.2 Nuclear magnetic resonance

Nuclear magnetic resonance spectroscopy (NMR) is an important technique that is used for determining the structure of molecules. The basic theory of NMR is common to all experiments and all nuclei. The fundamental property of the atomic nucleus involves a nuclear spin (*I*), which have values of 0, ½, 1, 1 ½, etc., in units of $h/2\pi$ (Young and Lovell, 1991). The actual value of spin of any given nucleus depends on the mass number and the atomic number of the nucleus, as shown in Table B-3

Table B-3 Mass and atomic number and spin of nucleus

Mass number	Atomic number	Nuclear spin
Odd	Even or odd	½, 1 ½ , 2 ½
Even	Even	0
Even	odd	1, 2, 3

Common nuclei such ^{12}C, ^{16}O and ^{32}S have even mass numbers and even atomic numbers and therefore zero spin, thus they are NMR inactive. The nuclear magnetic moment (μ) is directly proportional to the spin, i.e.,

$$\mu = \frac{\gamma I h}{2\pi} \qquad \text{A-2}$$

where γ, is the proportionality constant called the magnetogyric ratio and is constant for each particular nucleus (Young and Lovell, 1991).

Figure B-4 shows the orientation of atomic nuclei in the presence of an external applied magnetic field. The nuclear magnetic moments are randomly oriented and when placed in an external magnetic field, B, the nuclear magnetic moments orientate in the parallel or anti-parallel to the external applied field. Most of the nuclear magnetic moments will align parallel to the external applied field because lower energy is required for resonance

(McMurry, 2004). The energy difference between the two magnetic fields split levels is of the order of radio frequency (10^6 Hz). (McMurry, 2004)

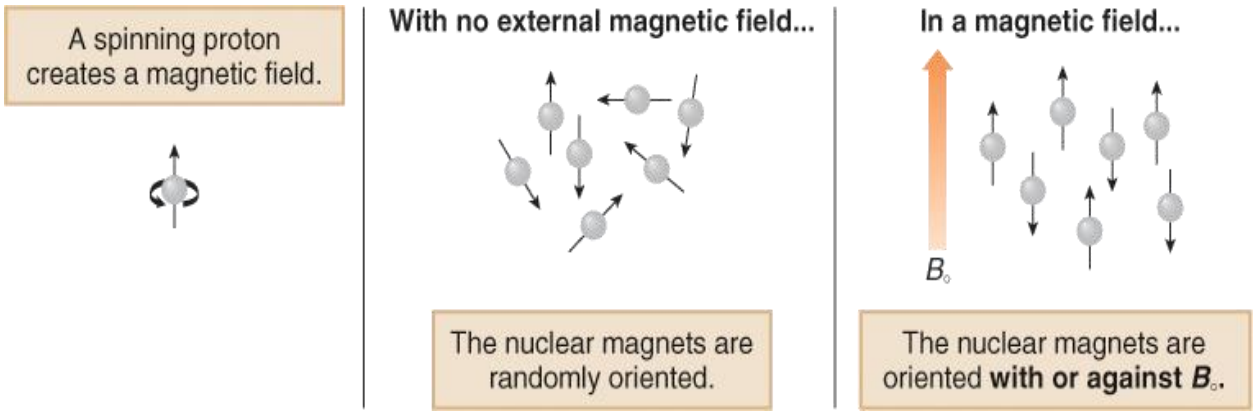

Figure B-4 Schematic representation of alignment of atomic nuclei in presence of the external magnetic field (McMurry, 2004).

The energy of interaction is simply proportional to the nuclear moment and the applied field and is represented by Equation A-3

$$E = -\frac{\gamma h}{2\pi} m_I Bo \qquad \text{A-3}$$

where B is the external applied filed and h is Planck's constant. The energy difference increases with the increase in the external applied magnetic field, B_o (McMurry, 2004).

The atomic nuclei have different gyromagnetic ratios, yield signals at different frequencies in a particular magnetic field and the nuclei of the same type can achieve the resonance condition at different frequencies. This occurs if the local magnetic field experienced by a nucleus is slightly different from that of another similar nucleus. If a molecule containing a nucleus of interest is put in a magnetic field, B_o, the magnetic field by the nucleus is reduced due to small magnetic field produce by the electrons around the nucleus, thus shielding the nucleus from the external applied filed. This local magnetic field, B_{local}, felt by the nucleus can be presented by Equation A-4.

$$B_{local} = B_o(1 - \sigma) \quad \text{A-4}$$

where B_{local}, is the local field experienced by the nucleus, and σ a dimensionless shielding constant. Therefore, the shielding and the resulting resonance frequency will depend on the exact characteristics of the electron environment around nucleus (McMurry, 2004). The shielding effect on the nucleus by electrons causes chemical shift in NMR spectra (Breitmaier, 2002). When an atomic nucleus shift is reduced is said to be shielded (high shielding field) and when shift is increased is said to be deshielded (low shielding filed) (Breitmaier, 2002).

A nucleus with a magnetic moment may interact with other nuclear spins resulting in a natural splitting of the NMR signal from each nucleus into mutliplets. The number of components into which a signal is split is 2n + 1, where n is the number of other nuclei interacting with the nucleus. The difference between any two adjacent components of multiplets is the same and yields the value of the spin-spin coupling constant, *J* (in hertz). The spin-spin splitting is independent of magnetic field strength, so increasing the magnetic field strength will increase the chemical shift difference between two peaks in Hz, but the coupling constant *J* will remain the same (Breitmaier, 2002; McMurry, 2004).

There are two basic techniques for recording high-resolution NMR spectra, i.e., the Continuous wave NMR (CW-NMR) and Fourier transform NMR (FT-NMR) techniques. In CW technique, the frequency of field of appropriate for the chemical shift range of the nucleus is swept by a continuously increasing radio-frequency. The duration of the sweep is long, around 2 Hz/s or 500 s for a sweep of 1000 Hz corresponding to 10 ppm in 100 MHz proton NMR spectra (Breitmaier, 2002). Rather than sweeping through a range of frequencies (or magnetic field strengths), in FT-NMR technique, the sample is placed in a magnetic field and irradiated with a short, intense burst of RF radiation (the pulse), which excites all the protons in the molecules at the same time. A typical pulsed FT-NMR spectrometer is shown in Figure B-5.

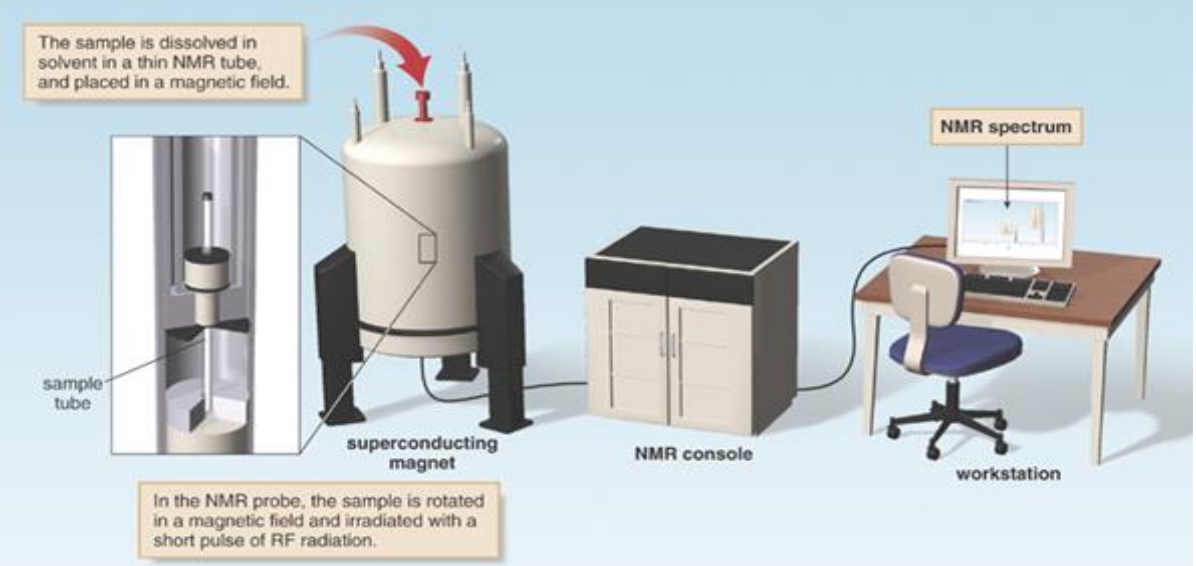

Figure B-5 A typical NMR spectrometer diagram.

NMR spectroscopy is most commonly used in structural characterisation of sample in solution than in solids. The following factors limit the response of solids compare to that of liquids: dipole-dipole interactions and chemical shift anisotropy (CSA). These factors give rise to line broadening in the spectra of solids due to lack of molecular motions. Line broadening occurs in solutions but is average to zero by molecular motion and their contributions are negligible (Andrew and Eades, 1962). The lack of molecular motions in solids causes the lines of the NMR spectra appear broad and relatively characterless. This considerably limits the characterisation of solids. The magic angle spinning (MAS) is one of the techniques developed to remedy the problems associated with line broadening. The following techniques have been developed to remedy the problems associated with line broadening: dipolar decoupling (DD) and magic angle spinning (MAS) (Mohajerani, 2001).

The DD and MAS techniques narrow the linewidth and subsequently provide well-resolved spectra. The MAS consists of spinning the rotor containing the sample around an axis at the magic angle $\theta = 54.74°$ with the direction of the external magnetic field (Alia et al, 2009). Figure B-6 represents the MAS experimental setup. Spinning the sample at the magic angle, the anisotropic part produces NMR spinning sideband. A sample is placed in a rotor and mechanically spun at high frequency about an axis oriented at the magic angle of $\theta = 54.74°$

to the static magnetic field yielding ($3\ Cos^2\ \theta - 1 = 0$). Employing faster rotations, the spinning sidebands are shifted away and the spectrum consists of narrow lines at the isotropic shifts (Alia et al, 2009).

For the low sensitivity of the ^{13}C nucleus, the problem can be overcome by the techniques called cross polarisation (CP) by transferring polarisation from magnetised-rich protons to the carbon nuclei (Mohajerani, 2001).

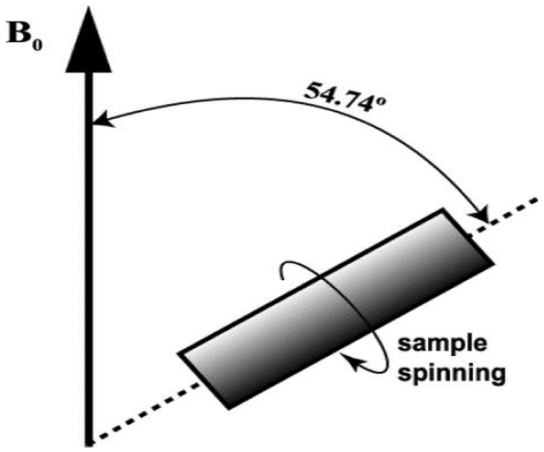

Figure B-6 NMR Magic angle spinning setup.

Solid state ^{19}F NMR

The ^{19}F nucleus, with spin quantum number I = 1/2 and a high receptivity (100% natural abundance and gyromagnetic ratio similar to that of ^{1}H, comparisons are shown in Table B-4), would appear to be well-suited for NMR investigations in solids. The large ^{19}F chemical shift range (~800 ppm, compared with the ~20 ppm typically found for ^{1}H) results in spectra which are particularly sensitive to the relatively small changes in local environment (Dargaville, 2002). However, the high natural abundance and large gyromagnetic ratio of ^{19}F can results in very strong homonuclear dipolar couplings that may hinder the resolution of distinct sites and the extraction of site-specific information (Dargaville, 2002).

Fluoropolymers are resistant to most common solvents and therefore have poor solubility (Emmons et al, 2008). This makes fluoropolymers difficult to characterise by solution-state NMR. The availability of ^{19}F high-resolution solid-state NMR has presented new opportunities in understanding the behaviour of fluoropolymers and changes in their chemical structures. The ^{19}F solid-state NMR does suffer from the limitations associated with solid analysis mention above. The difficulties arise due to strong homonuclear ^{19}F-^{19}F dipolar coupling interactions and chemical shift anisotropy (CSA), which results in line broadness and featureless resonance complicated by spinning sidebands. The MAS technique can be used to average both the CSA and dipolar interactions in the NMR spectra of solids. However, high spinning rates are required for efficient averaging of these interactions by MAS alone because of the great influence of ^{19}F-^{19}F interactions.

Table B-4 NMR behaviour of some common nuclei.

Nuclei	Unpaired protons	Unpaired neutrons	Net spin
^{1}H	1	0	½
^{2}H	1	1	1
^{13}C	0	1	½
^{14}N	1	1	1
^{19}F	1	0	½
^{23}Na	1	2	1 ½
^{31}P	1	0	½

Spinning rates in the excess of the static dipolar-broadened linewidth (>10 kHz) , see Figure B-7, shows a reduction in the width of the centre bands and spinning sidebands as the spinning rates increases, thus indicating the sidebands are partially caused by homonuclear coupling (Scheler, 1998). Another method that can be used to acquire a well-resolved spectrum is by applying heat to the sample to high temperatures greater than 300 °C while

acquiring the spectra without spinning. The high temperature causes molecular motions, and narrows the broad NMR lines and average dipolar interactions. The disadvantage using high temperature could cause the microstructure to undergo thermal degradation (Mohajerani, 2001).

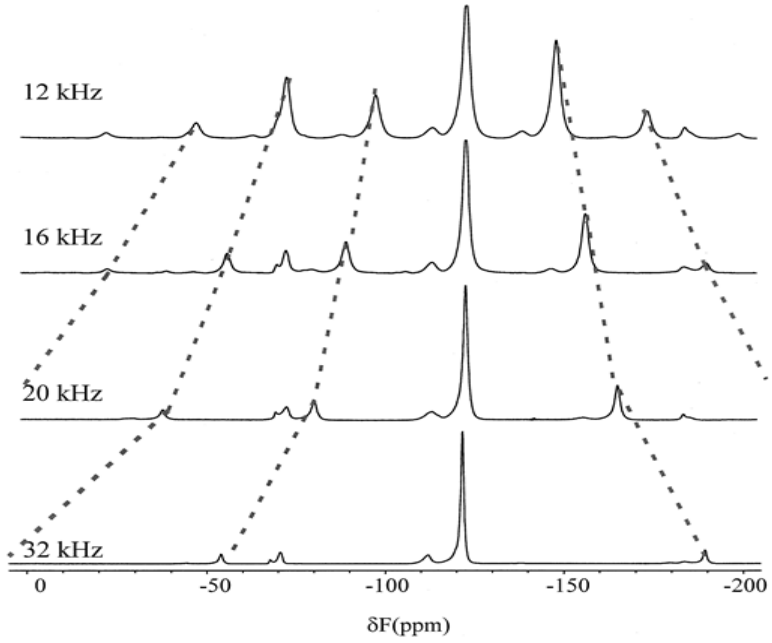

Figure B-7 ^{19}F spectra of FEP analysed using different MAS spinning frequencies (Scheler, 1998).

APPENDIX C ELECTRON MICROSCOPY

Electron microscopy uses high energy electrons that are generated from a filament using a large accelerating voltage (up to ~400 kV). The high momentum of such electrons corresponds to very short wavelengths (e.g. λ is ~ 0.025 Å for an accelerating voltage of 200 kV) according to the de Broglie equation (Söderlind, 2008). For accelerating voltage higher than ~100 kV, the relativistic effects have to be considered and the wavelength can be calculated using Equation C-1:

$$\lambda = \frac{h}{\left[2em_o U + \frac{e^2 U^2}{c^2}\right]^{1/2}} \qquad \text{C-1}$$

where $h\ is$ the Planck constant, c is the speed of light, e is the electron charge, m_o is the electron rest mass, and U is the accelerating voltage. (Söderlind, 2008)

The scanning electron microscopy (SEM) is a type of electron microscope with a capability of producing high-resolution images of a sample surface. The SEM produces an image that gives the impression of 3 dimensions. This SEM uses a 2 to 3 nm spot of electrons that scan the surface of the sample that is then detected by a sensor. The image is produced over time as the entire sample is scanned. The accelerating voltages used for SEM are considerably low, generally 5 to 20 kV (Söderlind, 2008). When these electrons impinge on the sample, secondary electrons, back scattered electrons, absorbed electrons, and characteristic X-rays are emitted. The emitted electrons are collected by detectors and used to form a 3D picture of the sample, providing both topographical and structural information (Söderlind, 2008). The characteristic X-rays emitted have energies characteristic for each element, and are used to qualitatively and quantitatively deduce the chemical composition of the sample, by energy dispersive x-ray spectroscopy (EDX) (Söderlind, 2008).

The formation of images in SEM occurs because of interaction between the electron beam and specimen. SEM requires the vacuum environment and specimen surface to be electrically conductive. Figure C-1 show the general schematic diagram of SEM. The specimen (or its surface) must be electrically conductive and vacuum compatible. For

conventional imaging, the specimens must be electrically conductive at least at the surface, and electrically grounded to prevent the accumulation of electrostatic charge at the surface. Metallic samples and alloys can be examined without coating, but organic materials, insulators and non-conducting materials (such as, rubber, plastics, concrete, ceramics, biological specimens such as bacteria and other biological specimens), tend to charge when scanned by the electron beam, and cause scanning faults and other image artefacts. This can be rectified by coating with an ultra-thin layer of electrically-conducting materials, such as carbon, aluminium, gold, etc. The coating is applied to the specimen by high temperature evaporation or by plasma discharge techniques. The coating of the sample prevents charging of the sample and, increase signal and surface resolution. The improvement in resolution arises because backscattering and secondary electron emission near the surface are enhanced and thus an image of the surface is formed.

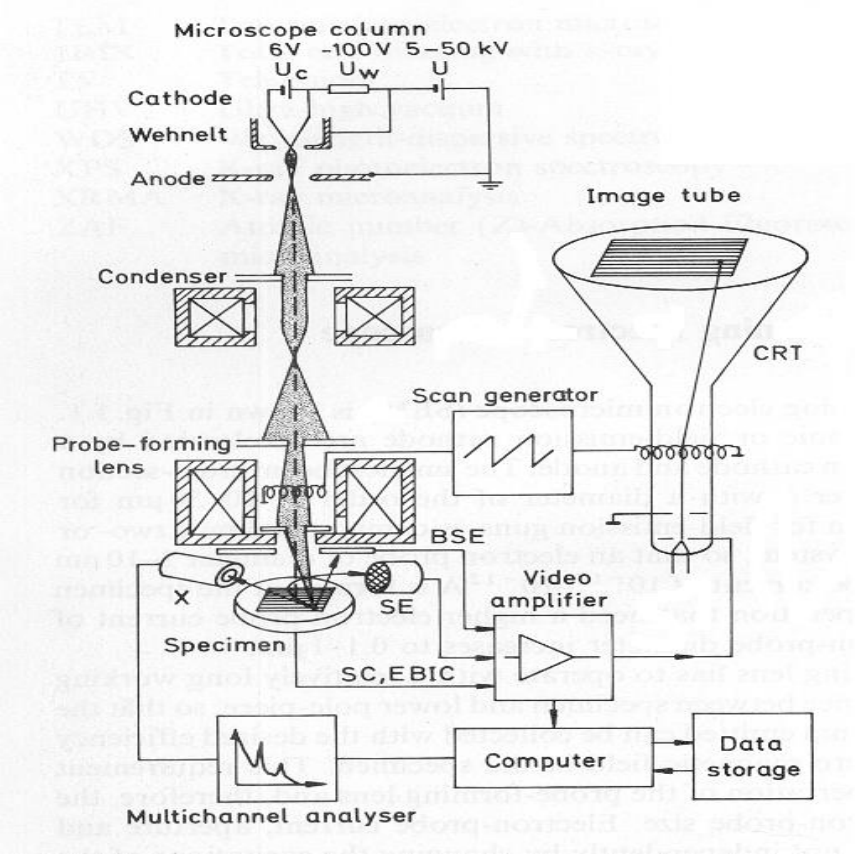

Figure C-1 The main components of a typical SEM are electron column, scanning system, detector, display, vacuum system and electronic controls.

APPENDIX D X-RAY DIFFRACTION

The X-ray region by definition is the portion of the electromagnetic spectrum that lies between the ultraviolet and gamma regions. XRD is a widely applied technique for material characterisation in fields as diverse as chemistry, solid-state physics, geology, etc. XRD analysis provides information about the chemical nature of the material including the crystallographic structure of the phase.

A material is composed of atoms or molecules that are periodically ordered at a distance of 0.1 to 0.5 nm from each other (Munekawa, 1988). Irradiating a material with X-rays having a wavelength approximately equivalent to the interatomic or intermolecular distance, a part of the radiation incident upon the crystal scatters from the crystal lattice and the X-ray diffraction phenomenon occurs (Munekawa, 1988). The X-ray diffraction pattern provides information about the size and symmetry of the unit cell. It also provides the location of the atoms within the unit cell. The X-ray wavelength, λ, is given by the Bragg's Law (Equation D-1):

$$n\lambda = 2d_{hkl}\sin\theta \qquad \text{D-1}$$

where d_{hkl} is the interplanar distance of the lattice planes hkl, θ the angle of the incident beam and n is the diffraction order (an integer > 0). The Bragg's law can be geometrically derived as shown in Figure D-1 (Söderlind, 2008). Thus the X-ray diffraction patterns can be employed to directly determine the 3-dimesnional structure of a crystalline material (Söderlind, 2008).

XRD can be used for estimating the degree of crystallinity in polymers. The degree of crystallinity in a semicrystalline sample is calculated from the ratio of the integrated crystalline scattering to the total (crystalline and amorphous) scattering (Lee et al, 1995; Mulla et al, 2012). This can only be possible if the crystalline and amorphous scattering in the diffraction pattern can be separated from one another. The crystalline scattering pattern is represented by a sharp peak. The crystalline scattering arises when X-ray beams are scattered by atoms in the crystalline regions of the sample according to the Bragg's law.

The amorphous scattering pattern is represented by a much broader peak, which originates when X-ray beams undergo diffuse scattering from the amorphous regions of a material.

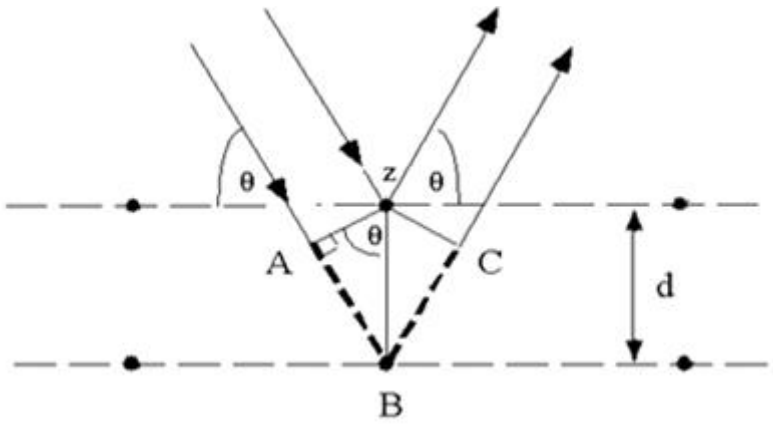

Figure D-1 Schematic representation of diffraction of X-rays in a crystalline material. Bragg's satisfied when the path length difference of the X-rays is equal to $n\lambda$. The diffraction angle θ is half the angle between the incident and diffracted X-rays.

A typical X-ray diffractometer comprises of the following: a source of X-rays, i.e. the X-ray generator, a diffractometer assembly, and an X-ray data collection and analysis system. The diffractometer assembly controls the position and orientation of both the specimen and the X-ray detector. XRD requires monochromatic radiation, generated by excitation of K-radiations from a pure metal target and then filtered the beam by interposing a foil which strongly absorbs the β-component of the K-radiation without any appreciable reduction in the intensity of the α-component. A good example is the use of a nickel filter ($E_{Ni\text{-}K}$ = 0.1488 nm) with a copper target ($E_{Cu\text{-}K}$ = 0.138 nm), which transmits the Cu-K_α beam (0.154 nm), but blocks the Cu-K_β component. Suitable parts of target and filter metals are given in Table D-1.

Table D-1 Anode, filter metals and frequency applied wavelenths.

X-Ray tube	K_α (Å)	K_β (Å)	Filter
Fe	1.9373	1.7565	Mn
Cu	1.5418	1.3922	Ni
Co	1.7902	1.6207	Fe
Cr	2.2909	2.0848	V
Ni	1.6591	1.5001	Co
Mo	0.7107	0.6223	Zr

APPENDIX E SPECIFIC IR RATIO

The Specific IR ratio, also known as HFPI (HFP index), is defined as the net infrared absorbance at wavenumber 982.32 cm^{-1} divided by net absorbance at wavenumber 2352.94 $cm^{-1}$of a film about 50 um thick. The film was produced by melt pressing 0.5 grams sample of a resin at 340 °C for 1 minute under 18143 kg force between the shiny sides of 12.7 cm square aluminium sheets having a combined thickness of 0.0762 mm in a 15.24 square. A 0.127 mm deep cavity of a mould assembly consisting of superposed flat planes separated by a centrally aperture spacer sheet, quenching the mould assembly in ice water, and dissolving the adherent aluminium foil away from the resulting film in hot (90 - 100 °C) aqueous 10 % sodium hydroxide. A clear portion of the film was mounted on the sample holder of a recording infrared spectrometer, and scanned in the ranges of from 2000 cm^{-1} to 2500 cm^{-1} and from 833 cm^{-1} to 1000 cm^{-1} while flushing the sample holder with nitrogen. (Bro and Sandt, 1960; Ebnesajjad, 2003)